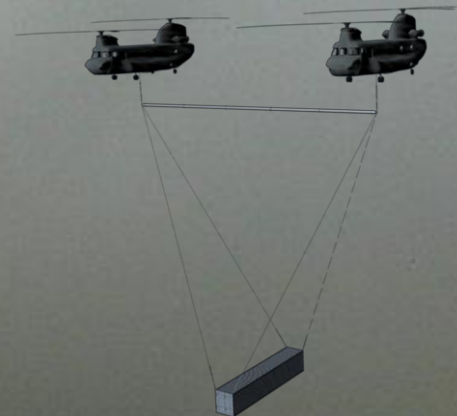27th Annual AHS Student Design Competition

Graduate Category

T.win-Lift
H.elicopter
O.perations
R.esearch

Daniel Guggenheim School of Aerospace Engineering

Georgia Institute of Technology

"THOR"

Twin-Lift Helicopter Operations Research

Department of Aerospace Engineering

Georgia Institute of Technology

Atlanta, GA 30332

In Response to the 27th Annual American Helicopter Society Student Design Competition

Graduate Category

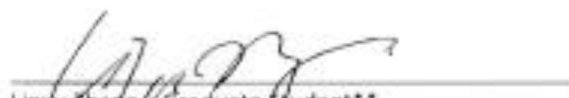Zachariah Morford – Graduate Student (Team Lead)**

Daniel Akins – Undergraduate Student*

Keeryun Kang – Graduate Student

Nicholas Austin – Undergraduate Student*

Stephanie Kersten – Graduate Student**

Corey Dillingham – Undergraduate Student*

Linyu Zhang – Graduate Student**

Arvind Krishman – Undergraduate Student*

Robert Schlein – Undergraduate Student*

*Student receives credit for AE4359: Rotorcraft Senior Design.
**Student receives credit for AE6334: Rotorcraft Design II.

Acknowledgements

Table of Contents

Table of Figures

Table of Tables

Table of Acronyms

AHS	American Helicopter Society
AS	Aircraft Separation
CA	Control Accuracy
CAAS	Common Avionics Architecture System
CI	Controllability Index
DAFCS	Digital Automatic Flight Control System
ELRS	Emergency Load Release System
FCS	Flight Control System
FCC	Flight Control Computer
FHA	Functional Hazard Assessment
FTA	Fault Tree Analysis
IPPD	Integrated Product & Process Development
IPT	Integrated Product Team
LD	Load Flat Plate Drag Area
LHI	Load Handling Index
LR	Load Release
LS	Load Sharing
LVDT	Linear Variable Differential Transformer
M&P	Management & Planning
M&S	Modeling & Simulation
MADM	Multi Attribute Decision Making
MCI	Mission Capability Index
MPH	Mid-Point Hover Time
OC	Operating Cost
OEC	Overall Evaluation Criteria
Osc	Oscillation
PC	Production Cost
PDS	Product Design Specification
PFD	Primary Flight Display
PSSA	Preliminary System Safety Assessment
QFD	Quality Function Deployment
RC	Remote Control
RDT&E	Research Development Testing & Evaluation Cost
RFP	Request for Proposal
RT	Response Time
SEP	Systems Engineering Plan
SFC	Specific Fuel Consumption
TLC	Twin Load Capacity
TOPSIS	Technique for Order Preference by Similarity to Ideal Solution
WLAN	Wireless Local Area Network

Twin-Lift System Characteristics

12 ft

100 ft

48 ft

100 ft

8 ft

8 ft
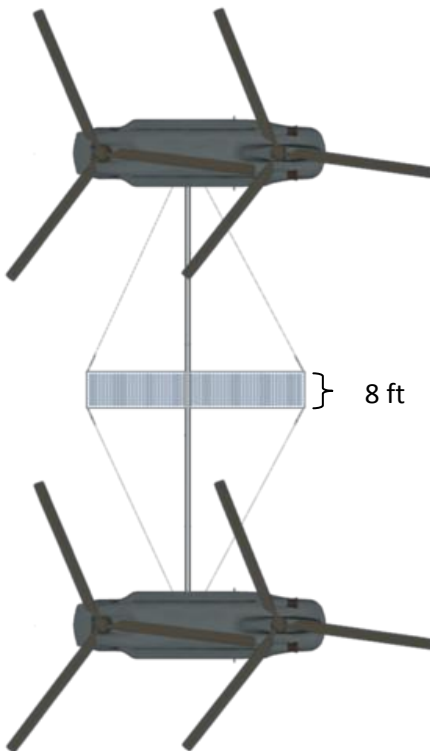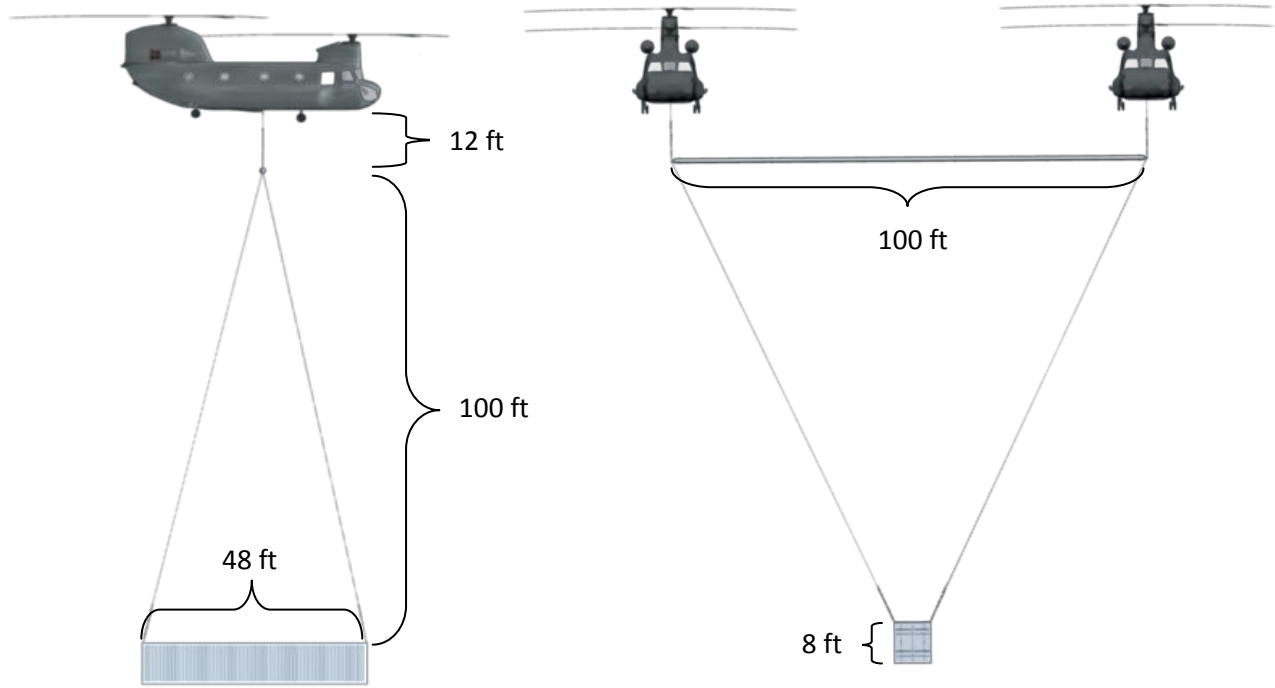
Aircraft Characteristics

Aircraft Gross Weight: 33,000 lb

Aircraft Max Gross Weight: 50,000 lb

Mission Design

Max Payload: 31,000 lb

Mission Range: 100 nm

Lift Capacity Gained in Twin Configuration: 90%

System Cost

System Cost Per Flight Hour: $866.86

Total System Cost: $39,300,000

Overview

Given the task of creating a twin-lift system utilizing two current off-the-shelf helicopters to simulate heavy lift, Team THOR decided to create a system of two CH-47F helicopters in side-by-side configuration using a spreader bar and longitudinally directed load. This configuration maximizes lifting capacity while minimizing drag. Although it does increase the need for precision control, with an appropriate load stabilization system and master/slave control for maintaining close formation flight this configuration can be safely flown in all modes of flight. Also included in the project was a flight demonstration where the lift of a remote control helicopter had to be improved by at least 5%. This was accomplished by increasing the RPM of the rotor, which increased the thrust by 20%. Also tested for this portion was using blades of different symmetries, but this only gave a 0.5% increase in thrust.

Throughout this semester, the team from AE4359 Rotorcraft Senior Design and AE6334 Rotorcraft Design worked through the IPPD methodology to select a concept for the 2010 AHS design competition. During this portion, the team selected to utilize the CH-47F as the baseline airframe because of its superior payload capabilities, stability with sling loads, and low disk loading. Based on safety considerations and equal load sharing, we selected to utilize a 100' spreader bar made of an Aluminum-Lithium alloy for basic load handling. This spreader bar was made to be divided into five 20' sections which are fully interchangeable. This allows the bar to be easily disassembled and transported in the back of a single aircraft. It also means that any damage will require replacement only in the section which was damaged; it also simplifies the procurement of replacement parts by limiting the spreader bar to only two unique parts: the 20' bar sections and the end caps. In order to control the high number of degrees of freedom, decrease response time and increase control accuracy, we decided to use a form of adaptive control. Once the concept was selected, we moved on to conceptual design where we refined the concept, sized the vehicle and spreader bar, maximized the payload for the mission, and began modeling the system with CAD software.

Once the conceptual design was complete, a model was created in Matlab which used equations from NASA Technical Paper 3280 on twin-lift operations. With this model, we were able to determine the controllability of the system, boundary conditions for controllability, and response times to maintain control. This information fed into decisions on the type of load stabilization system and formation flight system which were needed to safely control the system.

Next, numerous options for stabilizing oscillations of the load were looked at and researched. These options ranged from controls on the bar, to controls on the load, to sensing systems on the bar, before deciding upon an optical based sensing system with control logic for the pilot of the master aircraft.

In order to make this system work, a method of master/slave control had to be implemented that allowed the aircraft to fly side-by-side at very close range and with very little error. Once again, research was done on a wide range of systems from optical sensing systems, to mechanical altitude control systems, to photogrammetry and retinal sizing systems, before deciding upon a system utilizing key

features of the CH-47F Digital Automatic Flight Control System (DAFCS) to implement a master/slave system where the slave aircraft is flying in a mode that closely resembles an auto-pilot.

Once the preliminary design for the twin-lift system was complete, a safety assessment was done to ensure there were no undue safety hazards within the system. Based on this analysis, an emergency release system was created to eliminate several catastrophic outcomes.

Lastly, a cost analysis of the system was done which leveraged trades in designs and materials for the spreader bar as well as calculating the production costs, RDT&E costs and additional direct operating costs due to the addition of the twin-lift system. This found that a twin-lift system can be developed for slightly under $40 million and the system would increase the DOC of the aircraft by approximately $900 per flight hour.

This finalized the preliminary design for the twin-lift system, but there was still the practical demonstration of the flight test on an RC helicopter remaining. After doing theoretical research on different methods to improve thrust, two different methods were tested to achieve the required 5% increase in thrust. Despite the success of both methods in theoretical testing, only one of the methods showed results which exceeded the requirements dictated in the RFP. While changing airfoils was only able to increase thrust by 0.5%, changing the tip speed of the rotors improved thrust by 20%.

All calculations and information regarding the information given above can be found in the report.

Twin-Lift System Design

Introduction

The purpose of this paper is to provide a response to the 2010 American Helicopter Society's (AHS) Lift! More Lift! Request for Proposal (RFP). This response serves as a formal declaration of intent of the Georgia Institute of Technology to compete in the 2010 design competition.

The paper provides an analysis of the requirements stated in the RFP, as well as both a conceptual selection of the configuration most suitable for performing the mission and a preliminary design of a number of subsystems and functions of the system. The culmination of the effort is the use of in house modeling tools to provide an optimized preliminary design of the multi-lift system as well as verification that the system is capable of meeting the mission requirements. The method, shown in Figure 1, was utilized to complete this analysis and is called the Georgia Tech Integrated Product and Process Development (IPPD) Methodology for Rotorcraft Preliminary Design. This is a methodology that logically breaks the development process down from receiving requirements through delivery of the product and allows work to be done sequentially and in parallel.
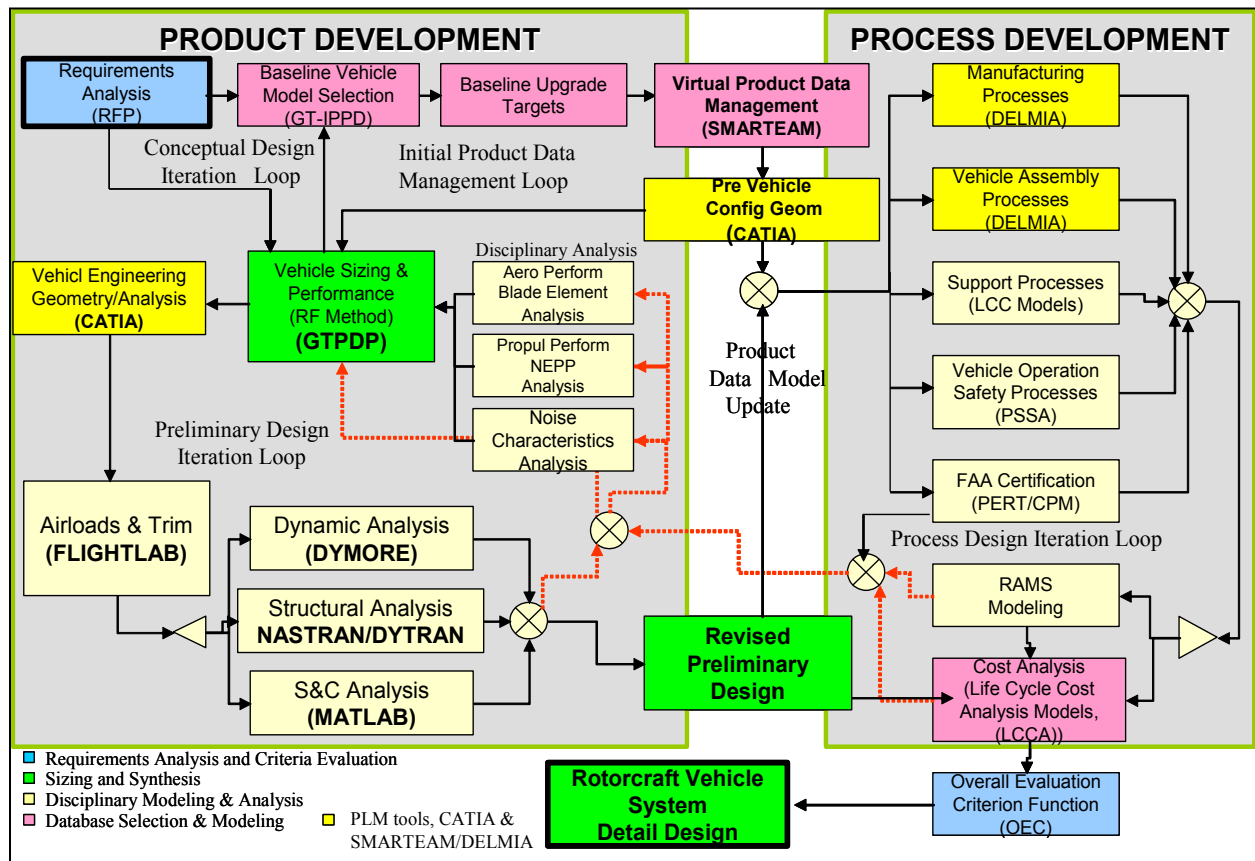
Figure 1: Generic IPPD Methodology for Rotorcraft Preliminary Design

Requirements Analysis

The 2010 AHS Student Design Competition Request for Proposal provides the requirements for the design of a multi-aircraft/lifting system capable of lifting 75% more payload than each of the individual aircraft could lift working alone. The RFP specifies that an in-service rotorcraft be selected as the baseline aircraft. The majority of the focus of the project is not on the design of the particular aircraft to be used, but rather on the multi-lift system capable of performing the requirements.

The general focus of the design effort is to be centered on the load lifting device, control scheme, and multi aircraft system stability. The specific requirements for the multi-lift system are as follows:

- Enough fuel needs to be aboard at takeoff for a 100 nm delivery distance, mid-point hover capability for 10 minutes and return without the payload.
- The baseline aircraft should have at least 5,000 lb useful load capability at Sea Level/ISA + 20 C conditions.
- A production heavy multi-lift load handling system should be able to accommodate 20' and 48' ISO containers, various wheeled or tracked vehicles, and large construction machinery.

These requirements if not the direct wording of the RFP, are derived from the text. The requirements regarding the baseline aircraft drive the selection of the off the shelf aircraft, while the requirements for the multi-lift system drive the design of the system as a whole.

Mission Analysis

From the requirements stated in the RFP, a mission diagram was developed. The stages of the mission required, coupled with the baseline parameters of the aircraft enable the determination of the weight ratio required to perform the mission. The aircraft mission, as derived from the RFP, consists of the following eleven stages shown in Figure 2.

1. 10 minutes for engine crank and warm-up.
2. 15 minutes at hover for load pickup and take-off.
3. Climb to 1000ft at a 2.5^o angle.
4. Fly in the twin-lift configuration for 100 nm at 100 kts.
5. Descend 1000ft at a 2.5^o angle.
6. Hover for 10 minutes with the load.
7. Drop the load and spreader bar.
8. Begin flight separately, climbing to 1000ft at a 2.5^o angle.
9. Fly 100 nm at 130 kts (approx 99% best range airspeed).
10. Descend 1000ft at a 2.5^o angle.
11. Land and shut down, mission complete with a 20 minute reserve.

Figure 2: Mission Breakdown

It is important to note that the 100kts speed was chosen based on aircraft sizing analysis, discussed later in this proposal. Above and beyond the information in the RFP it was necessary to make assumptions in

the development of the specified mission through the use of common aviation practices (such as the 10 minute crank and warm up) and safety standards (such as the 20 minutes of reserve fuel). While these are not captured in the RFP, they would commonly be requirements levied against a program during development.

System Decomposition

The physical architecture for the twin-lift system is included in Figure 3. This architecture includes the physical decomposition of the system into its main components. From the figure it can be seen that the system is broken down into aircraft, payload, load handling, and controls categories. The payload, load, and controls aspects are considered separately from the aircraft, due to the fact that these would all be carried on or attached to the aircraft at the time the mission is performed. The load handling devices can be further decomposed into the aircraft and load attachments, the method of separation, and the release mechanisms. The controls system will consist of flight controls and communication between the two load carrying aircraft.
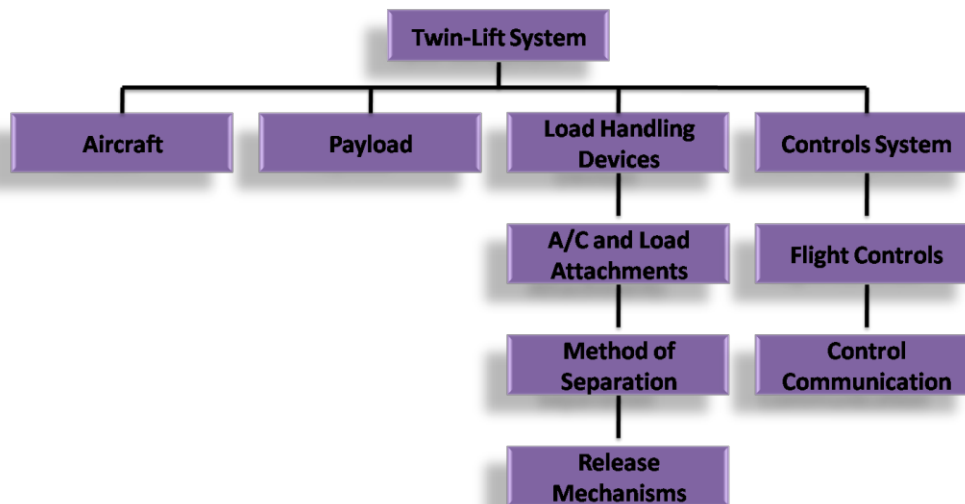
Figure 3: Physical Decomposition

Quality Function Deployment

With the system decomposed, attributes needed to meet the customer requirements were determined and prioritized in a matrix. This matrix gives a priority ranking of customer requirements, by comparing the requirements against each other[11]. The prioritization matrix for the twin-lift system is shown in Figure 4. The customer requirements were divided into separate categories including controls, performance, load, stability, and time.

The controls category includes aircraft coordination and safety as requirements. Aircraft coordination deals with the fact that there are two aircraft sharing one load. Where normally aircraft are carrying loads separately, in this effort two aircraft are physically connected to the payload. This implies that aircraft coordination is necessary in order to keep one aircraft in the correct position in reference to the

other aircraft. This also implies that safety should be another requirement, as the two aircraft are in close proximity to one another, posing a potentially dangerous situation should something go awry.

			10	Much More Important
			5	More Important
			1	Same Importance
			0.2	Less Important
			0.1	Much Less Important

		Controls		Performance		Load		Stability		Time	Weights	
		Aircraft Coordination	Safety	Range	Hover Capability	Load Sharing	Load Handling	Multi-Aircraft	Take-off/Landing Techniques	Total Mission Time	Weight	Importance (%)
Controls	Aircraft Coordination		1	5	10	5	5	10	10	10	56	32.56
Controls	Safety	1		10	10	5	5	10	5	10	56	32.56
Performance	Range	0.2	0.1		1	0.2	0.2	1	1	1	4.7	2.73
Performance	Hover Capability	0.1	0.1	1		0.2	0.2	1	1	1	4.6	2.67
Load	Load Sharing	0.2	0.2	5	5		1	1	1	5	18.4	10.70
Load	Load Handling	0.2	0.2	5	5	1		1	1	1	14.4	8.37
Stability	Multi-Aircraft	0.1	0.1	1	1	1	1		1	1	6.2	3.60
Stability	Take-off/Landing Techniques	0.1	0.2	1	1	1	1	1		1	6.3	3.66
Time	Total Mission Time	0.1	0.1	1	1	0.2	1	1	1		5.4	3.14

Figure 4: Twin-Lift System Prioritization Matrix

The performance category includes the range and hover capability requirements that are specified in the request for proposal. The range will be 200nm and 10 minutes of hover capability are needed in order to perform the mission.

Load sharing and load handling comprise the loads category of requirements. Load sharing is referring to the fact that two aircraft are connected to one load. Ideally, the load sharing should be equal between aircraft, with each aircraft is responsible for 50% of the total load. Load handling refers to the method in which the load will be connected to the aircraft, as well as any attachment or release mechanisms required.

The stability category includes multi-aircraft, and take-off and landing techniques. The multi-aircraft aspect of the mission is defined in the RFP, with two aircraft being the requirement. Stability concerns between the aircraft, and between the aircraft and the payload will comprise a significant portion of the design effort. Take-off and landing techniques will be investigated to guarantee the best stability.

The last category is reserved for total mission time. Although it is not a specific requirement in the RFP to complete the mission within a certain time frame, it was decided that the mission would need to be completed within a reasonable amount of time in order to be a practical use of the aircraft and equipment.

The importance column in the prioritization matrix represents the percentage importance for the requirements, with all requirements totaling to 100%. A Pareto Chart, shown in Figure 5, shows the

ranking of the requirements from highest to lowest. It is easy to see that the first three requirements, aircraft coordination, safety, and load sharing, will drive the decision making for the entire system, as they represent 80% of the total requirement weight. This makes sense, as safety is always an important factor to consider with aircraft operations.
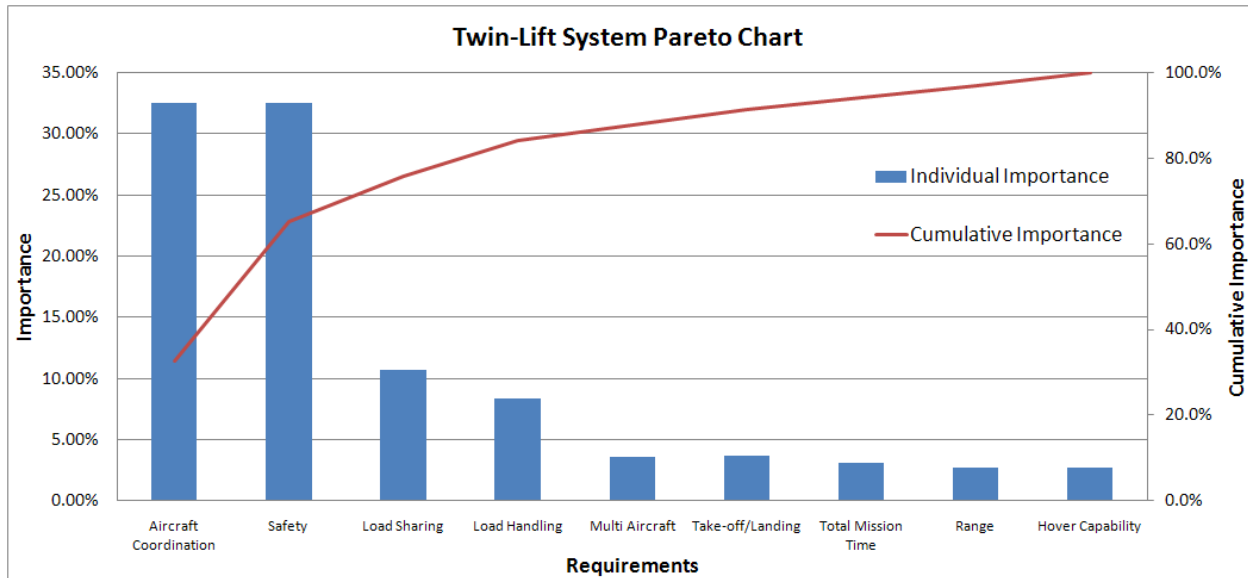
Figure 5: Twin-Lift System Pareto Chart

A quality function deployment, or QFD, was used to express the customer requirements in terms of system attributes. Target values are established for each system attribute, and the attributes are assigned a relative importance. This relative importance is based upon the prioritization of the customer requirements as well as the relationship between the requirements and the attributes. Once a difficulty is assigned to the task of attaining each target value, a relative risk can also be assigned to the attributes. [3]

Figure 6 shows the twin-lift system QFD. Each attribute has a corresponding target value, difficulty level, importance, and risk associated with it. The difficulty level is represented by a non-linear scale of 1, 3, or 10, with 1 being the easiest, and 10 posing great difficulty. The greater the difficulty and the importance, the greater the risk associated with achieving that particular target value.

Load Handling

Attributes under the load handling category include load release, aircraft separation, equal load distribution, load oscillation, and load drag.

The load release attribute has a target value of 97%. This corresponds to the load release mechanism having the minimum success rate of 97%. This is especially important under emergency circumstances, where the load may need to be released automatically by the control system if the balance between the aircraft is disturbed significantly.

Aircraft separation is the next load handling attribute. In order to maintain safety, it is ideal for the two aircraft to maintain a distance equal to 1.5 times the rotor diameter. This will be accomplished through the controls system.

Equal load distribution will also need to be maintained throughout the mission. This means that each aircraft is responsible for 50% of the total payload weight. Due to the magnitude of the payload, if one aircraft loses the capability of carrying its corresponding 50%, the entire load must be jettisoned. For this reason, it is especially important to maintain an equal load distribution between the aircraft.

The next load handling attribute is load oscillation. Oscillation is the periodic movement of the payload beneath the aircraft. Although some oscillation during flight is normal, it is important to minimize this parameter as much as possible. This will be accomplished through the control system and the design of the load handling system.

Load drag comprises the last load handling attribute. The drag for a standard ISO container is estimated to be nearly 100 ft^2, as it is not aerodynamic in shape. Although this drag is very large, adding shapes to the front and back of the container to make it more aerodynamic would not justify the production cost due to the fact that this mission is designed to be used only on occasion. Minimizing the drag can be accomplished by flying with smallest face of the container in the direction of flight.

Controls
The controls aspect was divided into two attributes, response time and control accuracy. Response time corresponds to the amount of time that it takes for the control system to have the desired output, after being given the appropriate input. Control accuracy is the deviation between the desired output and the actual output. Both of these parameters were assigned a difficulty level of 10, being the most difficult and time consuming aspect of this system design task. The control attributes also have the highest risk of all the categories.

Aircraft
The aircraft related attributes are divided into range, hover time, fuel consumption, total load capacity, and flight speed attributes. The range and hover time were specified in the RFP. It is ideal, then, to achieve the range and maximize the hover time. Fuel consumption is a significant attribute to consider for this mission, as it dictates the range, hover capability, speed, and payload of the aircraft. Although it is ideal to minimize fuel consumption, since this effort involves using off-the-shelf aircraft, it is a set value for each aircraft. Total load capacity represents the amount of payload that the aircraft are capable of carrying. This effort will include maximizing the total load capacity of the aircraft. Flight speed influences the amount of time that it takes to perform the mission. A balance must be achieved, between having a practical flight speed that is optimum for aircraft fuel burn, and accomplishing the mission in a reasonable amount of time.

Cost
The cost category includes three parameters, production costs, operations costs, and RDT&E cost. Production cost is the cost associated with fabricating the system components[3]. Due to the fact that this

system will not be mass-produced, reducing the production cost will pose some difficulty. Operation costs are recurring costs associated with using the aircraft and include fuel, maintenance, and aircrews[3]. Research, development, testing, and evaluation (RDT&E) costs are associated with the cost to develop the system so that it is ready for production[3].

Overall, the highest risk attributes are in achieving the controls attributes. This means that the majority of the effort involved in this twin-lift system will be in developing a working controls scheme.

Quality Function Deployment System of System View		Customer Importance	Load Release	Aircraft Separation	Equal Load Distribution	Load Oscillation	Load Drag	Control Response Time	Control Accuracy	Range	Hover Time	Fuel Consumption	Total Load Capacity	Flight Speed	Production Cost	Operating Cost	RDT&E Cost
Direction of Improvement			↑	○	○	↓	↓	↓	↑	○	↑	↓	↑	↑	↓	↓	↓
Controls	Aircraft Coordination	33.0%	○	◉	◉	◉		◉	◉					◉	◉		◉
Controls	Safety	33.0%	◉	◉	◉	◉		◉	◉					◉	◉		◉
Performance	Range	2.7%					◉			◉	◉	◉				◉	
Performance	Hover Capability	2.7%		○						◉	◉	◉	◉			○	
Loads	Load Sharing	10.7%	◉	◉	◉	○		△						◉			◉
Loads	Load Handling	8.4%	◉	○	○	○	○							◉	◉		◉
Stability	Multi-Aircraft	3.6%	◉	◉	◉	◉		◉	◉	○	○		◉				◉
Stability	Take-off/Landing Techniques	3.7%	◉	◉				◉	◉	△	△				◉		◉
Time	Total Mission Time	3.1%						◉	◉				◉				
How Much			97%	2*D	50%	<10% Perterbation	100 ft^2	0.1 sec	+/- 5%	200nm	10 Min	SFC < 1	175%	> 100 kts	<$500,000	<$15,000	<$100,000
Organizational Difficulty			1	1	1	3	1	10	10	1	1	1	3	3	3	1	3
Weighted Importance			6.3	7.9	7.5	6.8	0.5	6.7	6.6	0.9	0.9	0.5	1.5	7.0	7.0	0.3	8.3
Absolute Risk			6	8	7	21	0	67	66	1	1	0	5	21	21	0	25

File: Top Level QFD V2.BIP
Date: 11/30/2009 15:50

Weight
- ◉ Strong Symbol 9
- △ Weak Symbol 1
- ○ Medium Symbol 3
- ↑ Larger The Better 0
- ↓ Smaller The Better 0
- ○ Norminal The Best 0
- ✳ Negative -1
- ✕ Strong Negative -3
- ◉ Strong Positive 9
- ○ Positive 3

Figure 6: System Quality Function Deployment

Overall Evaluation Criteria

The QFD is used to establish the Overall Evaluation Criterion, or OEC, as a quantitative method of assessing a proposed solution's suitability to perform the mission specified. The system was broken down in Table 1.

Table 1: Overall Evaluation Criteria

Overall Evaluation Criteria	Engineering Requirements from QFD	Weighted Importance		Relative Importance
Mission Capability Index/Aircraft				
	Total Load Capacity	1.6		53.3
	Range	0.5		16.7
	Hover Time	0.5		16.7
	Fuel Consumption	0.4		13.3
	MCI Total		3.0	6.7
Controls Index				
	Control Response Time	6.3		50.4
	Control Accuracy	6.2		49.6
	SI Total		12.5	27.7
Load Handling				
	Load Release	6.7		22.6
	Aircraft Seperation	7.9		26.7
	Equal Load Distribution	7.6		25.7
	Load Oscillation	6.8		23.0
	Load Drag	0.6		2.0
	LHI Total		29.6	65.6
Cost Index				
	Production Cost	7.2		61.5
	Operating Cost	0.3		2.6
	RDT&E Cost	4.2		35.9
	CI Total		11.7	
OEC = 0.067(MCI) + 0.277(SI) + 0.656(LHI)/Cost_Index				

As shown in the table, the system was decomposed into four categories, a mission capability index (MCI), a controllability index (CI), a load handling index (LHI), and a cost index. The overall evaluation of the system is as follows:

$$OEC = \frac{0.067(MCI) + 0.277(CI) + 0.656(LHI)}{Cost}$$

$$MCI = 53.3\left(\frac{TLC}{1.75LC}\right) + 16.7\left(\frac{MPH}{10\ min}\right) + 16.7\left(\frac{Range}{200\ nm}\right) + 13.3\left(\frac{1\ ^{lb}/_{hp}}{2SFC}\right)$$

$$CI = 50.4\left(\frac{RT}{0.1\ sec}\right) + 49.6\left(\frac{CA}{100\%}\right)$$

$$LHI = 22.6\left(\frac{LR}{100\%}\right) + 26.7\left(\frac{AS}{2D}\right) + 25.7\left(\frac{LS}{50\%}\right) + 23.0\left(\frac{Osc}{90\%}\right) + 2.0\left(\frac{LD}{100\ ft^2}\right)$$

$$Cost = 61.5\left(\frac{\$500,000}{PC}\right) + 2.6\left(\frac{\$15,000}{OC}\right) + 35.9\left(\frac{\$1,000,000}{RDTE}\right)$$

Preliminary Sizing and Performance

Sizing and performance analysis was needed, in order to determine which aircraft is most appropriate for the twin-lift mission. In addition, it was necessary to find the maximum amount of payload that the aircraft could carry. Part of the mission requirements included selecting an aircraft that is currently in-service and has the capability of lifting 5000lb. Many aircraft fit this requirement, however, focus was placed on cargo rotorcraft, as they specialize in heavy lift situations. Utilizing cargo rotorcraft in a twin-lift configuration was deemed most beneficial, as the need to build a new heavy-lift rotorcraft would then be eliminated.

Vehicle Sizing Methods

Several vehicle sizing methods were used to perform the preliminary sizing and performance analysis, including the Fuel Ratio (R_F), Georgia Tech Preliminary Design Program, CIRADS, and FalconView.

Fuel Ratio

The R_F fuel balance method provides a way to determine minimum gross weight that meets a balance of required and allowable fuel. This fuel fractional method is founded on solving equations containing performance information simultaneously, to determine gross weight. It is assumed that a minimum gross weight solution is preferable. Figure 7 shows the flow of information required to complete a sensitivity analysis using the R_F method. Parameters used in R_F calculations include weight ratios, disk loading, hover requirements, range requirements, efficiencies, and correction factors.
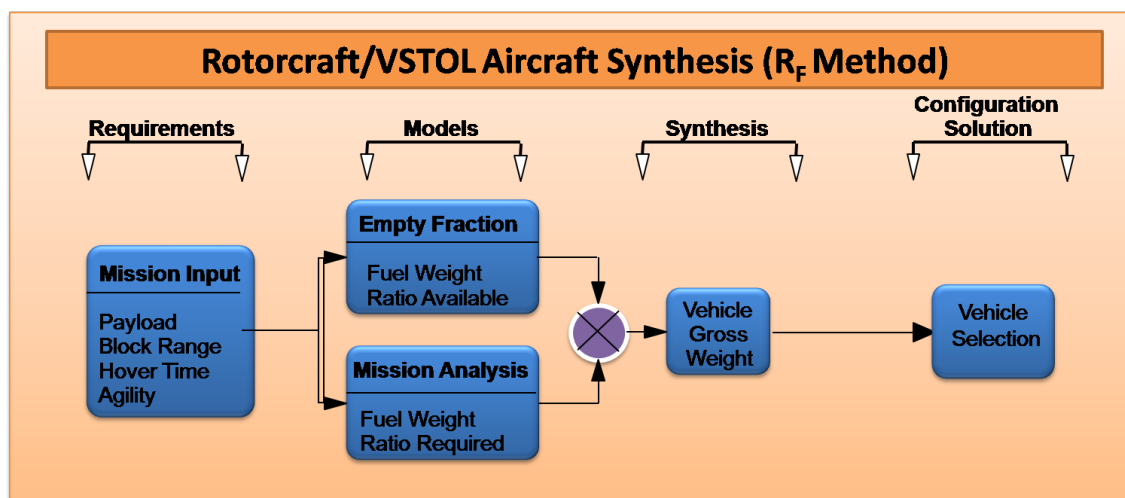
Figure 7: Fuel Ratio Method

For this R_F sizing analysis, the mission was divided into 11 segments, as discussed in the mission analysis section. The fuel required at each stage was determined, and at the end of the mission, the total fuel weight was found. An iterative process was used to maximize the amount of payload that the aircraft can carry, while balancing the fuel required and fuel available over the length of the mission. This method was used to compare the maximum payload capability of three cargo rotorcraft, the CH-47F, CH-53E, and CV-22. Figure 8 shows the results of the analysis. It is clear that the CH-47 aircraft has the greatest payload capability of the three, and was recommended for use in the twin-lift system design.
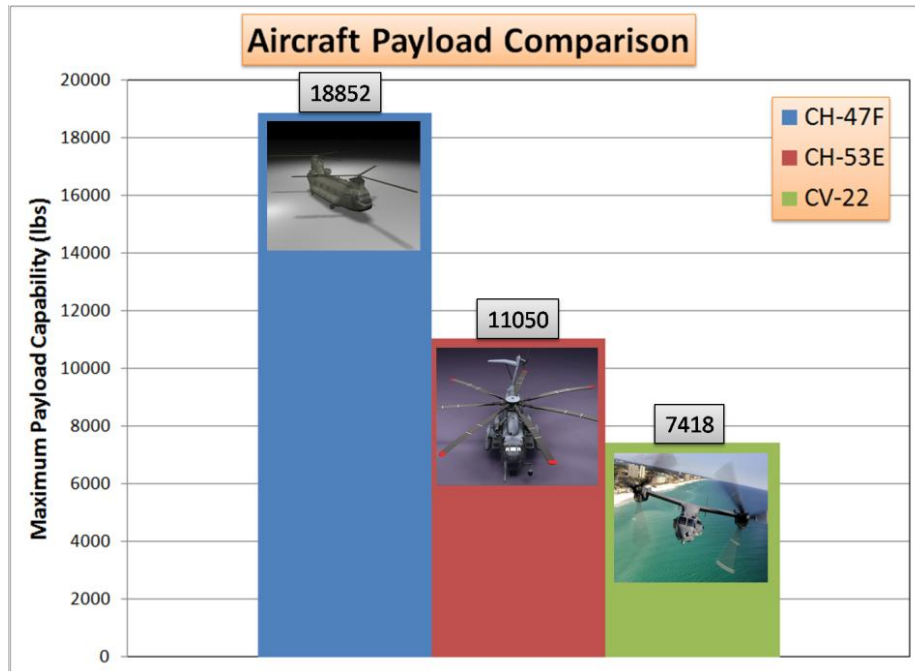
Figure 8: Aircraft Payload Comparison

Once the CH-47F was selected as the desired aircraft, two additional studies were performed. The first, shown in Figure 9, is a study to determine the maximum payload as a function of airspeed. This airspeed corresponds to the speed at which the aircraft fly with the payload. The return airspeed was kept constant at 130kts, the speed corresponding to maximum endurance for the CH-47F. Both hot day and standard sea level conditions are shown, allowing for a 'worst case scenario' in terms of flight conditions to be used in this study. From the figure it can be seen that as the aircraft speed increases, the payload capability also increases, due to flying closer to the max endurance speed. A safety limitation has been placed for speeds greater than 100kts, due to operating restrictions for the aircraft. For this mission, the best scenario is to fly with the load at 100kts, to maximize payload capability. Note that this 100kt speed was used to define the mission in the mission analysis section of this report.
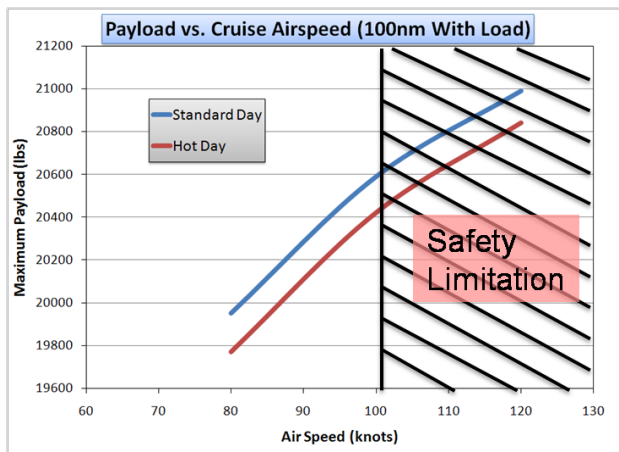
Figure 9: Payload Optimization via Airspeed
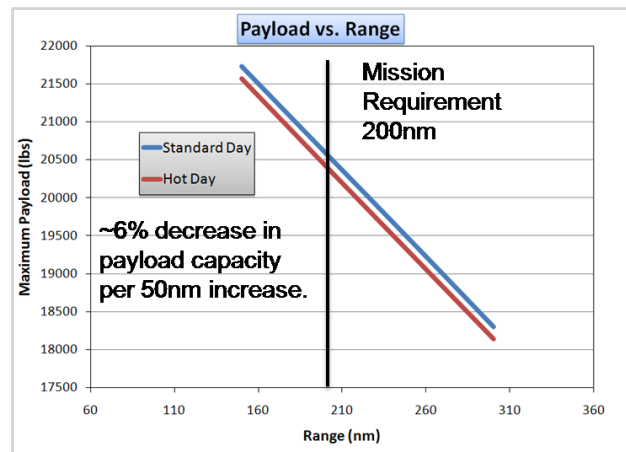
Figure 10: Payload Optimized via Range

13

The second study is shown in Figure 10. This study involved keeping the aircraft airspeed constant and varying the range, allowing for maximum payload to be determined. As expected, when the mission range increases, the payload capability of the aircraft decreases. In fact, for each 50nm increase, the payload capability falls by nearly 6%. This decrease becomes significant as the range increases past 200nm. This study suggests the twin-lift system can also be utilized for short-range, heavy-lift missions.

The mission requirement of 200nm is plotted to show that the maximum payload for this mission will be near 20,500 lbs. Once crew weight is subtracted, the maximum payload becomes 19,900 lbs for each aircraft. This gives a total payload capability of 39,800 lbs for both aircraft. Notice that this is nearly a 100% increase from an individual aircraft's load carrying capability. Note that the RFP requests a 75% increase. Although these numbers suggest that this increase can approach 100%, further analysis that includes drag affects, as well as the weight of the load handling system, will reduce this number.

Georgia Tech Preliminary Design Program (GTPDP)

GTPDP is a preliminary in-house helicopter design code. It is made to be a simple, quick method to obtain a rough configuration for a user's specifications. It has capabilities of minimizing maximum gross weight, mission fuel weight, noise and cost as well as maximizing endurance, dash speed and hover ceiling. Also, by the specified configurations it can estimate the performance of the vehicle. Originally, GTPDP was developed to analyze a conventional helicopter, but a capability of handling a tandem rotor configuration was added to the source code in 2005. A preliminary estimation of the system performance is an output of the GTPDP tool.

GTPDP was used for estimating the performance of CH-47F, the vehicle chosen by the fuel ratio analysis. By selecting an in-service aircraft, focus could be placed in designing the additional lift capability for the aircraft. Before considering the performance of the multi-lift configuration, a single and clean lift mission performance of CH-47F needed to be investigated, in order to validate the model in GTPDP as well as to compare it to multi-lift mission performance.
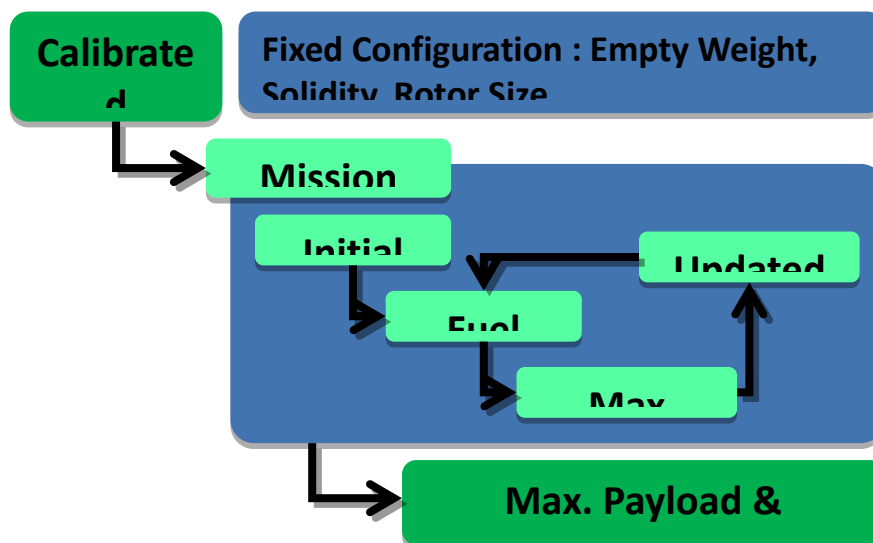
Figure 11: Aircraft Sizing Analysis

Figure 11 shows the process of mission analysis with respect to the fixed helicopter configuration. Based on the configurations, significant parameters such as empty weight, solidity, and rotor size can be determined. By using those parameters, power required & available also can be obtained as shown in Figure 12.
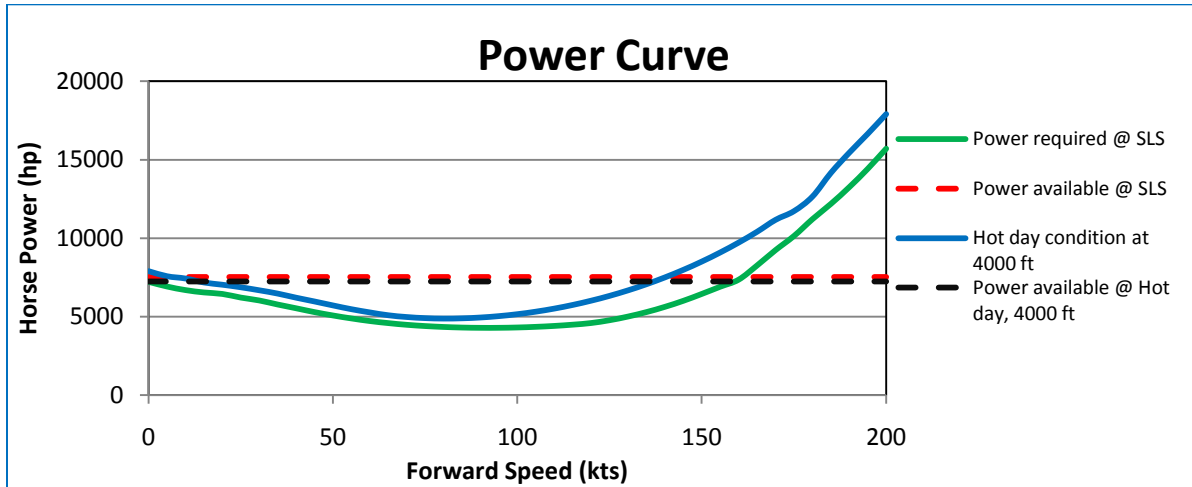
Power Curve

Figure 12: Power Curve at 54,000 lb Gross Weight

Based on the baseline mission profile as well as the calculated model characteristics, the relationship between the mission range and the maximum payload was investigated. The red dotted line in Figure 13 represents the maximum payload that the helicopter can carry and was constrained by the structural limitation. A vehicle with 54,000 lb of maximum gross weight can carry approximately 20,000 lb of maximum payload up to 200 nm for the given mission. Once the mission fuel weight approaches the maximum fuel weight, the payload is compromised by fuel weight. Beyond a certain range, the consequences of having to carry additional fuel outweighs the practicality of the twin-lift mission.

Payload vs. Range
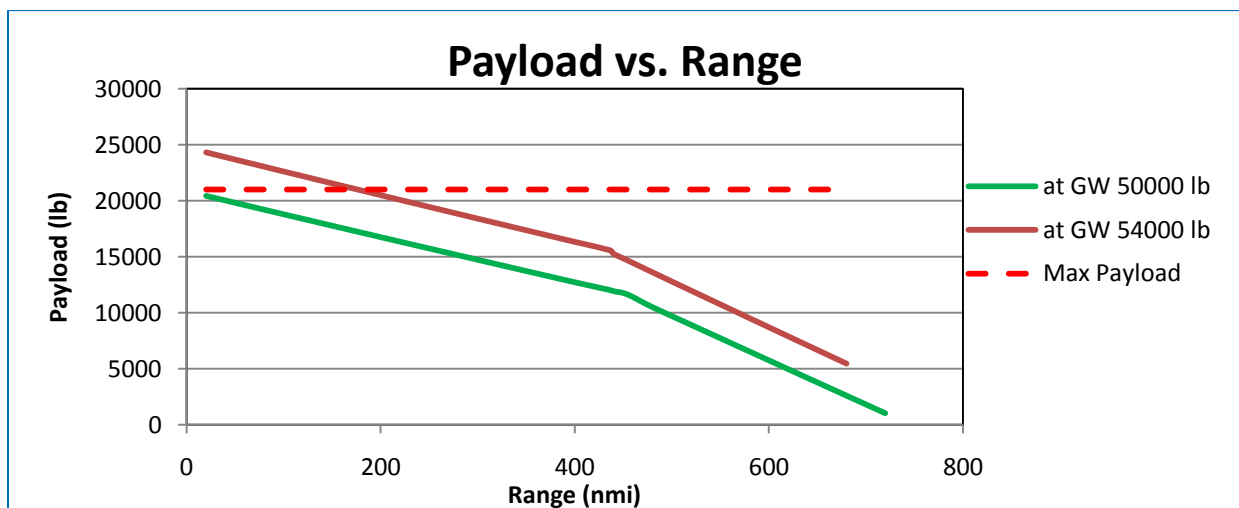
Figure 13: Payload-Range Diagram

Gross Weight	Payload		Remarks (@ 2000 ft)
	Baseline Mission	Mission at Best Range Cruise Speed	
54000 lb	20503 lb	20846.5 lb	141.5 / 143.5 (kts)
50000 lb	16756.2 lb	17131.4 lb	148.0 / 143.5 (kts)
45000 lb	12048.4 lb	12406.2 lb	155.0 / 148.5 (kts)
40000 lb	7313.4 lb	7601.4 lb	153.0 / 148.5 (kts)
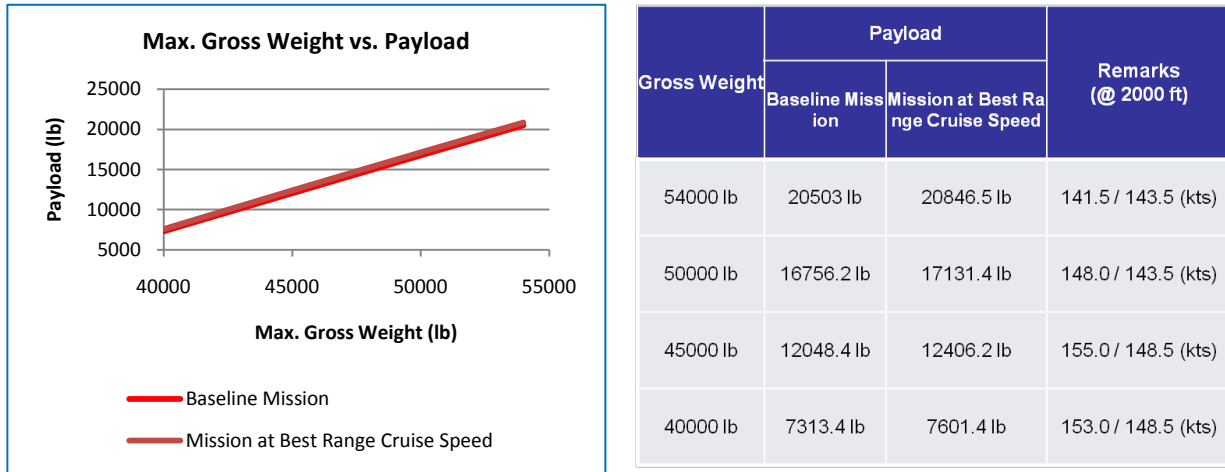
Figure 14: Max Payload Comparison at Different Flight Conditions

Figure 14 represents the cruise altitude and the forward flight speed slightly adjusted for maximum payload performance. Note that these preliminary results do not take account of any oscillations of the external load or interactions between vehicles. Therefore, the analysis should be conducted with other analyses simultaneously to determine a more precise payload capability.

CIRADS

CIRADS is a conceptual design tool with a facile user interface used to quickly assess and size rotorcraft configurations of multiple types: single main rotor, coaxial, tilt rotor, tail sitter and tandem. Based on the requirements of the project, CIRADS was utilized to model the CH-47F at different gross weights, as shown in Figure 15 and Figure 16.
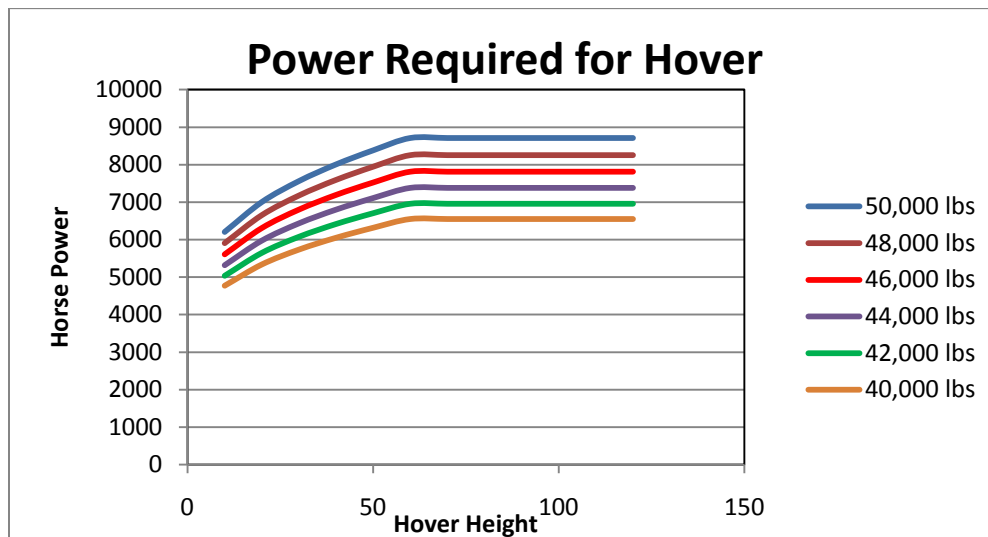
Figure 15: CIRADS Assessment of CH-47D Hover Power at Different Gross Weights
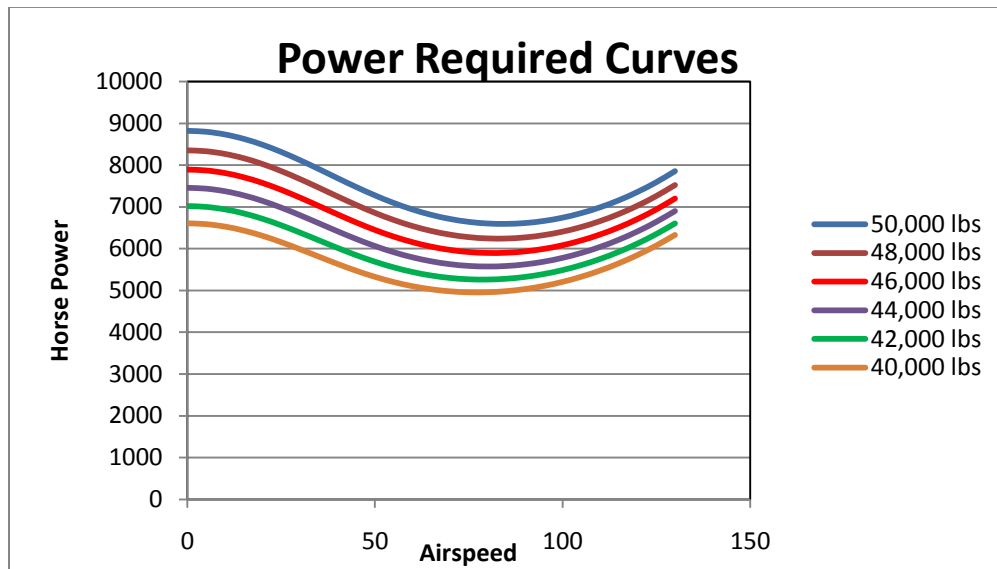
Figure 16: CIRADS Assessment of Power Required at Multiple Gross Weights

In the end, the numbers from CIRADS never matched the known values for the CH-47F, especially at a hover. Because the requirements for this project were to use an off-the-shelf helicopter, there are known values for power consumption. Since these values were not matched, a different method of sizing the mission was required. To do this, the US Army's flight planning software FalconView was used.

FalconView™

FalconView is a PC based mapping application developed by the Georgia Tech Research Institute for the Department of Defense. FalconView is an integral part of the Portable Flight Planning Software (PFPS)[13]. PFPS is an integrated suite of planning tools used by the Army for flight planning. Since the CH-47F is an aircraft currently in service with the US Army, it seemed natural to use the same program in use by the Army for CH-47F mission planning. One of the tools integrated into PFPS that was the most helpful was the automated performance planning, which constantly evaluated and updated the fuel burn rate for the aircraft throughout all modes of flight.

In order to properly utilize the tool, the exact mission specifications had to be properly defined, using standard times for the mission as well as Army regulations for remaining fuel. Note that the mission breakdown is shown in Figure 2.

Using this mission profile, PFPS was used to determine the maximum payload that could be carried. In addition, the program was used to calculate another interesting mission profile; the round-trip distance that could be travelled with the aircraft at maximum gross weight. For this mission, the aircraft's design gross weight was set to 33,000 lbs and its maximum gross weight was set to 50,000 lbs. Table 2 shows the results for these two mission profiles. Note that the maximum gross weight of 39,000lbs estimated by the fuel ratio method is similar to that estimated by FalconView.

	Meets Requirements	Max Weight
Load Weight	31,000 lbs	34,000 lbs
Mission Distance	100 NM	78 NM

Summary

The CH-47F was selected to be the most advantageous for the twin-lift mission. The CH-47F is the most prominent tandem rotorcraft in-service. It represents the best selection for the baseline vehicle to perform the multi lift mission. For the remaining analysis, the CH-47F was used as the baseline aircraft.

The Boeing CH-47 Chinook is a versatile, twin-engine, tandem rotor heavy-lift helicopter. Its top speed of 170 knots is faster than utility and attack helicopters of the 1960s and many of today. Its primary roles include troop movement, artillery emplacement and battlefield resupply. It has a wide loading ramp at the rear of the fuselage and three external-cargo hooks. The Chinook was designed and initially produced by Boeing Vertol in the early 1960s. The helicopter is now produced by Boeing Integrated Defense Systems. With its triple-hook cargo system, the CH-47D can carry heavy payloads internally and up to 26,000 pounds - for example, bulldozers and 40-foot (12 m) containers - externally, at speeds over 155 mph (250 km/h). In air assault operations, it often serves as the principal mover of the 155 mm M198 howitzer, 30 rounds of ammunition, and an 11-man crew. Like most US Army helicopters, the Chinook has advanced avionics, flight controls and electronics, making it an ideal choice for a twin-lift mission.

Multi-Lift System

For the purposes of the competition, the subjects necessary to be analyzed in detail are the load lifting device, the control scheme, and the aircraft stability. Additionally, a focus of this section is on the performance of the multi-lift system in order to show that the selected design can meet the mission requirements for range and useful load.

Load Handling System

The CH-47F aircraft is capable of lifting payloads in its interior and also as a sling load below the aircraft. The design of the multi-lift system will take advantage of the sling-load capability of the aircraft in order to lift the required payload.

Several options were considered for the load lifting device. The results of this analysis indicated that the optimum method of lifting the required load is through a spreader bar attached to the sling load device of each aircraft. The bar will then be attached to the required payload. The purpose of the bar will be to ensure that the weight is evenly distributed between the two aircraft and additionally to provide some level of safe separation between the two aircraft.

The focus of design on the spreader bar will be a minimization of drag and weight of the bar. However, it will also need to be strong enough such that it will not buckle under adverse inputs to the system such

as gust loads. Additionally, there is a requirement for the carrying of specified standard ISO containers as well as miscellaneous equipment. The dimensions of the containers in addition to the safe separation of the aircraft needed to be considered in determining the length of the spreader bar.

With the selected configuration the design of the multi lift system consists of two CH-47F aircraft with a spreader bar attached to their center hook and the payload suspended from the sling legs.

Load Handling System Trade Study

The main considerations for the spreader bar are weight and drag. Drag and weight in turn are specified by the necessary structural buckling requirements of the bar. The first step in determining the optimum bar configuration was to determine the loads that the bar is capable of withstanding. For a high-level conceptual sizing of the bar, an Euler buckling analysis was used. The critical buckling force F on a bar is given by the equation in Figure 17:

$$F = \frac{\pi^2 EI}{(KL)^2}$$
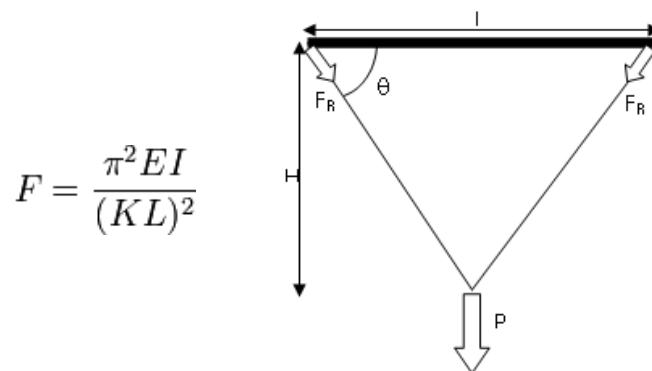
Figure 17: Load Handling Geometry

E is the material modulus, I is the area moment of inertia of the bar's cross section, L is the length, and K is a constant that was determined by boundary conditions. The critical force required was determined for the twin-lift geometry, shown in Figure 17. A load of force P hanging at distance H attached by two cables below a bar of length I will produce a reaction force F_R in each cable. The component of the reaction force which puts the bar in compression is $F_R \cos \theta$. For our twin-lift system, P was assumed to be 60,000 lbs, which is about 1.5 times the 43,000 lbs that corresponds to the maximum weight for a fully loaded ISO container. It assumes a 1g maneuver. For L=H=100 ft, the compressive force on the bar is 11,375 lbs.

The cross-section of the bar was designed as an annulus, shown in Figure 18, where r1 represents the inner radius and r2 represents the outer radius. The area moment of inertia for such a cross section is given by the equation, also in Figure 18.

$$I_0 = \frac{\pi}{4}\left(r_2{}^4 - r_1{}^4\right)$$
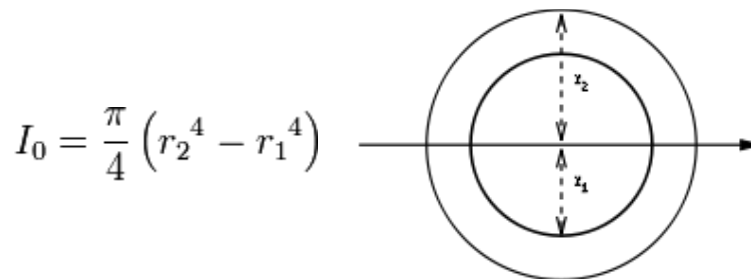
Figure 18: Spreader bar Cross Section

A sizing study was conducted by first solving for the smallest possible outer radius capable of carrying the necessary load, which would necessitate a solid cross-section (r_1=0). This geometry would yield the lowest drag but highest weight solution. The outer radius was then stepped-up, solving for the necessary inner radius to carry the load, in order to find the weight of the bar as a function of outer radius. The relationship is shown in Figure 19, assuming that the bar is made of aluminum. The plot clearly illustrates that the relationship between the weight and the annulus is non-linear, and therefore trades were necessary to find the optimal design.

Bar Weight vs Outer Radius
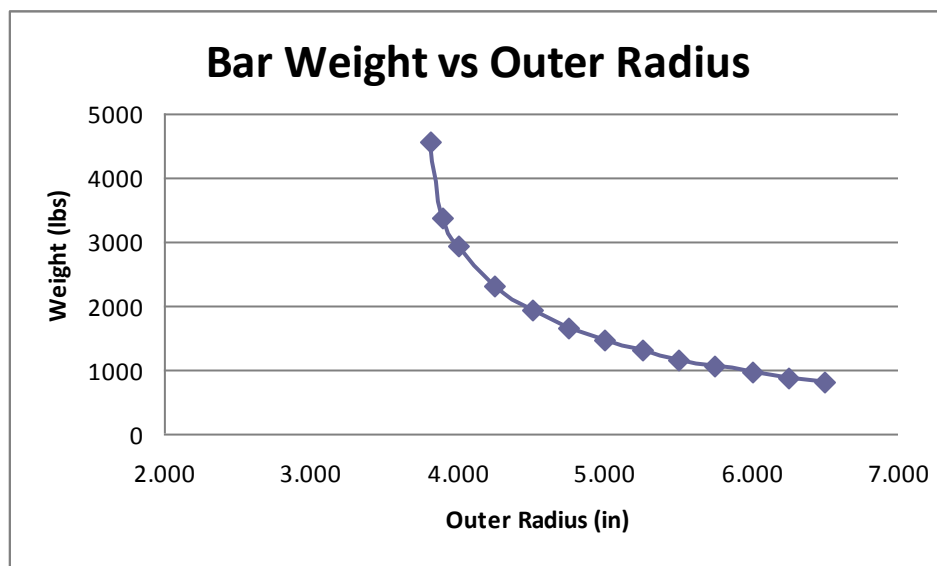
Figure 19: Spreader Bar Weight per Outer Radius

Because this is a stiffness driven design, lighter weight alloys or composite materials could be used to reduce weight compared to an aluminum bar. Composites give the advantage of being able to tailor the material properties to the design by altering the layup.

Euler buckling analysis showed that the weight of the bar can be minimized by increasing the radius; however, the drag of the bar sets a limit to how large the radius of the bar can be in practicality. The drag of a cylindrical bar is highly dependent on Reynold's number as seen in Figure 20. When flying at 100kts while carrying the slung load, this optimum Reynold's number can be approached by utilizing a spreader bar with a smaller radius, as seen in Figure 21.
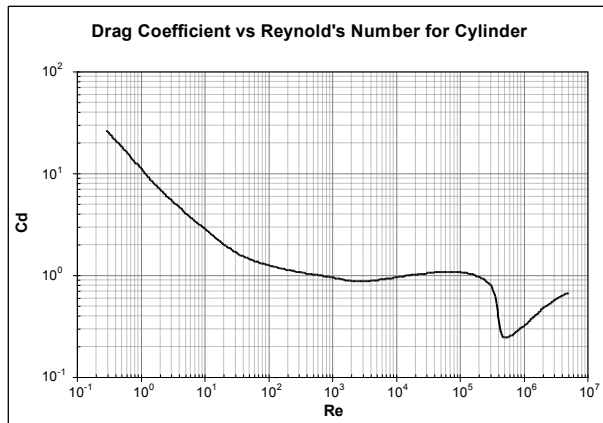
Figure 20: Cylinder Drag Coefficient
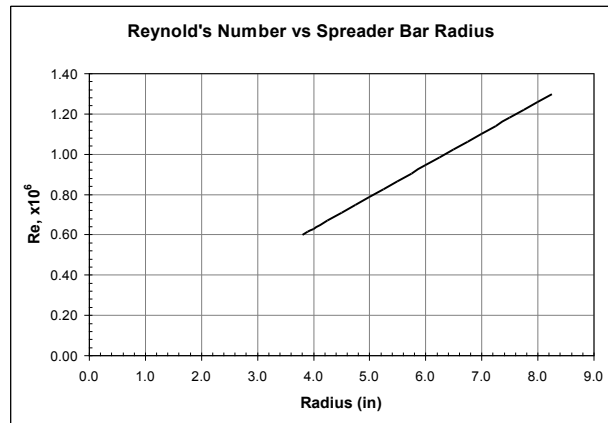
Figure 21: Spreader Bar Radius per Reynold's Number

Although the lower Reynold's number expected to be seen based on airspeed and bar radius helps to reduce drag, the drag coefficient, and consequently the drag force over the entire bar, sees a large variation in magnitude. Figure 22 and Figure 23 demonstrate the range of drag coefficient and ultimately drag force over the entire spreader bar as the radius of the bar increases.
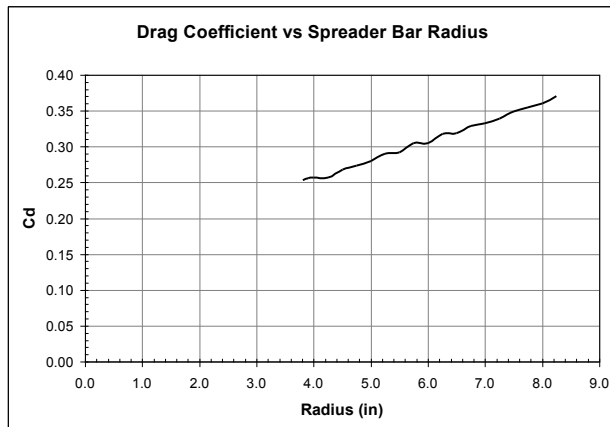
Figure 22: Spreader Bar Radius at Various Drag Coefficients
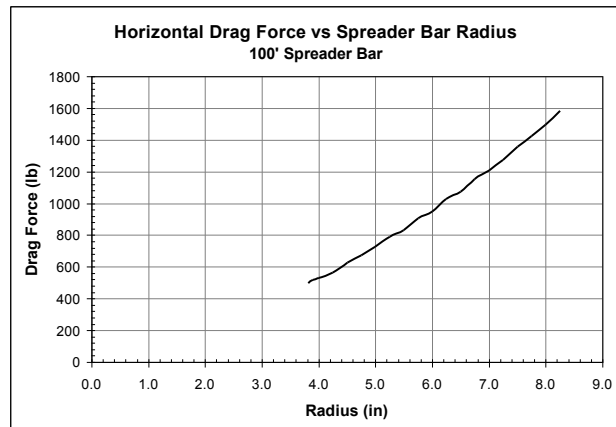
Figure 23: Influence of Drag Force on Spreader Bar radius

Earlier, it was seen from Euler buckling analysis that weight can be minimized by increasing the outer radius of the spreader bar. However, the drag of the bar can be minimized by decreasing the outer radius of the spreader bar. Simply put, weight and drag of the spreader bar are competing characteristics, as shown in Figure 24. From the typical power required curve for rotorcraft, it can be seen that less power is needed to keep the aircraft in the air (induced power) at moderate speeds, as compared to hover, due to additional airflow through the rotor from the aircraft's own forward speed. At the same time, the power required to pull the aircraft through the air (due to parasite drag) is increasing. At moderate airspeeds the impact of these two power requirements are becoming fairly equal in determining total power required. Thus, for the design, it is safe to assume that weight and drag are equally costly. Based on this assumption, the goal in sizing the spreader bar is to minimize both weight and drag equally.

Graphing both weight and drag against each other as well as their sum gives a graphical representation showing the design point where the weight and drag are minimized. Figure 24 shows the total weight and drag, along with the sum of these two values. It is seen that the sum of weight and drag of the spreader bar is minimized when the outer radius of the bar is around 6.5".
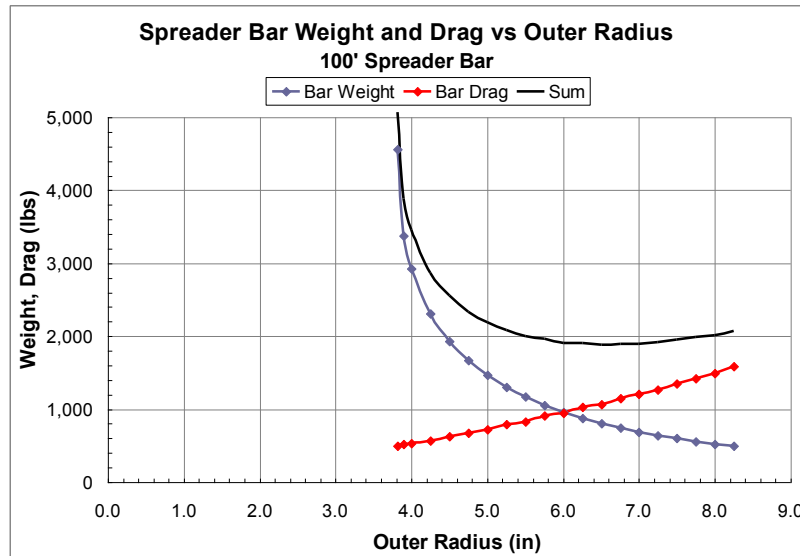
Figure 24: Influence of Weight and Drag on Spreader Bar Radius

Cost is also a significant aspect which must be considered in the design of the bar. While composite materials may be beneficial from a weight standpoint, they are more expensive in both material and processing costs when compared to aluminum. In order to choose the best design for the spreader bar, different materials were compared using the Euler buckling analysis as well as a Designer's Cost Trade-off tool to bring cost into the overall comparison. The Designer's Production Cost Trade-Off Tool from the Price H Model is a very powerful instrument in allowing us to quantify the total Manufacturing Cost by adding together both the Material Cost and the Tooling Cost for different materials. The tool uses a formula which take machining, precision and tooling into account in addition to the overall weight of the bar.

For each alternative material, the outer radius-inner radius combination was chosen from the weight-drag trade-off tool done in the Euler buckling analysis. The radii were chosen such that the weight and drag were a minimum while the wall thickness was set to a minimum of 0.25". Once this weight was determined, the cost trade-off tool was used to determine the production cost for a single bar. It must be noted that this trade-off tool models relative production cost based on general relationships between the principal manufacturing parameters and manufacturing effort; because the tool does not account for economic or business factors, it does not produce valid cost estimates.[21] Using this knowledge, a comparison of 4 different materials was done so they could be compared. The results are in Table 3.

Table 3: Comparison of Spreader Bar Production Costs

	Aluminum-Li	Aluminum	Al w/ foam	Composite
R_2, (in)	6.50	6.50	6.50	6.25
R_1, (in)	6.25	6.25	6.35	6.00
W, (lbs)	1106	1202	1487	693
a	0.853	0.85	0.85	0.854
b	438	287	287	527
c	20000	20000	20000	40000
Material Cost	$172,900.89	$119,069.55	$142,674.45	$140,538.98
Tooling Cost	$1,106,000.00	$1,202,000.00	$1,487,000.00	$1,386,000.00
Total Cost	$1,278,900.89	$1,321,069.55	$1,629,674.45	$1,526,538.98
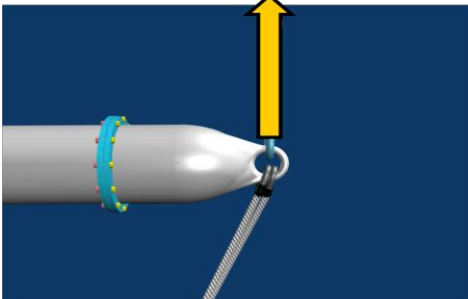
Using this analysis, the spreader bar should be made of an Aluminum-Lithium alloy with an outer radius of 6.5" and an inner radius of 6.25". It can also be seen from our analysis that the tooling costs involved with the production of the bar are very high, especially for such a small production number. Because of this, if there are options, the bar should be bought from a manufacturer rather than manufactured by the company in order to reduce setup costs and overall price.

End Cap Design
When designing the bar another main concern was the design of the end caps to allow clearance of the cables and prevent shearing of the eyelet. To fix the shearing complication, we calculated the sheer stress due to the tension force, and solved for the radius of the steel eyelet.

To calculate the shear stress we used the equations below. Where F is the tension in the cable above the eyelet, and r is the radius of the steel. From this it is seen that the minimum allowable radius would be .77" for the maximum shear stress. The team concluded that we will use a diameter of 2", with a factor of safety of 1.3. A cone shape was chosen for the end caps because the design allows for clearance of the cables, and superior strength to a standard eyebolt. Total length of each end cap is 2ft.

$$\mathbf{F} = 30{,}000 \text{ lbf}$$

$$\tau = \frac{F}{A} = \frac{F}{\pi(r^2)}$$

$$\tau_{max} = .577 \times \sigma_y$$

$$\sigma_y = 32 \text{ kpsi}$$

Figure 25: End Cap Eyelet Sizing

Modal Analysis

With the spreader bar sized, the stiffness characteristics of the bar are known. The bar properties can be used in a simplified finite element model (FEM) in MSC Nastran to determine natural frequencies of the twin-lift system. In this simplified finite element analysis, both aircraft and the slung load were assumed to have mass and no inertia. Also, the flexibility of the aircraft and the slung load were ignored. The FEM, which is depicted in Figure 26, consisted of the following:

- Two CH-47F aircraft at 33,000 lb each (1)
- 45,500 lb slung load (2)
- 100' aluminum cylindrical spreader bar with OD=13", ID=12.5" (3)
- 10' pendant from each aircraft to ends of spreader bar (4)
- 111.8' pendant from ends of spreader bar to sling (5)
- 10' sling to the load (6)

The aircraft and the slung load were modeled as lumped masses (CONM2), the spreader bar was modeled as an Euler beam (CBEAM), and the pendants and sling were modeled as tension/compression members (CONROD).
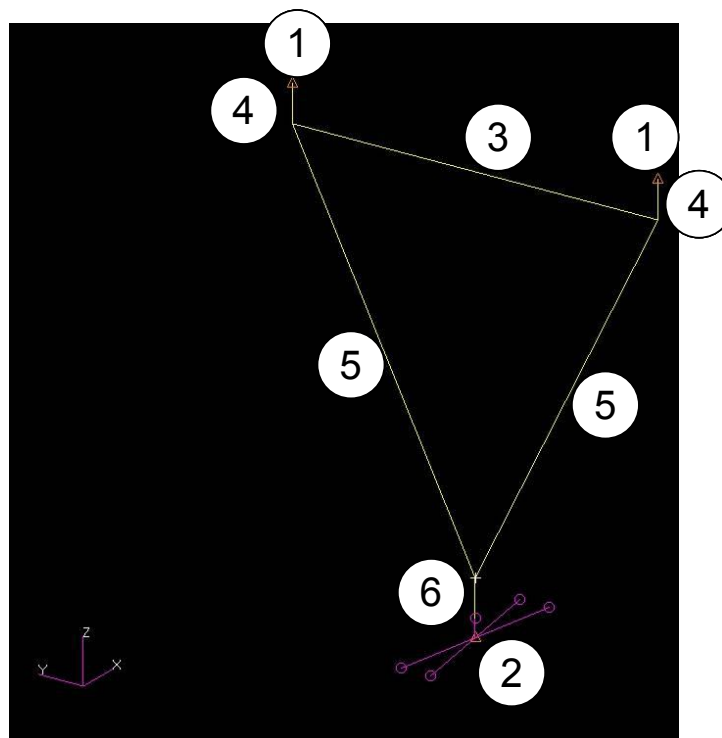
Figure 26: Twin-Lift System Modes

Modal analysis was performed to determine the natural frequencies of the aircraft – slung load system. Aside from the 6 rigid body modes, the simplified FEM of the system had three natural frequencies as shown in Figure 27, Figure 28, and Figure 29. The mode shapes of these three natural frequencies can be seen in the three figures.
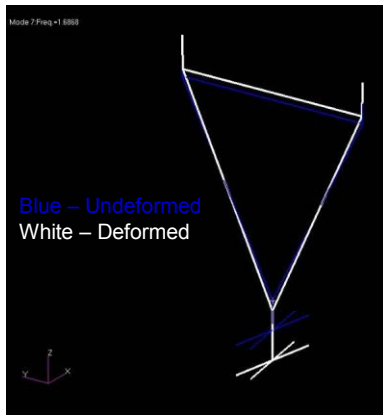
| Figure 27: Mode 1: 1.69 Hz | Figure 28: Mode 2: 17.10 Hz | Figure 29: Mode 3: 20.04 Hz |
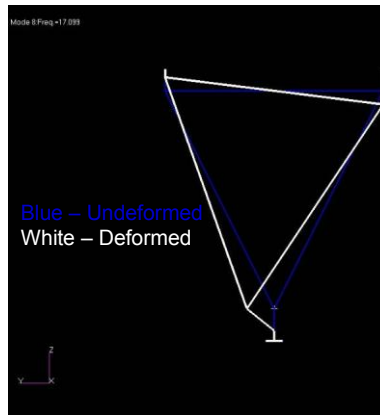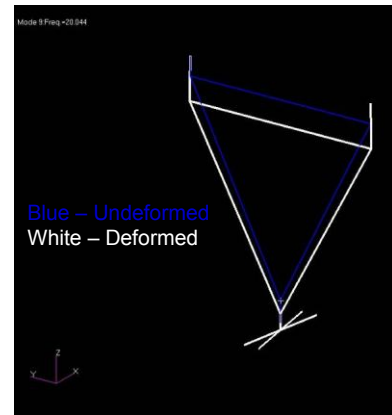
Often in slung load missions, the modes of the external load are below 1P and have the potential to cause stability issues. On the CH-47F, 1P is 3.75 Hz. The first slung here is at 1.69 Hz. Such low frequency modes are susceptible to pilot induced oscillations. These modes must be taken into consideration during control system design. Above 1P, it is usually common practice to ensure that fixed system modes are not near the blade passage frequency and its harmonics. Avoid bands at each harmonic +/- 10% are usually put in place. On the CH-47F, the three bladed rotors have a blade passage frequency at 3P, or 11.25 Hz. The first harmonic is at 6P, or 22.5 Hz. Here it is seen that the second mode, the spreader bar roll mode, is at 17.10Hz which is well separated from both 3P and 6P. The third mode, the spreader bar bounce mode, is at 20.04 Hz, which is just outside the 6P avoid band. Having this mode near 6P is considered low risk since energy at 6P is generally lower than the energy at 3P and many rotorcraft control systems filter out higher frequency signals (>10-15 Hz). However, its proximity to 6P should still be noted in terms of aircraft vibration and control system design.

Aircraft Trim Analysis

In order to begin construction of the control system for the vehicle, the trim states needed to be determined. Trimmed states are beneficial in that, while they don't necessarily give final control state, they give required geometry and effort of the system. This can be simply converted into control inputs. Although the steady state trim condition is something that will only briefly achieved in this system, oscillations about the steady state are quite common. The steady state trim control settings are used in the design overall design of the control system in state space.

It was decided that an analytical approach should be used in order to determine the trim states of the vehicle. Unfortunately the entire system itself proved difficult to solve all at once, so the system was solved as two separate parts. The first section solved was the lower two bodies, with the assumption that the steady state condition of the system will have the carrying hooks fixed relative to the spreader bar and the slung load. The next assumption made was that the cables holding the loads were not rigid bodies and were axially elastic.
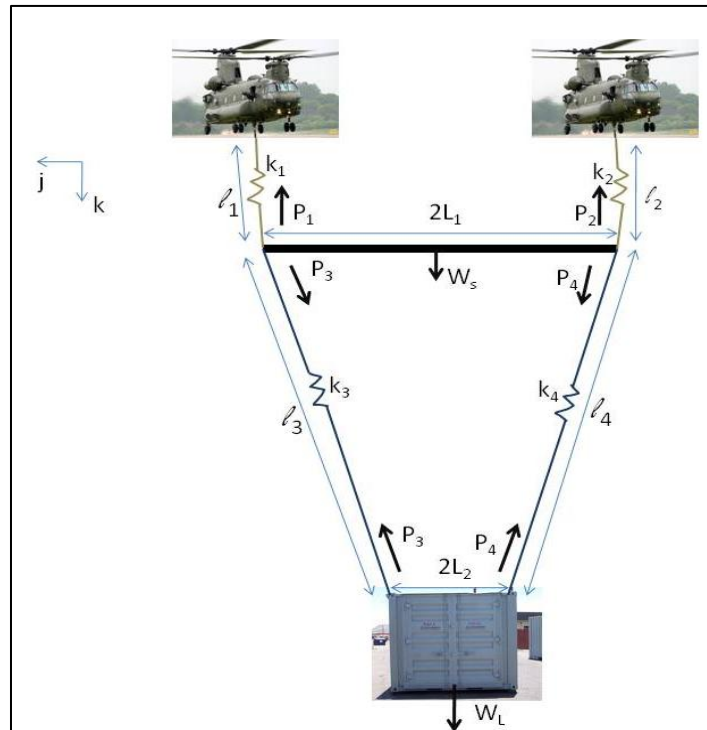
Figure 30: Twin-Lift System Dynamics

After the forces acting on the spreader bar, the hanging mass, and tension in each cable were determined, the forces acting on each helicopter were determined and summed for a given slung load setup, as seen in Figure 30. Once these calculations were made, it was apparent that the cable forces -- caused by the slung load in steady state forward flight-- acting on the helicopter were near identical. Because of this, the cable forces calculated from hover were used for all velocities. After this, through use of the Newton-Raphson method of iteration the trim conditions for multiple velocities were determined using multiple controller configuration, due to the symmetry of the CH-47. Additionally, in steady state forward flight, each vehicle would have the same steady state trim conditions, so the trim settings below are for both vehicles.

The first controller configuration used was only using body pitch attitude, and collective thrust control for the front and rear rotors. Using only these controls works because in neutral positions, both rotors of the CH-47 act only in the x-z plane, and only generate torque about the y axis. In Figure 31, the unloaded CH-47 has almost identical controller inputs to those derived in NASA TN D-8159. In Table 15 (Appendix 3) are the derived unloaded controls for the CH-47 at varying forward velocities. Figure 32 and Table 16 (Appendix 3) are the derived control inputs for the loaded system.
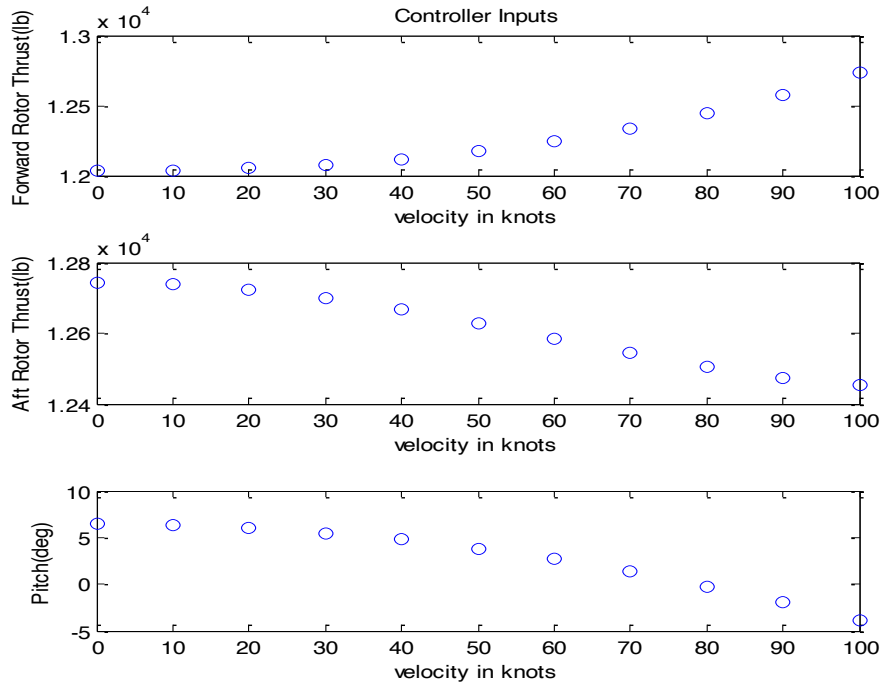
Figure 31: Unloaded Chinook input using only rotor Collective and body pitch attitude
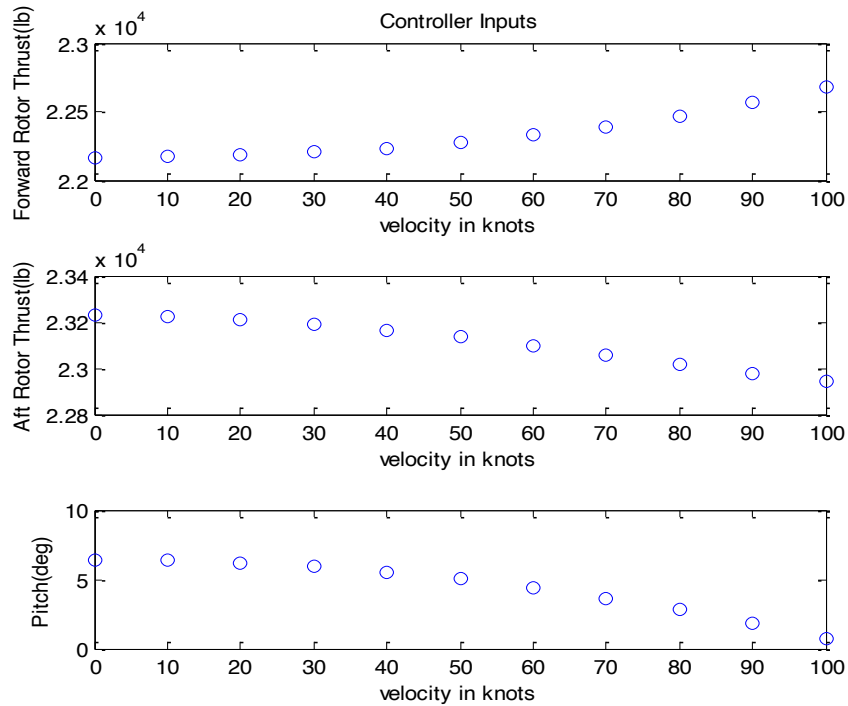
Figure 32: Loaded Chinook Controller Input using only rotor collective and pitch attitude

The next configuration utilized all parts controls of the CH-47, controlling the full swash plate of each rotor, the collective pitch and the body angles of body pitch and roll. Figure 33 displays data for the scenario without loading, and Figure 34 shows results from the scenario with loading. The full swash plate control is represented in the flapping angles B1s and B1c as well as the rotor thrust for both the front and rear rotor. Again, the vehicle is trimmed at no loading in order to compare the results of this method to a previously done method published in NASA TN D-8159.
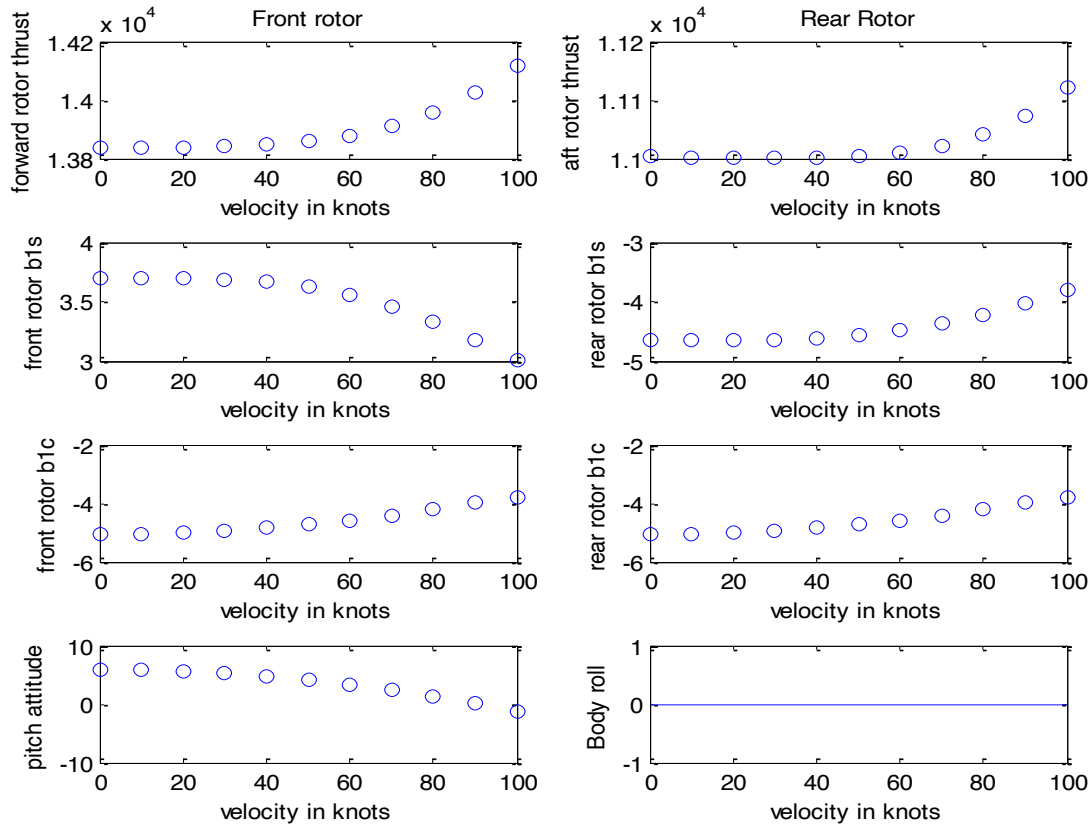
Figure 33: Controller Inputs Without Loading
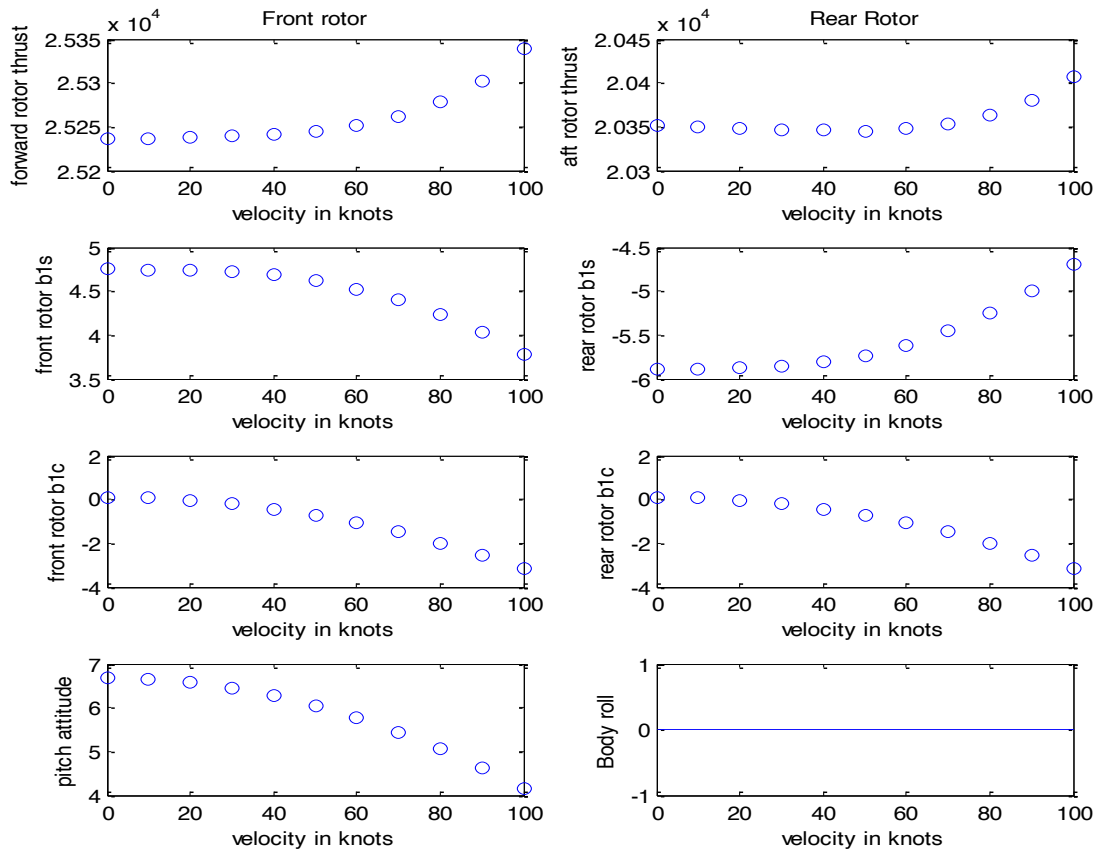
Figure 34: Controller Inputs With loading

Load Handling System Configuration

Blender 2.49b, an open-source 3D modeling program, was used to provide visualizations of the THOR system design. The overall system configuration is shown in Figure 35. Two CH-47F aircraft are separated by a 100ft spreader bar, which is connected to the load via four nylon ropes. The load handling system components are connected together in accordance with the Army Multiservice Helicopter Sling Load: Basic Operations and Equipment manual[22], as shown in Figure 36.

The spreader bar was designed in five interchangeable 20ft sections. The length of the section was chosen such that it does not exceed the maximum weight that can be lifted by two individuals. The sections are connected together via 2 flanges, 12 bolts, 12 nuts, and 24 washers. The section connection is shown in Figure 37. The flange was designed based on standard flange sizes, and extends 3in in diameter and has a 3/4in thickness. In order to provide an interchangeable connection for the spreader bar to the sling ropes and chains, it was necessary to design an end cap for each end of the spreader bar.

Figure 38 shows the end cap, which was designed to tolerate the high shear and compression forces experienced at the connection point. The design was derived from pulling heads, which are built for pulling large loads. As shown in the figure, the end caps connect to the spreader bar segments using the

same flange and bolt components. This enables the end caps to be interchangeable with any spreader bar segment. The total length of the end cap is 2ft.
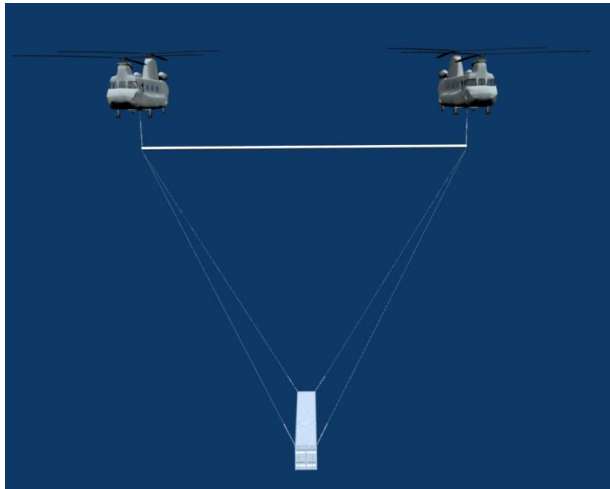
Figure 35: Twin-Lift System Configuration
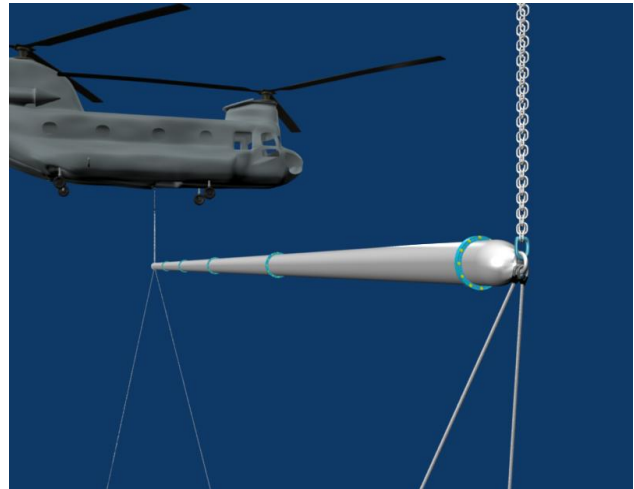
Figure 36: Spreader Bar Connections

Having the spreader bar separable into 20ft sections allows it to be loaded into either aircraft after the load has been delivered. The load handling system was designed such that the entire thing can be disassembled and loaded into a single aircraft. The aircraft can then deliver the equipment back to the original location, or to a new location.
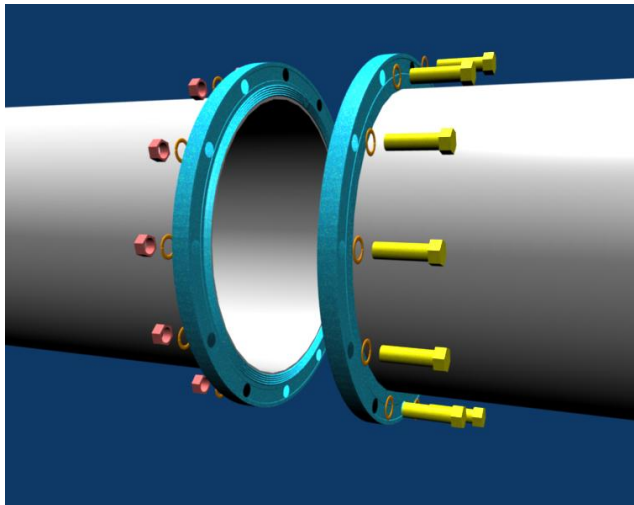
Figure 37: Spreader Bar Section Connection
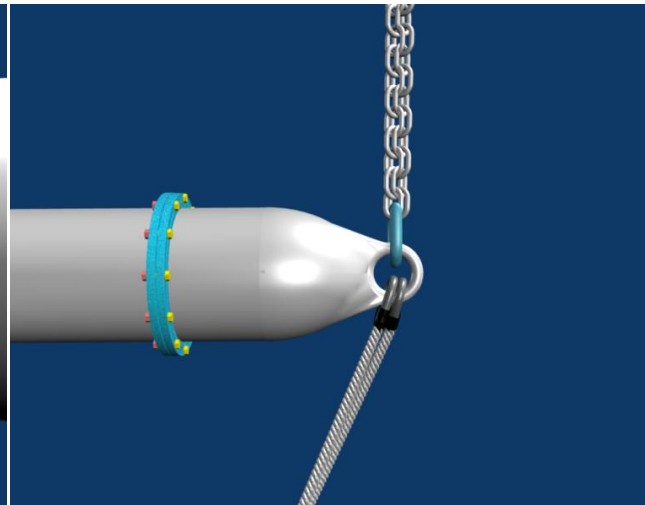
Figure 38: Spreader Bar End Caps

Figure 39 shows how the load, an ISO container in this case, connects to the sling legs. A nylon rope extends down from the spreader bar until it is 8 feet from the load itself. The rope is then joined to a chain via an eye and grab hook, as shown in Figure 40.
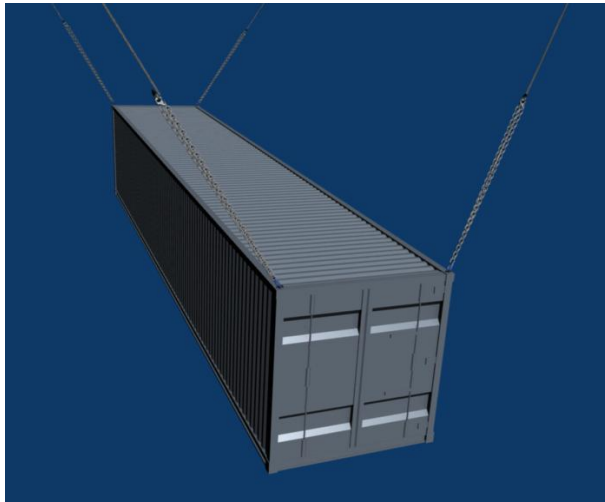
Figure 39: Load Connections

Figure 40: Rope, Eye, Grab hook, and Chain Assembly

Control System

The CH-47F is an in-service aircraft, and the majority of the controls present are mechanically based. In order to ensure safe operation of the multi-lift system it will be necessary to add an additional level of control related to control of the multi aircraft system. In order to support the payload on the spreader bar in the sling load configurations it will be necessary that both aircraft respond and behave in a similar way. If there is too much ability for the aircraft to move independently, it could result in a collision between the two aircraft. Additionally, a suitable control system will need to be in place to respond to gusts loads and other inputs to the multi-lift system.

Adaptive control is a technique by which the gains on the system input commands are adjusted based on changes to the aircraft configuration and flight environment. In industry, some effort has been made to utilize adaptive controls in order to allow aircraft to respond to failures of certain systems such as flight control surfaces. As a particular control surface is loss, the gains on the commands to the other flight control surfaces are adjusted to maintain stability and control. An example might be the loss of an aileron which is compensated for by increased gain on the redundant aileron or in the rudder and elevator.

For the purposes of the AHS project, the use of adaptive control will allow for the gains on the system to adjust based on the weight of the payload carried, as well as the atmospheric conditions present. As mentioned, the implementation of this system will be in a control scheme that essentially operates as an outer loop to the aircraft system. Figure 41 is a block diagram of the arrangement.
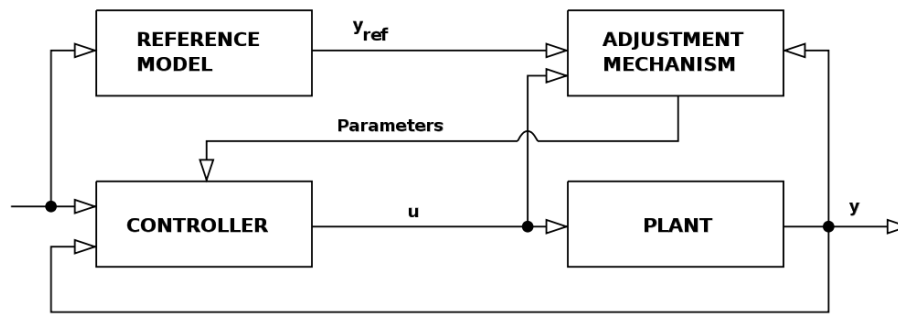
Figure 41: Model Reference Adaptive Control (MRAC)

The functional diagram of the adaptive control system shown in Figure 41 does not show the sensing elements, but sensors will be fundamental to providing feedback to the Controller and Adjustment Mechanism. The error sensed in the Plant output (y) relative to the Reference Model predicted result (yref) is used by the Adjustment Mechanism to modify the gains of the control laws implemented by the Controller. To make the development of the control system reasonable in scope and complexity, the Reference Model frequently models the Plant behavior as a linear system as shown below, where A and B are linearization coefficients. This linearized model is developed based on the ambient atmospheric conditions and range of gross weights most frequently encountered.

$$\bar{y} = A + B \cdot \bar{u}$$

Vehicle operation outside of the primary design conditions will result in reference model errors relative to the plant output. In these situations the adjustment mechanism serves to update the controller's operating laws though the linearization coefficients to improve the accuracy of the plant inputs in order to produce the desired system response. In the design of the adjustment mechanism, limits must be imposed on the magnitude of the adjustments possible, to assure system stability. The quality of the sensor data used by the adjustment mechanism must also be considered, so that noise in the data signals from various instruments do not result in unacceptable or oscillating adjustments to the controller gains.

Some basic requirements for the control system include maintaining safe separation between the aircraft for all flight orientations, equal load sharing and provisions for auto-jettison to protect the aircraft structure, as well as robust communication and sensing between the aircraft. The aircraft must sense not only the position, velocity and accelerations of the partner, but communicate the control system motions as they are made. This type of communication will allow the two aircraft to work cooperatively to maintain acceptable load sharing and relative positioning, improving the flying qualities of the twin-lift system. Without the communication between the two control systems, the system would become a master/slave arrangement, and the slave would be forced to react to the actions of the master to maintain coordination. This reaction-based system puts higher excess power demands on one of the aircraft (the slave), which will degrade handling qualities and system stability.

The connection between the two aircraft and the payload and spreader bar results in the overall system having a large number of degrees of freedom (DOF's). These degrees of freedom must be accounted for

in the development of the control laws. Because most of the DOF's are closely coupled, all of the cross-coupling terms in the linearized control system must be considered. Each aircraft by itself has 3 translational and 3 rotational degrees of freedom, totaling 12 between them. If the aircraft were rigidly fixed together, as proposed in Frank Piasecki's multi-lift patent, there would be only 6 aircraft DOF's, but here all 12 are present because the aircraft are free to move relative to each other. In addition to the aircraft DOF's, the Spreader Bar can tilt and yaw, and the Payload has pendulum modes in all 3 axes. The summation of these degrees of freedom yields a total of 17 for the entire system. As stated previously, these modes are coupled. For example, if one aircraft increases its vertical height relative to the other, this will also induce spreader bar tilt and rotation of the payload. If the tensions on the cables supporting the spreader bar force the cables to be vertical, then vertical offset between the aircraft will also induce rotation bringing the aircraft closer together horizontally.

The system is complex, and care must be taken in analyzing the technical risk and cost when determining the degree of automation in the control scheme. A fully manual approach is unfeasible because it puts excessive workload on the pilots, while a fully autonomous CH-47 twin-lift system is unrealistic given the time and cost which would be required to implement and certify such a system. There is significant risk in implementing an augmented control system with the mechanical flight controls of the CH-47, so effort must be devoted to developing not only the control algorithms but also the physical flight control system integration.

Modeling and Simulation

The use of flight simulation provides an efficient means of testing the load's oscillation motions and finding stable boundaries for various operations to be accomplished. It also provides criterion and certification for control logic.

The simulation of the whole system is fulfilled with Simulink from Matlab. A code is written using general simulation equations for the rigid body motion of twin-lift system. The simulation integrates dynamic features of the helicopters, spreader bar and load and can reflect how the three parts interacts with each other. Equations for the general system are obtained from the Newton-Euler rigid-body equation with introduction of generalized velocity coordinates.

Moreover, the flexible initial setting offers a wide range of states for the system to start from and outside disturbance can be performed arbitrarily during simulation process. This feature gives the simulation high compatibility for simulating all kinds of motions. Thus the simulation depicts how the system responds to all kinds of outside disturbance and various operations. It builds a path through which we can know a sequence of certain operation without repeatedly doing complex and tedious Euler dynamic calculation.

Equations

The base equations applied in this simulation are derived from the Euler Equation. When applied in the twin-lift system we combined the model dynamic equations of helicopters, spreader bar and load with following simulation flow diagram, Figure 42.

$$fo = fg + fa - X - D\left(\dot{A}u + \dot{B}\dot{p} + B\ddot{p}\right)$$

$$\delta, p, \dot{p} \longrightarrow \quad fc = \left\{ \begin{array}{l} \sum_{j=1}^{M} hj \max\{0, Kj(lj - loj)\} \\ -\Lambda[\Lambda^{T}D^{-1}\Lambda]^{-1}\Lambda^{T}D^{-1}f0 \end{array} \right\}$$

$$sf = D^{-1}(fo + fc)$$

$$A^{-1} \quad \dot{u} \quad \int \quad u \quad z_u u + z_p \dot{p} \quad \dot{z} \quad \int \quad z$$

$$\dot{p} \quad p$$

$$z \qquad \dot{z}$$
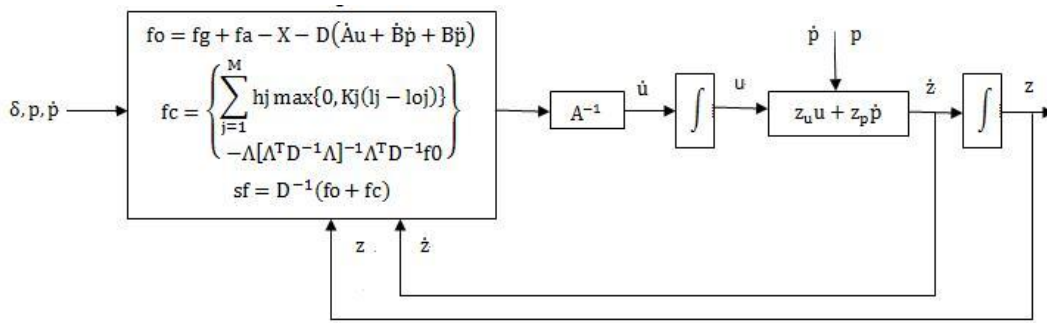
Figure 42: Simulation Flow Diagram

Detailed explanations of these equations are not given here due to space constraints and because this is not our priority. Instead, with this fulfillment several tests are done to test the stability of system under different conditions and then derive the stable boundaries for various operations. Our interest especially lies in testing helicopter or load offset in different direction and the treatment of operations like forward flight, take-off and landing.

Initial Condition Settings

Initial settings, determined by the conceptual load handling system design, are shown in Figure 43. The length of spreader bar was set to 100ft, the height from the center of the spreader bar to the center of the load was set to 100ft, and the height from spreader bar to the helicopter was set to 12ft. Note that this analysis does not include the two 2ft end caps.

Y-axis

X-axis

100feet

12 feet

100 feet

TIME : 3.12 sec
HEL. : 0.02, -15.24 m
LOAD: -0.00, 0.00 m
TGT. : 0.00, -0.01 m
ERR. : 15.24 m

Initial swing
angle 5 degree
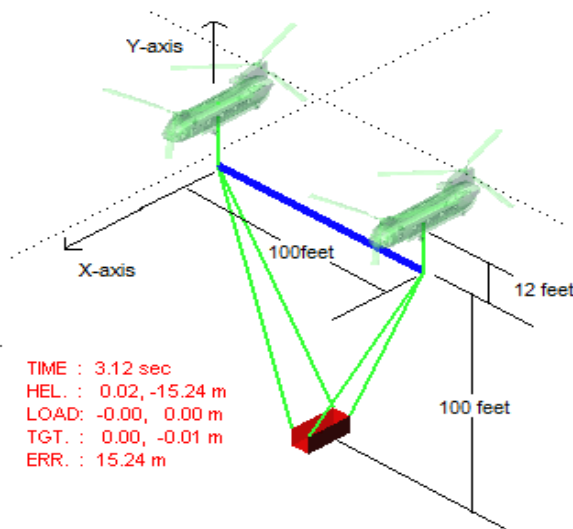
Figure 43: Twin-Lift System Overview   **Figure 44: System with Initial Swing**
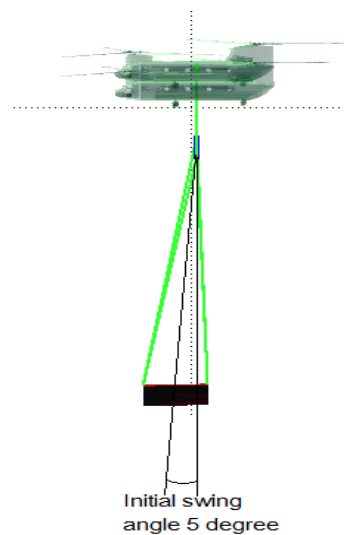
Considering as it is a common situation that an outside force like the aerodynamic force is acting on the load, we can never make the load totally static. Plus that is different from the single load system, the twin-lift system involves highly coupled oscillation motion from both spreader bar and load which makes it hard to totally eliminate the oscillation motion even when control is added into the system. It is advisable to use a state with a small oscillation angle to define the "normal stable condition" which is shown in Figure 44. This assumption pulls the simulation closer to the actual situation and provides a

wide range of possibility for future operations. In this way, we consider the "normal stable condition" as one with a small load oscillation angle.

Also, this is a rough simulation and does not represent a high degree of accuracy. Therefore these are representative and not exact values; we expect around 90% - 95% percent accuracy for these results.

Before we start the tests, we tend to learn some feature of the system about how it responds to disturbances. We set the helicopter to hover and give the load a larger initial oscillation angle of 13 degree. Thus the initial position of load in X axis is $100 * \sin(13) = 20$ feet. We do this setup to make the results clearer and effective; in most of the tests below we carry on these settings. Refer to Figure 45 we can see that the oscillation motion of the load is a perfect cosine curve (red line). One other feature is that the frequency of spreader bar oscillation is much higher than that of the load (blue line). This again states the fact that the motions of two objects are non-linear. Also we can observe that the frequency of load is about 1/12 second. It states that the load is actually moving very slowly. The feature gives more margins for the feasibility of control.
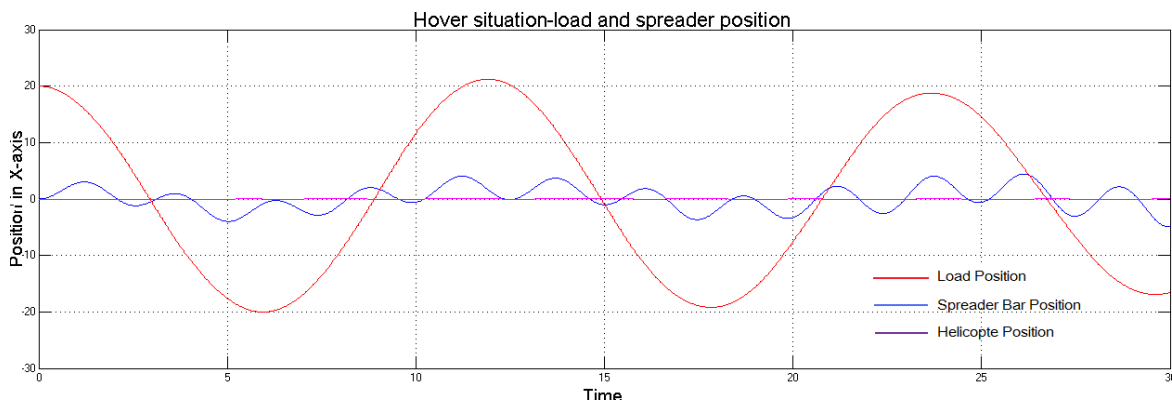
Figure 45: Load Oscillation

Test 1: Changing airspeeds
In this test, we start by setting the entire system to cruise at constant speed with no acceleration. Relative to the helicopter, the load starts at the same speed but with a given longitudinal offset, which will infuse the load with an oscillatory motion in the longitudinal direction. This kind of oscillation is one of the most common situations happening in actual forward flight. It is easily caused by a sudden outside force acting on the load, e.g. strong gust.

Assume that the aerodynamic force acting on load is small relative to the weight of load. Simulation shows that the level of stability of the system does not vary with the speed. Compared with Figure 46 and Figure 47, we find that the two cases start with the same initial load oscillation amplitude. The only difference lies in that the former case cruises with a constant speed of 12.5 feet/second while the latter case cruises with a constant speed of 25 feet/second. We use the same range in vertical axis to represent the position of the x-axis, which generates a clear view. But we do not find any clue that hints the oscillations are damped or enforced with increased speed. Instead it is evident that the oscillation amplitude remains the same from 12.5 to 25feet/second. This leads to the conclusion that with the

same initial load oscillation motion, the increase in speed neither enlarges nor decreases the oscillation motions.
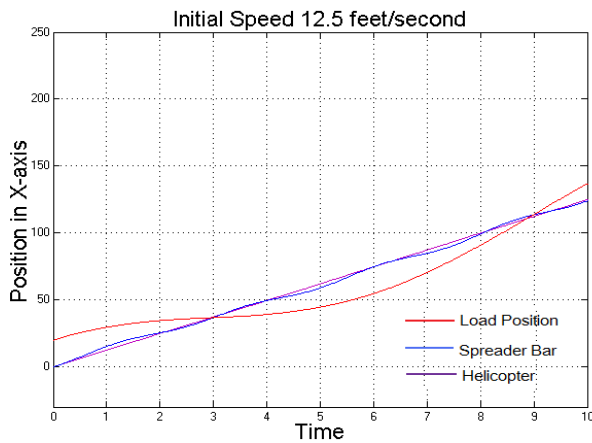
Figure 46: Cruise at 12.5 ft/s
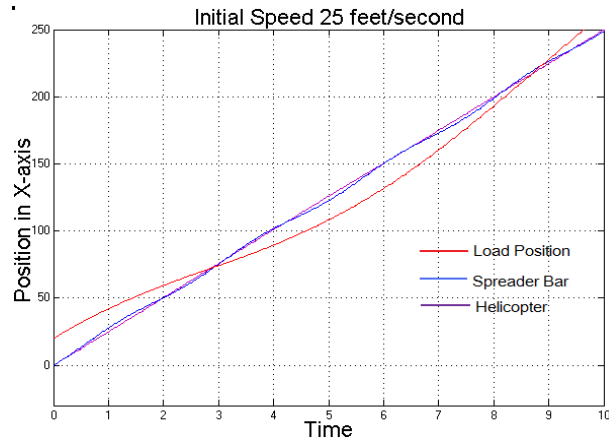
Figure 47: Cruise at 25 ft/s

Test 2: Accelerate at different rates

In this test, we start by setting that the entire system starts at speed 0 but accelerates at different levels. The load starts at speed 0, but with a given longitudinal offset. This test simulates the hover-forward flight situation, which happens at take-off. The results can also be correlated to the approach to landing.

The simulation shows that the stability varies widely according to the acceleration rates and the way of acceleration. One of the most interesting features of the results is that the stability changes according to the start time of acceleration. The theory of control is illustrated in Figure 48.
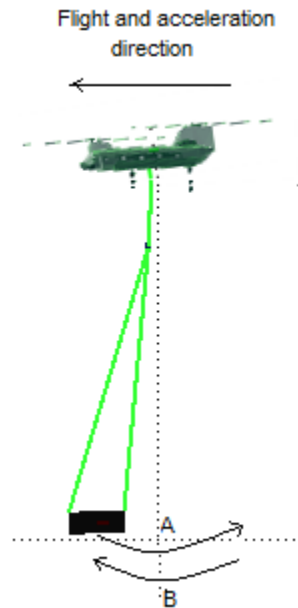
Figure 48: Load Oscillation Track

In the right hand side Figure 48, the two curved lines represent the oscillation trail of the load. Point A is the lowest point on the right-moving trail (the upper curve) and point B is the lowest point on the left-moving trail (the lower curve). Assume that both helicopter and load are moving to the left and the acceleration rate is positive, which means the system is accelerating. When acceleration happens at point A, the stability will be jeopardized. The degree at which it is jeopardized depends on the magnitude and duration of acceleration. On the contrary, when acceleration happens at point B, and the rate is not excessive, the system will remain stable and stability can even increase. This theory is tested by simulation and the results are shown in Figure 49 and Figure 50. The two graphs respectively show the situation that acceleration happens at point A and point B. Notice that in Figure 49, acceleration happens at around 3 seconds while in Figure 50, acceleration happens at around 9 second. The sequence of this difference leads to huge variety in oscillation motions. In Figure 49 where acceleration happens at point A, the amplitude of oscillation is enlarged. On the contrary in Figure 50 where acceleration happens at point B, the oscillation amplitude remains constant. The same logic can be seen in the deceleration case. The results show that regarding to the acceleration case, the system is highly non-linear. This result will play a key role in control logic implement.
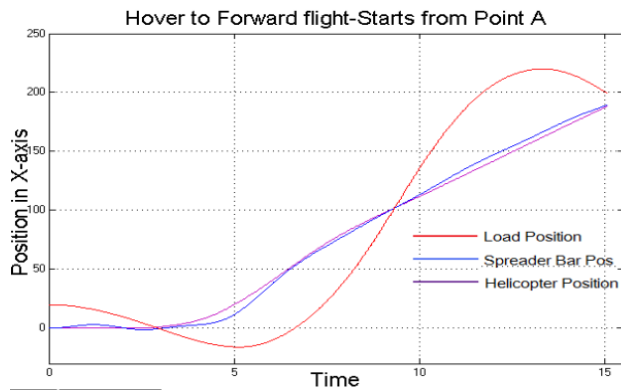
Figure 49: Accelerating at Point A
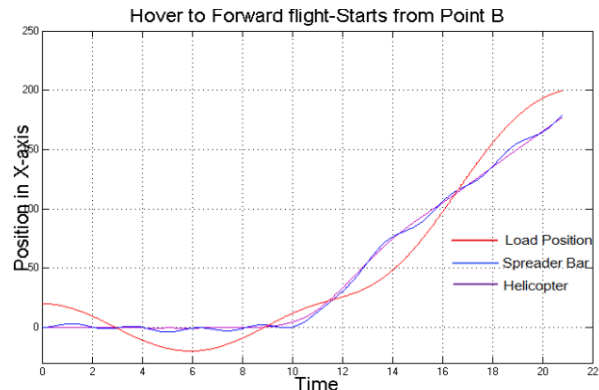
Figure 50: Accelerating at Point B
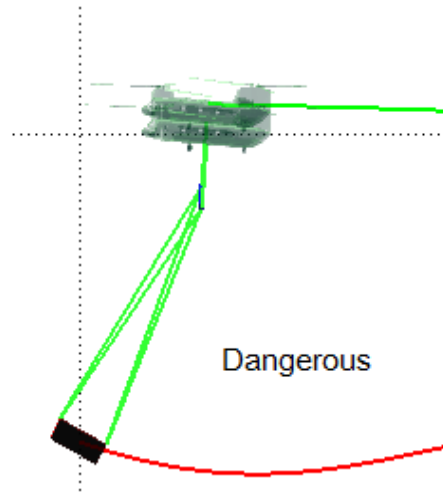
Figure 51: Hazard Condition

As mentioned above, by using the simulation, one of our most important objects is to derive the operational boundary. So we build a set of stability/safety criterion, which can help to define the operational boundary. We use the oscillation angle between y-axis and slung load to classify the stability/safety criterion. The reason why we use this value to do the classification is that it is measurable and most efficient. Figure 51 shows the logic of this classification.

If the angle exceeds 30 degrees, the situation is dangerous. If the angle exceeds 20 degrees but is less than 30 degrees, caution is needed. If the angle remains less than 20 degrees, the situation is safe, although utilizing control logic is highly recommended needed.

The logic applied in this criterion lies in that the range of stress in the cables varies according to the oscillation angle. When the amplitude of oscillation increases, the range of stress in cables also increases. Though this variety can be balanced by helicopter's trim control, there will be a heavy pilot workload to stay focused on sustaining the frequently alternating operations. Thus we claim that though it is still feasible for helicopters to remain in flight with a large oscillation angle, it is quite dangerous for pilots to operate in such conditions and control is urgently need.

One other thing should pay attention to is that throughout this test, acceleration happens at time point A. We do this in order to simulate a worst-case scenario. Because as the initial oscillation angle is small and the pilot cannot always exactly check the location of load; it is difficult to correctly decide the right time point to start acceleration. In this way, we will deal with the worst case rather the best situation.

Four tests were done to record the largest oscillation angle, acceleration duration and acceleration rate. The initial angle is 5 degree and the initial speed is 0. We concluded the following results:
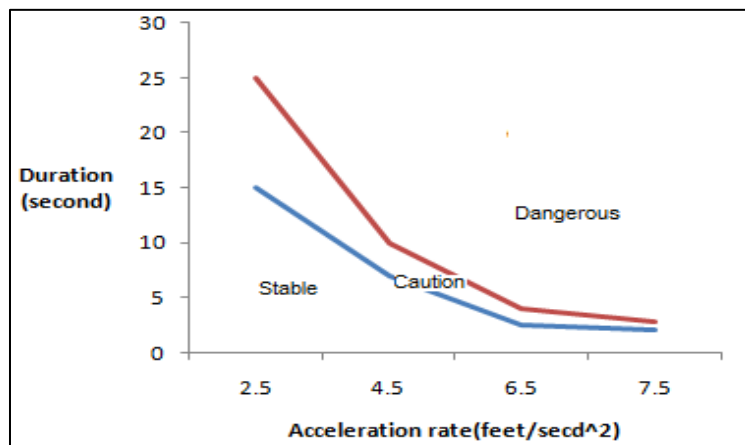
Figure 52: Operational Boundaries

Operational boundaries are specified in Figure 52. Three sections in the graph respectively stand for stable, caution and dangerous region. Notice that the curves that define operational boundaries are not perfectly linear. This is due to the complexity of twin-lift system.

Obviously we can see that for the system to remain stable, the smaller acceleration rate allows for the longer maximum duration. When the helicopter accelerates at rate of $7.5 \, feet/sec^2$, the allowable

duration is only around 2 seconds. When the helicopter accelerates at the rate of $2.5 \, \text{feet/sec}^2$, the margin is much larger than the case of $7.5 \, \text{feet/sec}^2$. The maximum allowable duration reaches 15 seconds. Thus it is highly advisable that pilots accelerate the helicopter slowly but constantly, instead of sharply.

Test 3: Different helicopter offset

This test simulates with the situation that there is an offset between the helicopters. The offset can either be in the vertical, lateral, or longitudinal direction. These kinds of offsets, which are most caused by outside disturbance, happen frequently in high speed flight. Though the helicopter itself has a damping characteristic, a slight disturbance of helicopter's state will still lead to significant offsets relative to each helicopter's state. Special attention should be paid when the helicopters make a sharp turn. Detailed analysis will be given in later chapters. To fulfill this test, different values are adopted to evaluate how the systems respond to the offset.
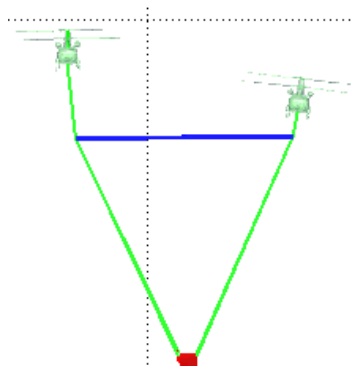
| Figure 53: Vertical Offset | Figure 54: Lateral Offset | Figure 55: Longitudinal Offset |
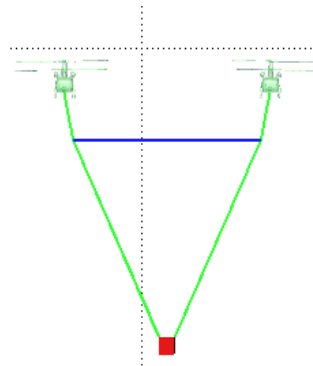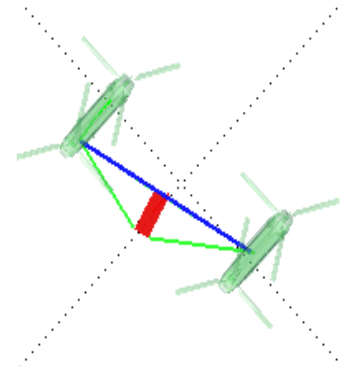
Figure 53, Figure 54, and Figure 55 show three main kinds of offsets which are vertical, lateral, and longitudinal respectively. Also notice that there are other kinds of offsets like the yaw angle offset, pitch angle offset, roll angle offset. However, as the hook attaching cables are located in the center position of helicopter, it is reasonable to assume that compared with main offsets, the yaw angle offset, pitch angle offset and roll angle offset will not dramatically endanger the stability. Also there are a number of coupled disturbances that we can't void consideration. These coupled offsets are the most danger situations we may face and special work should be done. However, it is extremely complicated and effort consuming to finish the job. So we will not focus on analysis these coupled offsets though we will still forward some basic logic in dealing with them later.

It is significant that there are other kinds of disturbances act on the load. Apart from the longitudinal offset we have already discussed in Test 2, the load may have other motions like rotating motions and rolling motions. However, as the elastic modulus in cables is large, the rotating or rolling motions will be all gradually and automatically damped. We will not consider these motions of our interest.

One of the features that differs this test from above ones is that we will develop a new safety/stability criterion which is suitable for this test. We claim that if the simulation starts with a given offset and the

system can last longer than 6 second, than the offset is within safety criterion. If the system broke down within 6 second, we claim that the offset is beyond safety criterion and urgent control is needed.

The tradeoff between this safety criterion and the one applied in Test 2 is that, for Test 2, the system can still remain in flight even if the load has an oscillation motion; for Test 3, the system is vulnerable to certain kinds of offsets. As in many cases, the system broke down immediately when large offset happen. It is no longer feasible that we use oscillation angle to represent the level of stability. Thus we need a new criterion which can evaluate how the system responses to disturbance and we come to the idea of using sustaining time.

One thing needs to be mentioned here is that we choose 6 seconds as the boundary and this value will also be used as the dividing line of pilot manual control and computer automatic control. Investigation reveals that the average recognition time for the pilot is about 3 seconds, the average response time is 1 second and operation time is 2 seconds, which makes up the 6 seconds. This means that if the disturbance will crash the system within 6 seconds, it is unfeasible for the pilot to sense and respond. Otherwise there is enough time for pilot to respond and manual control is feasible.
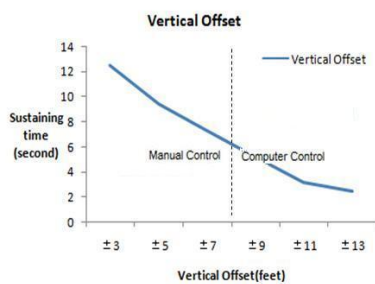
Figure 56: Vertical Offset
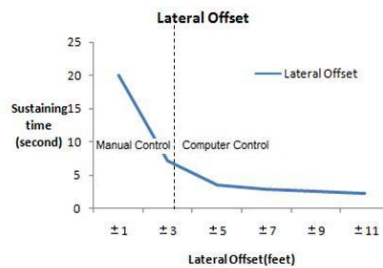
Figure 57: Lateral Offset
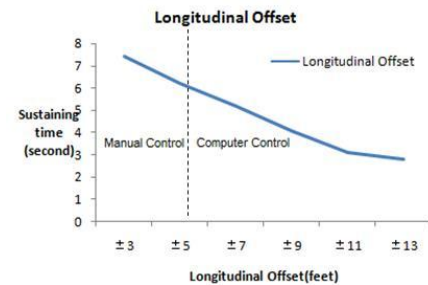
Figure 58: Longitudinal Offset

In Figure 56, Figure 57, and Figure 58, the positive and negative sign indicates the relative helicopter offset compared to the original position. For example, +5 and -5 in lateral offset means the two helicopters move apart or toward each other for respective 5 feet in lateral direction. Figure 54 exactly shows this situation. It is also adoptable to set the offset value to +5 and 0 which means that one helicopter is moving and the other remains stable.

These three figures reveal something interesting. We observe that even the three kinds of offsets have hugely different sustaining time. For lateral offset case, even an offset as slight as 5 feet will quickly destroy the system. This is due to the nature of the twin-lift system. It can be seen that the cable attaching the helicopter and spreader bar is only 12 feet long which at some extent "amplify" the offset. In this case there will be a large angle between the cable and vertical axis. The horizontal force acting on the helicopter will hugely increase due to the offset and make trim control infeasible.

Also from the figure we can see that with different sorts of disturbances, the system responds differently. Sustaining time boundaries are given regarding to various disturbances. The most dangerous

cases happen when there are lateral or longitudinal disturbances. These numerical results will also be applied in later operation analysis and set the baseline for control logic.

Implementation of Control logic
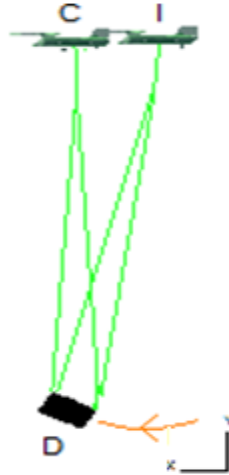
Figure 59: Control Logic

The control logic described here is similar to the logic used in Test 2. The initial purpose of this logic is to decide when to start acceleration. However, we can as well apply this logic to damp the oscillation. Here we will not again elaborate on the logic which decides start time point, but illustrate the control logic by Figure 59. We first test the control logic for the oscillations in the longitudinal direction and later we can expand it to other kinds of oscillations. We claim that to damp the oscillation, we want to make the following things happen:

Assume that in Figure 59 point I is the helicopter initial position and the initial motion of load is moving from right to left. As the load moves to point D, where it reaches its highest location and its tangent velocity reduces to 0, the helicopters reach point C (which is in the same X plane as point D) and the helicopter's velocity also becomes 0. In this manner, the load and helicopter will be relatively static. No tangent force will be acting on load and the swing motion will be negated.

When applying this control logic into simulation, and integrating trim control into the system, we start the simulation by giving the system a different initial speed. It shows that when there is longitudinal oscillation motion, the control logic works well in both the initial speed case and zero-initial speed case. We will trace the load oscillation amplitude and check if the oscillation motion is damped during the process. Figure 60 shows that the system starts with hover situation and load's initial oscillation amplitude is 20 feet.
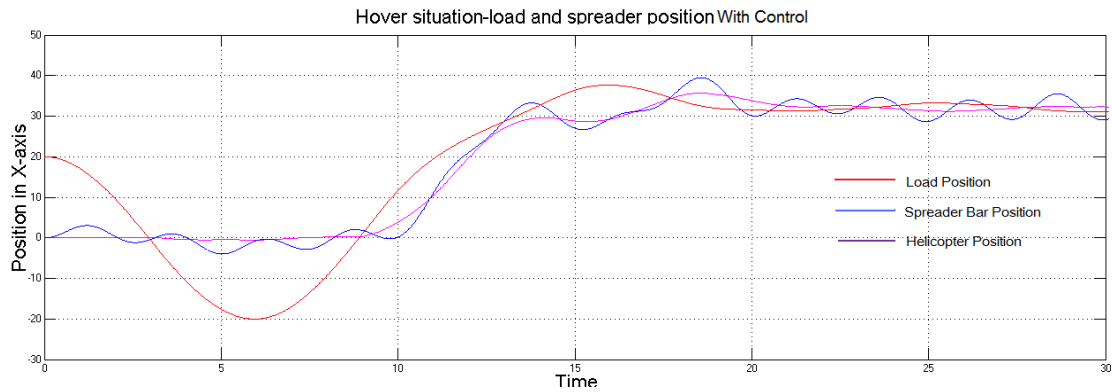
Figure 60: Hover with Control Implemented

Figure 61: Forward Flight With Control Implemented

As we illustrated before, the control should start when the load is moving in the same direction with helicopter and the load reaches the lowest point in this period. According to this logic, we start control at point B.

It can be seen from Figure 60 that after control starts at 8 seconds, the oscillation begins to be efficiently damped. The amplitude gradually drops from 20 to 0. This demonstrates that our control logic is useful to damp the oscillation. Similar results can be seen from Figure 61 which shows the case that the system starts with an initial speed of 25 feet/second and load's initial oscillation amplitude is 20 feet. As the speed is 25 feet/second, and the vertical axis has a much larger range, the three curves overlap. But we can still figure out that at the beginning, the oscillation amplitude is 20 feet. While we apply control logic, the oscillation motion starts to drop. When the system reaches stable, it is hardly to distinguish the three curves. This indicates that the system is quite stable. Detailed control logic can be found in later chapters.

However, we also observe that when we eliminate the load oscillation motion, we failed to damp the spreader bar oscillation motion. Figure 57 also reveals that when the load oscillation is damped, the spreader bar oscillation is not effectively damped. On the contrary, the frequency of the spreader bar oscillation increased slightly compared with the load. This is due to the complexity of the twin-lift system. The two motions are highly coupled and bring difficulty to complete damping.

Besides the above situation, there are many other coupled oscillation cases. We claim that we can still apply this simple control logic but integrating them from different directions and treat the motions respectively. Our simulation is only utilized to demonstrate that stability of the system that can occur through the control logic, not to determine the exact control logic that must be implemented.

Cable Cut Logic

All above analysis are done to maintain stable flight. However, if there are severe oscillations of the load, it will have to be released in order to save the helicopters. One additional test was done to find the critical angle between of the sling legs and the spreader bar which decides when to cut the cables.

Results show that it is advised that the critical angle apply the same logic of stable criterion. If the angle between the sling legs and y-axis exceeds 30 degrees, immediate action should be taken to release the load.

Note that even when the swing angle reaches 40 degrees, we can still apply the control logic and bring the oscillations under control. But when the angle exceeds 30 degrees, the tension in the cables undergoes large changes for a period. It is quite dangerous to operate the helicopter in such conditions. Any additional control may make it too late to safely release the load.

Detailed cable cut method is given in the Safety and Certification section of this proposal.

Control System Design

The simulation built for this design shows that the system is controllable to a point, but many modes can be excited that require auxiliary control. Oscillations of the load are one such mode that if excited, by high magnitude oscillations caused by fast accelerations, will cause catastrophic failure. To avoid this, methods to stabilize the load and minimize the load oscillations by controlling acceleration were investigated. Bar alignment also is vital to ensure system stability. Simulation results showed that small misalignments in any axes could quickly lead to failure. A closely related issue to bar alignment is formation flight. Usually formation flight is a maneuver reserved for highly skilled pilots and not often performed, especially close formation flight. For this twin-lift concept, close formation flight is standard operating procedure. To assist in both bar alignment and formation flight additional control must be used to offload the pilot and ensure bar alignment.

Load stabilization is vital to ensure system stability. As found by the simulation, if the oscillations of the load become too great the system will become unstable, and crash shortly thereafter. Several methods for load stabilization were investigated. The various methods included adding both active and passive damping to the load or bar and augmenting the DAFCS control system currently available on the CH-47F. Many of the methods attempted that did not involve augmenting the DAFCS, making the system independent of the helicopters, required large equipment on the spreader bar or load. With the requirements for such equipment to stabilize the load these helicopter independent methods were found unfeasible. The designed load stabilization system uses various sensors and logic, derived through simulation results, that adds a flight director mode to the DAFCS aiding the pilot in controlling the system acceleration.

Formation flight and bar alignment are flight conditions that must also be controlled to ensure system stability. All methods looked at for this type of control considered DAFCS augmentation, requiring dependence on the helicopter. It was quickly found that passive methods and relying on dual pilot control were unfeasible. Several methods for DAFCS augmentation were investigated with a formation flight autopilot found to be the optimal solution.

When considering any augmentation to the DAFCS it was assumed that a master/slave configuration was being used. Based on trade studies discussed previously it was found that a master/slave configuration yielded the most efficient solution. The master/slave allows for the fastest and simplest implementation of the control systems. In addition to a master/slave control configuration it was found that a single pilot controlling both systems is required. The simulation show that under many conditions the time required to save the system is barely enough for a single pilot to realize and respond and far too small to allow for dual pilot coordinated control. The control systems selected focus on the ability for a single pilot, that of the master helicopter, to have the ability to control both helicopters, while the slave helicopter is under computer control. The formation control system is used to accomplish single pilot control.[9]

Load Stabilization Control System

To ensure system stability load stabilization is required. This was found from the results of the simulation. When the helicopters are in steady-state cruise the load is stable. During accelerated flight, if the acceleration is not carefully controlled, load oscillation instabilities are excited. To safely accelerate to and from cruise and hover load stabilization must be used. The system will be used to assist the pilot to keep the load stable while accelerating.

Several systems were looked at that did not call for augmenting the DAFCS, making the load stabilization system independent of the helicopter. These included a smart load, spring-damper system and a reeling system in the bar.

Helicopter independent control methods

Smart Load

One of the concepts for load stabilization was placing a means of thrust on the load in order for the load to sense and stabilize its own oscillations. This concept is based on undocumented research being done at Georgia Tech with unmanned aerial vehicles. Sensors placed on the load determine oscillations and utilize directed thrust vectors to stabilize these oscillations. To accomplish this, a series of ducted fans were controlled by computerized logic to stabilize the load. In limited testing, this system performed admirably in a single sling load configuration.

When this concept was looked at for utilization for the twin-lift concept, several aspects became unfeasible. The concept was tested using a 5 lb load that can be controlled with smaller fans that require little energy. When this is scaled up to control a 40,000 lb load, the fans and fuel required to power these fans become extremely large. The entire system added approximately 1,500 lbs of additional weight as well as additional bulk to the load. There are also questions as to the interchangeability of this

system if loads other than ISO containers are to be carried. Because of excessive weight added and inability to suit all possible loads, this system was deemed unfeasible for use in the twin-lift system.

Spring-Damper

A spring damper system consists of a shock absorber mechanism attached to each cable, from bar to load, in a way such that when the load oscillates, the system nullifies the motion and keeps the load in a stable state. The system was preliminarily designed as four individual systems—one at each cable. As the load would swing to one side, the tension would increase in the respective cable. The motion would be countered by the spring, and the damper would counter the rate of motion. With the two working in conjunction, the load would soon be brought back to a stable oscillation. Upon refining the system, four systems were not necessary; instead only two were needed. As tension was applied to one end much of that tension could be nullified by the corresponding tension on the opposite end. The second design had two systems in the middle of the bar connecting the cables from opposite end. Again after further refinement, it was concluded that due to the shape of the spreader bar (long and skinny), we would only be able to resist lateral motion. The fore-aft longitudinal motion would create too great of a torque that could not be resisted by the corresponding bar moment of inertia. The final proposal had only a single, large system located at the center of the bar designed to resist only lateral motion. It had both of the cables on one end of the bar connected to one side of the spring-damper, and both cables on the other end of the bar connected to the other end of the spring-damper.

While the spring-damper system offers a simple solution the ability to only control lateral oscillations and the weight of the system make it an unfeasible option. Basic sizing equations based on the force the spring-damper may encounter estimate a system weight in excess of one ton. This is almost double the weight of the spreader bar. The simulations also show most oscillations will be in the longitudinal axis. With this system only able to control lateral oscillations, its benefit of simplicity does not outweigh the cost of its ineffectiveness.

Reeling System

The reeling system utilizes four winches on each sling leg from the bar to the load. These winches would be used to increase or decrease the length of each cable, thereby controlling the oscillations. With control on all four sides the ability to dampen oscillations in both lateral and longitudinal axes was available. To control the reeling system a control system was necessary, in addition to a power source for the winches and control system. The control system would require some way of monitoring the load to determine what adjustments must be applied. This could potentially be accomplished with some kind of tension monitoring or optical system. The details of this system were never investigated. The first aspect investigated was the size of winch required. It was assumed that each winch would need to be able to control 25,000lbs, this is assuming each line splits the 40,000lb load evenly and adds a considerable safety factor. To get 25,000 lb of control authority over the 100ft of cable a very large winch is required. By using a sizing guide from Thern[16], a company specializing in heavy-duty winch manufacture, such a winch would way in excess of 3000 lb each. This alone made the reeling system unfeasible. Adding four 3000 lb winches represents a considerable portion of the total lift available between both helicopters. Although the reeling system had potential as a way to keep the load

stabilization system out of the helicopters, the weight of the winches instantly made it an unfeasible option.

With the helicopter independent systems being found unfeasible, the focus turned to creating a control system to be added as a module to the DAFCS and being dependent and specific to the particular helicopter platform. While this limits the use of the system by requiring aircraft involved to be retrofitted for use, it was found as the only feasible way to accomplish load stabilization control.

Helicopter dependent control methods

Focus was turned to these methods as the helicopter independent methods were quickly found unfeasible. With the load stabilization now being actively controlled by logic in the helicopter flight control system effects of acceleration can be controlled. In steady-state load stabilization control is not entirely necessary. The simulation found that in steady state oscillations are stable. This system is mostly being used for the acceleration phases of flight while accelerating to or from hover and cruise. Although the simulation results showed safe values of acceleration, this system will assist the pilot in maintaining stable acceleration rates and therefore stable load oscillations.

The simulation also found that with knowledge of the relative position, velocity and acceleration of the load, logic could be written able to determine helicopter accelerations necessary to bring load oscillations to a stable level. Efforts were turned to finding a solution that could effectively and accurately determine the position, velocity and acceleration of the load. Helicopter position, velocity and acceleration are already available through the EGIs that are part of the DAFCS.

Two systems were investigated for the purpose of providing load position, velocity and acceleration information. One utilized an optical system and photogrammetry, while the other used GPS sensors.

System Descriptions

Optical System

This system utilizes two optical sensors on each helicopter and coded targets on the load and bar. Through photogrammetry the position of the load will be available to the system. This will be accomplished by using several coded targets on the load and bar that will be visible by the cameras on the helicopters. For use in low visibility environments the targets will be IR reflective and IR-LEDs can be added to the helicopter to illuminate the targets. By using an image processing technique known as photogrammetry the pictures will yield the position of the load and spreader bar, by using multiple successive pictures velocities and accelerations can be calculated. This provides the necessary information needed by the control logic to determine accelerations needed for control. Our optical system is loosely modeled after the iMar/DLR built iSLD-IVC helicopter flight director load control system currently in production. The iSLD-IVC system has proven ability in determining flight director cues that will damp load pendulum oscillations[6].

GPS Sensor System

It has been proven that putting multiple GPS receivers in close proximity the signals received by each can be used to determine the attitude of the object they are mounted on, much like an inertial attitude

gyro would, in addition to position and velocity[1,8]. This system calls for several of these GPS sensors to be placed on the bar and load to provide position, velocity, acceleration and attitudes of the bar and load to the control system.

Both of these systems will utilize a wireless inter-ship control link that will allow for the passing of flight control information between the helicopters flight computers. This will allow the helicopters to share information such as positions and control solutions for comparison and added redundancy. Additionally, the link can be used to communicate the GPS information from the bar or load to the helicopters. This link will play a much larger role for the formation control and will be further explained at that time.

Trade-study

After investigating the pros and cons of each system it was clear that no individual system would provide a reliable and accurate solution. A summary of the multiple load positioning methods is shown in Table 4.

Table 4: Load Stabilization Control Trade Study

	Advantages	*Disadvantages*
Optical	• Proven ability in similar configuration • Low visibility use with IR reflective targets • Active components only on the helicopter • Increased redundancy, multiple cameras	• Potential short periods where targets are unable to be seen by camera system • True positions more difficult to determine
GPS	• No doubt in position measurements • All weather utilization	• Power and communications to load and bar • Active components on the load and bar • Mounting sensors on load can be troublesome

The optical sensors have problems in not knowing the exact positions of at least a few targets. Photogrammetry requires knowledge of the position of a few, at least three, targets that the system will use to tie the rest of the targets to. The purely optical system does not offer that. The optical system does allow for the only active components to be on the helicopter, which is very desirable.

The GPS system will always provide very precise and accurate position, velocity and acceleration information about the load. However, the added complexity of providing power and communication to the load is a big factor, not to mention mounting the sensors on the various loads now able to be lifted by this system. The desire to keep the load a passive component calls for this system not to be used.

With neither individual system able to accomplish the desired results a combination of the systems was investigated. Keeping the load passive was a key factor. That requires the optical system, at least in part. For the optical system to work properly the exact position of a few targets is necessary. By placing GPS sensors on the bar, along with targets, the pictures now have a fixed reference from the GPS position of the sensors on the bar. It is not unreasonable to run the sensors and a wireless transmitter off of battery power for duration of the flight. With the bar only 12ft below the helicopters it is also not unreasonable

to assume if a WLAN type inter-ship control link is in place that the GPS sensors could communicate with this type of system.

The system selected to provide the position, velocity and acceleration of the load is a combination of both the optical system, with two cameras and targets on the bar and load, and the GPS system with GPS sensors on the bar providing accurate positions of the targets on the bar for photogrammetry to use as a reference.

Detailed System Description

The final control system for load stabilization selected is a combination of the optical and GPS sensor system. There are various components being utilized; they fall into four main categories: optical components, GPS components, other components and the control logic.

Optical Components

The optical components consist of two cameras mounted on the underside of each helicopters, several coded targets on both the bar and on the four lines connected to the load as well as the photogrammetry logic.

The cameras will be mounted under the helicopter, near the center cargo hook. Wide-angle lenses will be used and a FOV of 60° can be safely assumed. The cameras will also be mounted such that they are tilted 24° to the center of the system. This tilt allows for the center of the FOV cone to be at the center of the load. Using simple trigonometry and knowing that cameras will be located 112 feet above the load the field of view at the load will be approximately a 130ftx130ft square, this is more than sufficient for complete view of the load along its travel. It will also allow for overlap by the second camera. Figure 62 illustrates the FOV cone available with the described mounting.
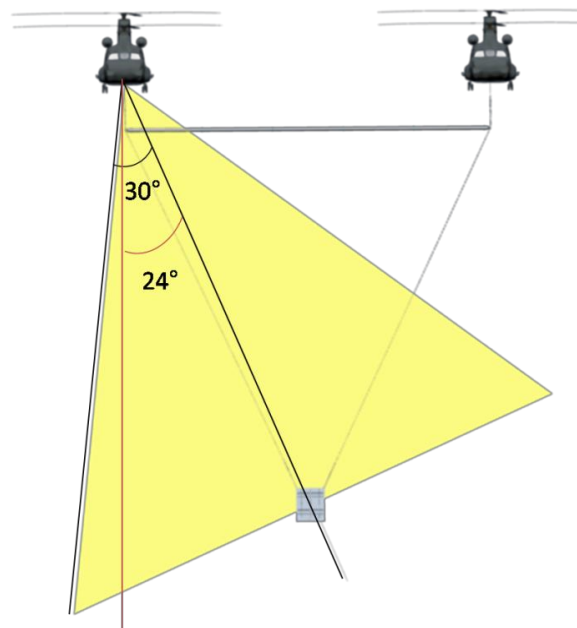
Figure 62: Camera FOV cone and mounting

However at 12ft below the cameras, where the bar will be, the field of view is only 14ftx14ft. This does not allow for any overlap, but leaves space for several targets to be in view on the bar. These targets are extremely important as the GPS sensors will give the exact location for these targets and provide a reference for which photogrammetry measurements can be made from. In addition to camera mounting and FOV, high speed capture cameras will also be utilized. The higher the capture speed the better picture of the load oscillation trend that can be obtained. It is not unreasonable to assume a camera with a 30Hz capture rate be used as most video cameras capture at 30 frames per second. 30Hz should provide a satisfactory capture rate, as the period of the entire oscillation is 10sec.

The targets are circular coded patterns. These patterns are recognizable by the computer and are differentiable so the computer will know which target is which. Figure 63 shows an example of the targets.
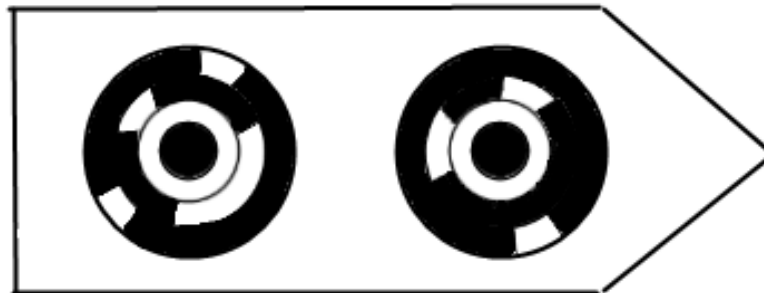
Figure 63: Example of photogrammetry target

The targets are also to be IR reflective. This reflectivity allows the system to be used in low visibility conditions. IR-LEDs located on the helicopter will be able to illuminate the targets and with the reflection the targets will be visible by the camera. The iSLD-IVC system uses this method for low visibility operations[6]. To make the bar pieces interchangeable the targets on the bar will be removable and can be placed in position on the bar section nearest the helicopters. Guides will be painted on the each bar section showing where the various targets need to be placed.

The targets for the load will not be placed on the load, but attached rigidly to sling leg connecting the bar to the load. These targets will be on a disk so that they are able to be removed and replaced if necessary. About 8ft above the load the cable changes to a chain. At this transition point a circular target will be attached rigidly to the line. Being only 8ft above the load the oscillations of the cable will be the same as that of the load. By putting the load targets on the cable sling leg, the system is independent of the size and shape of the load. It can be used for any load being carried. Figure 64 and Figure 65 show the mounting of the targets on the bar and the load respectively.
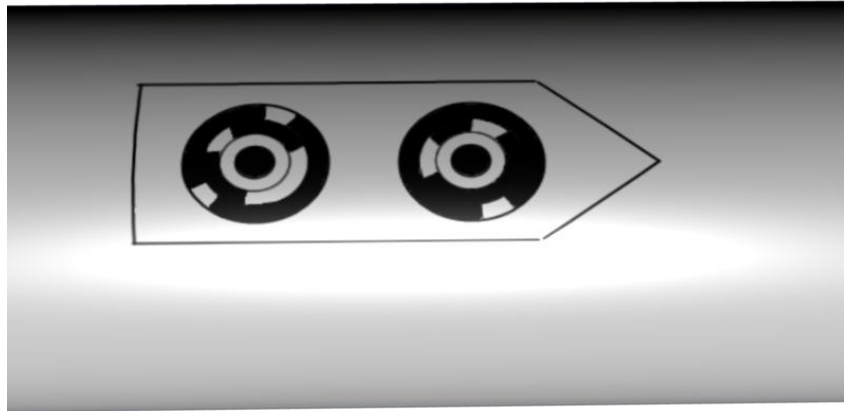
Figure 64: Mounting of the targets on the bar
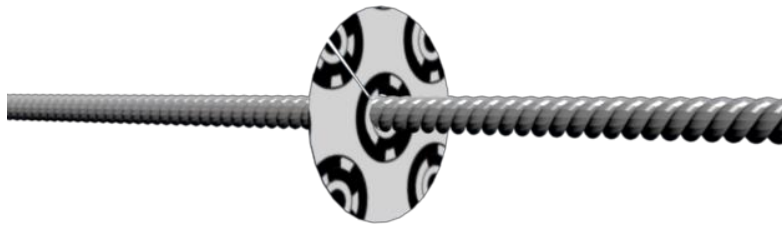
Figure 65: Target disk mounted on the load sling leg rope

The final optical component is the photogrammetry logic. This will be part of the overall system logic. Photogrammetry works by recognizing targets in a picture and measuring the position of those targets, this provides the ability to assign a position to every pixel in the picture. Photogrammetry needs to see and have knowledge of at least three targets to assure accurate measurements. The bar targets are being used as the known targets and will have position knowledge via GPS. With those targets' positions known the load targets will accurately be found. Several computer programs are commercially available that have this ability and building custom software would not be that difficult.

To assure accurate results the optical components will require calibration before every flight. The exact calibration procedure is undetermined, but it can be assumed it will not be time consuming or computationally taxing. Likely, pictures would need to be taken with the position of the load and bar known, such as immediately before the load lifts from the ground. With these know positions the system can calibrate and be ready to operate for the remainder of the flight.

GPS Components

The system also uses GPS components on both the bar and the helicopters. The GPS components on the helicopters provide the position, velocity and acceleration of the helicopters. EGIs currently installed as part of the CH-47F control system will be used to gather this information.

On the bar the GPS sensors will be mounted very near the targets on the bar. These GPS sensors are very important to the overall system as they provide the accurate position of the bar targets to the photogrammetry system allowing accurate measurements of the load position to be determined. To allow the bar sections to be interchangeable the GPS sensors will also be removable. Guide holes will be drilled into the bar where the sensors should be placed and in what positions.

A problem with putting GPS sensors on the bar is powering and communicating with them. Communicating with them is simple when using the inter-ship control link. This is a wireless connection similar to a common WLAN being used for wireless Internet access. Components can be added to this network and communicate with each other. Transmitters can be attached to each GPS sensor allowing them to communicate with the network. To power the sensors and transmitters it can e assumed that battery power will suffice. Neither GPS sensors nor WLAN transmitters require a great deal of power, a single rechargeable battery pack should provide enough power for the roughly 2.5hr mission profile.

Other Components

As previously stated, the inter-ship control link will be similar to a WLAN network and will be discussed in detail in the formation flight control section. For the load stabilization system the inter-ship control link will be used to allow the helicopters to exchange EGI and load position, velocity and acceleration information.

The GPS sensors will also communicate with the helicopters via this system. Determinations of the logic can also be sent between the helicopters for FCC voting to assure the solution is the same across the entire system, this ensures redundancy and allows for automatic switching of the master and slave aircraft if problems are detected.

The CAAS built by Rockwell Collins and standard equipment on all CH-47F aircraft will also be utilized for this system. The load stabilization system will not have control authority due to the fact that once the load oscillations become uncontrollable catastrophic system failure will happen so quickly the emergency cable cutter, discussed later, will have already cut the load loose before control will be regained. Therefore the output of this system is flight director cues. These cues will be shown on the attitude indicator as part of the CAAS systems. They will provide pitch cues to the pilot advising accelerations or decelerations using common flight director visual cues. The CAAS is visible in Figure 66 showing a mockup CAAS implemented in a MH-47G cockpit, very similar to the CH-47F implementation.

The screens on the far right and far left show the PFD and on them the main attitude indicators, the blue and brown circles, where the flight director cues will be displayed as standard flight director visual markers. All pilots should be able to easily understand the cues.

Figure 66: MH-47G cockpit mockup utilizing Rockwell Collins CAAS system[15]

Logic

The most important part of the system is the logic. This logic is partially discussed in the simulation section. The point is to keep the helicopter in a position behind the load oscillations. The idea is to know where the load oscillation is heading and as the tangential velocity reaches zero the helicopter will accelerate to be directly on top of the load. This will allow the relative velocity of the load and the helicopter to be equal thereby stabilizing the load. The system will provide cues to the pilot to maintain his position behind the oscillations and when the logic determines that the load oscillation tangential velocity is about to reach zero the pilot will be given a cue to accelerate and catch up with the load.

If the pilot keeps the accelerations in the safe range, as discussed in the simulation section, the accelerations required to catch up with the load as it reaches a zero tangential velocity should not be very large. A control flow for this system is available as Figure 67.
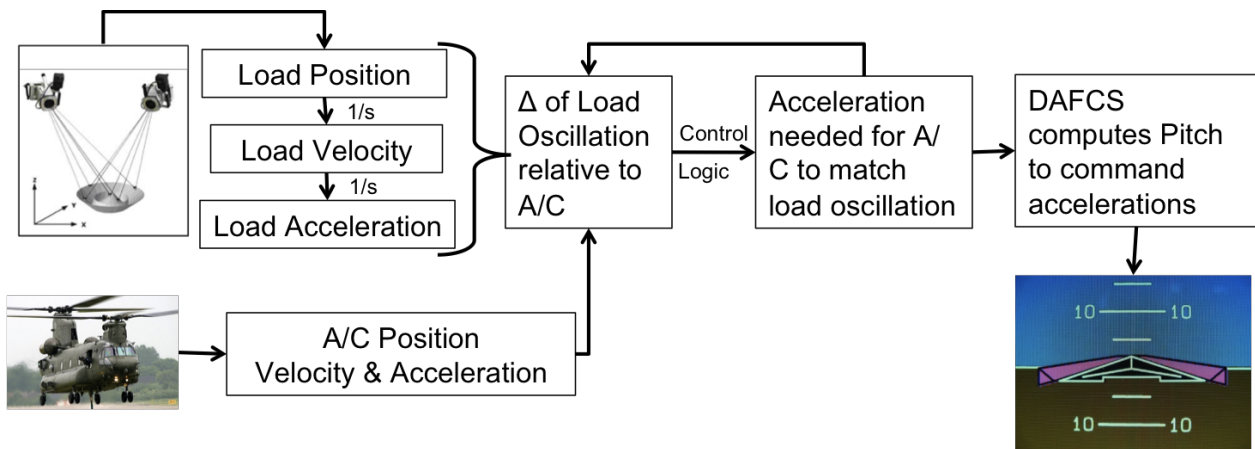
Figure 67: Load stabilization control flow

As is shown in Figure 67 the load position is provided by photogrammetry and can be integrated to determine the velocity and acceleration; the helicopter position, velocity and acceleration are provided directly by the EGIs. The load oscillation position relative to the helicopter is determined as is the change

in that position from the previous time step. The logic will determine the acceleration needed to keep the helicopter behind the load oscillation in a position to catch up. When the load tangential velocity reaches zero a command to the helicopter to catch up with the load will be given. The feedback loop is allowing the logic to constantly reevaluate the necessary accelerations as the relative position and acceleration command changes. As the acceleration command is determined, the DAFCS determines the pitch necessary to accomplish the acceleration, which is then sent to the CAAS to be displayed to the pilot.

The pilot getting the cues is the pilot of the master aircraft. The system while in multi-lift configuration will be under the control of a single pilot. The slave aircraft will be under computer control following the command of the master via the formation control system, discussed in the next section.

Formation Control

Close formation flight is a dangerous and high precision maneuver. Usually only skilled pilots participate in formation flight and their workload is very high throughout the maneuver. For this system, close formation flight will be standard operating procedure. The current spreader bar sizing calls for the helicopter fuselages to be 100ft apart, equivalent to about two rotor diameters. The distance between the rotor tips is a slim 40ft, less than a single rotor diameter. In order to maintain this extremely close proximity flight safely requires the formation flight control, even for highly skilled pilots.

The simulation results also find that the helicopter position relative to each other is very important. Consider the nominal state of the helicopters as being directly over the bar with a right angle formed between the bar and the helicopter sling leg. Simulation results show that small offsets from that nominal will cause the system to quickly become unstable. Offsets on the order of only a few feet, so small that pilots will not be able to visually see, can drive the system unstable. A computer is the only way to determine these slight differences, another duty of the formation control.

Coordinated flight has a direct impact on the helicopter offsets from nominal. System stability depends on maintaining very small offsets from the helicopter nominal positions and the small offsets depend on coordinated flight. Asking the pilots alone to maintain coordinated flight is impossible. The pilots will already be working very hard to keep their helicopters from hitting in the very close formation, requiring them to coordinate movement will easily over burden them. Formation flight control will take care of this problem as well as provide single pilot operation during multi-lift missions.

While in the multi-lift configuration the system will be flown by a single pilot. In order to accomplish this the formation control system will have full control authority of the slave helicopter. The dual piloted system was originally investigated, but the very small time frames required for pilot response before failure preclude both helicopters from being piloted separately. With the formation control having knowledge of the exact position of both helicopters an offset can be specified and the slave helicopter will fly such to maintain that offset.

Focus turned to finding systems capable of providing the exact position of the helicopters. It is quite simple for the slave to find its own position, which can accurately come from the onboard EGIs. The

problem comes when trying to sense the position of the master helicopter. Several systems were investigated: optical systems, LVDT and a GPS formation flight autopilot.

Brief System Descriptions

Optical System, Photogrammetry
Utilizes a camera looking at targets and through photogrammetry is able to find the position of the other helicopter. This system will be augmented with a range finder to provide better lateral distance information and provide a reference for the photogrammetry system. This system is very similar to the optical system being utilized by the load stabilization system.

Optical System, UAV methods
Another optical system was investigated using an omnidirectional catadioptric camera system with the ability to associate every point in the frame with a unique ray to the focal point. This ability allows a system with the appropriate ability to determine the state of an object seen in the image[2]. With these states known the relative position of the object relative to the camera can be determined. Research has been done using this method for UAV formation flight control with reasonable results[6]. This system has potential, however for the system to work properly it must be able to determine the object it is trying to sense; this may require a staggered formation.

LVDT
An LVDT could be placed on the bar at the connection point of the helicopter sling legs. Their null position will be 90°, the nominal position of the helicopters. By measuring the voltage induced by the LVDT the angle between the bar and the helicopter sling leg can be determined. This will allow for the vertical offset to be determined. With the vertical offset known, the DAFCS altitude control can adjust the system to maintain a zero vertical offset. Pilots would be responsible for lateral and longitudinal offset.

GPS Formation Control
The GPS formation flight autopilot will be similar to a system used by NASA in their F-18 formation flight autopilot. This system uses the built in EGIs already in the aircraft to determine inertial positions and velocities of each aircraft. By utilizing a wireless inter-ship control link the slave aircraft receives the 3D position and velocity of the master. The controller has a set separation to maintain from the master and by knowing its and the master's position and velocity the slave is able to maintain close formation flight, the observed error is under ±9ft, usually lower than ±5ft error[7].

For this system the position and velocity information will be augmented with control input feed-forward from the master aircraft. This allows for the slave aircraft to instantly know that the master has commanded movement and provide a degree of anticipation.

Trade-study

Table 5: Formation Control Trade Study

	Advantages	*Disadvantages*
Optical, Photogrammetry	• No inter-ship communication required • Full 3D autopilot capability • Able to work in many, if not all, conditions with IR reflective targets • Slave does not need information from master to operate	• Lateral offset determination may be problem (mitigated with range finder augmentation) • Target must be in view on master aircraft • Large delay in slave response while movement is detected • Complex system
Optical, UAV methods	• Proven on small UAV scale • No inter-ship communication required. • Full 3D autopilot capability • Slave does not need information from master to operate	• May require helicopters in staggered formation to work properly • Good visual conditions required for uninhibited view of master • Large delay in slave response while movement is detected • Complex system
LVDT	• Very simple • Accurate determination of relative vertical position • Will work in any environmental condition	• Only 1D autopilot capability • High pilot workload • Requires bar (LVDT)-helicopter communication
GPS Formation Autopilot	• Very accurate in all axes • Uses sensors already part of CH-47F DAFCS • Full 3D autopilot capability • Proven system for similar application • Able to work in any environmental conditions • Master control input feed-forward allows for anticipation	• Requires inter-ship communication • Highly complex system

Table 5 shows a comparison of each method. Unlike the load stabilization system a single system is able to perform all the requirements of the formation flight control system.

The optical systems are able to, but major drawbacks for each system exist. The photogrammetry system may have compromised accuracy without known positions of a few targets, like the targets on the bar for the load stabilization system. The rangefinder will provide the lateral offset and will help tighten the accuracy of the photogrammetry system, however concerns still exist. Another large problem with the photogrammetry system, as well as the UAV system, is the large delay inherent to the system. The optical systems need to wait for large enough motions to occur that will be sensed by the optics, therefore the system will not be able to respond until after the master has moved a considerable amount. This large amount of movement and time needed for the system to respond could cause the system to become unstable. The UAV method has other problems beyond the delay. The UAV method will require good visual conditions to operate in. Unlike the photogrammetry system where IR reflective targets can be used, the UAV method requires an uninhibited view of the other aircraft. Additionally, it

may require the helicopters to fly in a staggered formation in order to work; this is not possible as a staggered formation is impossible to fly with the limited offset positions permissible before the system becomes unstable.

The LVDT is not usable as it only works in one axis. The LVDT is very accurate at determining the vertical offset between the helicopters, but does little for lateral or longitudinal axes, requiring the pilots to be responsible for those axes. The GPS formation flight system will be used to reduce pilot workload as well as allow for single pilot operation. The LVDT does neither.

The GPS formation flight autopilot is able to very accurately supply the offset positions via the EGIs already installed on the CH-47F as part of their DAFCS. The only drawback of the system is the requirement of the inter-ship control link. However, this system is a required component of the load stabilization system and will need to be installed either way.

Detailed System Description
The selected system utilizes the GPS formation flight system similar to the system used by NASA Dryden in their F/A-18 formation flight autopilot. Research was done on this at the Dryden Flight Research Center in Edwards, CA in the early 2000's. In these experiments they used two F/A-18s in which one was the leader and the other was the follower. The leader was mostly a stock F/A-18 while the follower had an auxiliary mode added to its autopilot. The autopilot took in EGI position and velocity from both its own control system and from the leader aircraft. Through custom logic a relative position of the follower to the leader was determined. The engineers gave a specified offset from the leader for the follower to maintain. From their experiments it was found that the system never exceeded the ±9ft error limit imposed in all axes in steady flight, and was mostly under ±5ft of error. The leader aircraft shared its EGI information with the follower via a high frequency (2.4Ghz), high bandwidth (2Mbps) wireless connection. This link was found to be satisfactory in its ability to share the EGI measurements between the aircraft[7].

GPS Components
The formation flight system will utilize the onboard EGIs that are part of the CH-47F DAFCS. These devices use rate and attitude gyros augmented with GPS; they provide very accurate position, velocity, acceleration and attitude information. The GPS formation flight system will utilize the position and velocity measurements. They will be fed to the control logic where relative position and velocity will be determined. This exchange of information from the master aircraft to the slave aircraft will be accomplished using the wireless inter-ship control link.

Inter-ship Control Link
The inter-ship control link is an important part of both the load stabilization control and the GPS formation control system. The system incorporates a fairly standard WLAN type communication system. A WLAN system is the type of network used to connect computers to the Internet wirelessly via a transmitter on the computer and access point at the router, in use in many homes and business. A similar approach is being taken with the inter-ship control link. Access points will be placed on each helicopter capable of transmitting information between them and allowing for permitted devices to

communicate on the network as well, e.g. the GPS sensors on the bar as part of the load stabilization system. WLAN networks work very well within a small range of the access points; usually on the order of a few hundred feet (many common IEEE 802.11g networks have a useful range of 450ft from the access point). The systems can also be encrypted to protect the data being transmitted. Both the range of the network and encryption add a level of safety to the system. An errant signal would not only need to break the encryption, but also have high enough strength at very close range to become a problem. A potential problem of the wireless inter-ship control link is signal jamming by the enemy. Heavy lift systems are rarely sent into hot zones where these types of threats exist. With the multi-lift system being even more fragile than a common heavy lift platform, it is reasonable to assume that this type of system will not be dispatched to zones where jamming devices exist, therefore mitigating that concern.

Other Components

In addition to the EGI measurements being sent across the inter-ship control link the system will also have access to the control stick positions and DAFCS control inputs. These positions and control inputs are already being measured by the DAFCS and will be easy to obtain. This information will be provided to the system as a feed-forward. The feed-forward of the control inputs will allow the system some degree of anticipation of movement, speeding up the response. The aircraft plant model will know what type of motion the control inputs correspond to. By knowing what is being commanded in the master aircraft the slave response time will be lower as that movement can be anticipated.

Control Logic

The control logic for this system is fairly straightforward. The system will be told the three-dimensional offset the helicopter is to maintain relative to the master aircraft. Comparing the EGI measurements of the slave helicopter and the master helicopter, via the inter-ship control link, will provide the relative position and velocity. The controller will determine the motion necessary to achieve the desired offset and will send that information to the aircraft plant model, along with the master helicopter control input feed-forward. The plant model will determine the control inputs necessary for the slave aircraft to fly in order to maintain its desired offset. A diagram of the control flow is available as Figure 68. This logic can also be added to both helicopters allowing for on the fly changing of the master and slave configuration, or automatic change if a problem is detected.
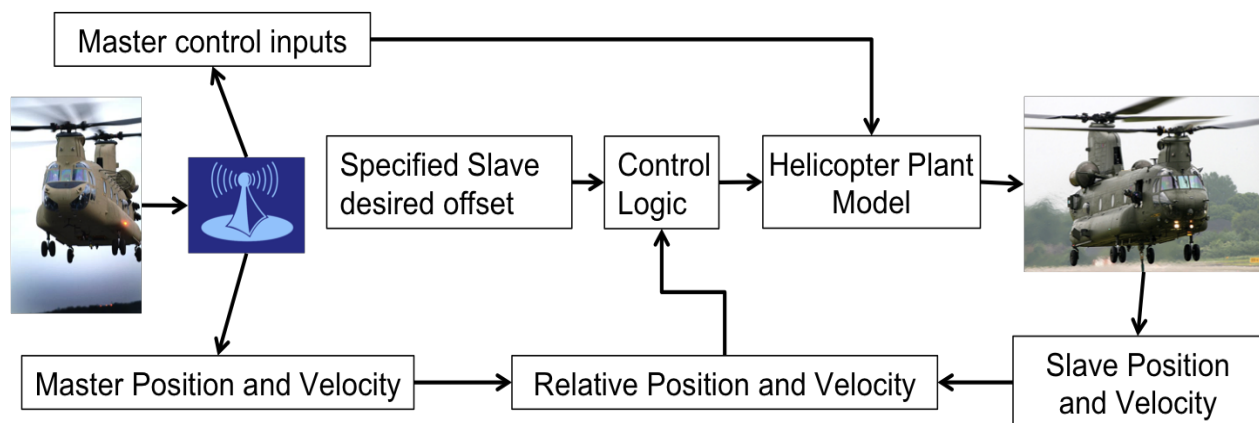
Figure 68: Formation control system control logic

Desired Offset

The desired offset will be such that it will keep the helicopters aligned in the vertical and longitudinal directions and 100ft apart laterally. The 100ft separation represents the length from the center cargo hooks. This distance will not be correctly measured by the EGIs and will need to be accounted for, the EGIs may not measure the position of the center hook. If the cargo hooks are 100ft apart the sling legs will be strictly vertical as the spreader bar is 100ft long.

Expected Error

As stated previously the system is expected to perform no worse, if not better, than the NASA F/A-18 system. This means that in steady state the error should be at a maximum of ±9ft. The results of the simulation say that ±9ft can quickly lead to failure. This must be clarified. The error of the formation control system is assuming that the master helicopter will remain perfectly aligned and only the slave will possibly be up to a ±9ft error from the desired position. This is essentially saying that it could only be 9 feet in any direction from the desired offset. The results from the simulation are modeling both helicopters moving off alignment. Thus, the ±9ft offset talked about then represents up to 18ft of total offset from nominal, while the formation flight only represents up to 9ft. With this understanding it is now clear that the maximum expected error would not have an impact on system stability.

Figure 69 shows the error observed by NASA during the F/A-18 formation flight testing. The error of this system is expected to be the same if not better than that which NASA observed, due to the control input feed-forward.
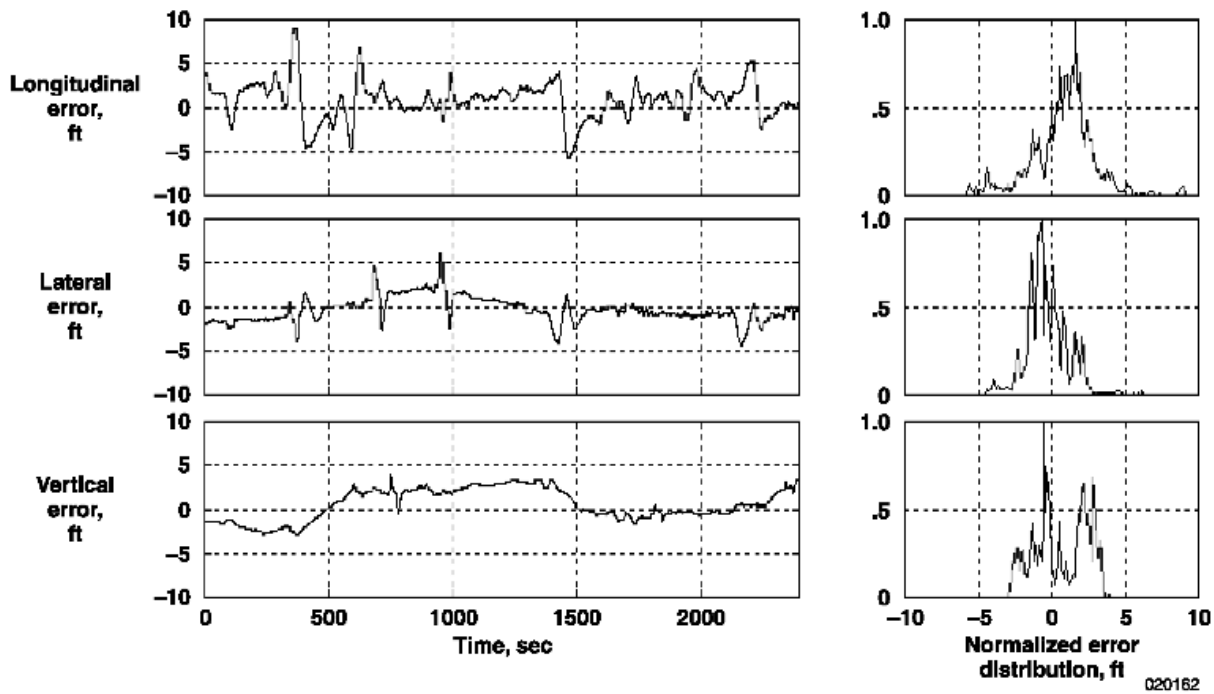
Figure 69: Error plots from NASA F/A-18 formation flight autopilot[7]

Slave Autonomous Control

One focus of the formation control logic is to offer single pilot control of the entire system. The logic of this system allows for that. The formation control system will fly the slave helicopter autonomously as to keep the helicopter at the desired offset. With the control input feed-forward the delay between motion being detected and the slave responding should be short enough to be considered negligible. While in multi-lift configuration the formation flight control will be operating and the slave aircraft will be under computer control. The CH-47F DAFCS allows for this. The control actuators on each control stick and swash plate already have the necessary control authority. This system will command the proper control via the actuators to maintain the desired offset.

Twin-Lift System Normal Operations

Crew Member Certification

In normal operation, the twin-lift system will be operated by 8 individuals, 4 pilots and 4 crew members. At a minimum, the pilots-in-command (PIC) should be certified on the twin-lift system (including both a ground certification and a flight certification), and the Flight Engineers (FE) should be certified on the operations of the hardware comprising the system.

The ground certification for pilots should consist of familiarization with the components of the system, but more importantly with the flight cues from the load stabilization system. The flight training should begin with an update to the CH-47F simulator which will allow for multiple simulated flights with the appropriate visual cues to be included in the training regimen. This will lead to multiple flights in the aircraft with an Instructor Pilot before a pilot is qualified to fly as a PIC during twin-lift operations.

Certification for the Flight Engineers will be equally rigorous. The ground certification will consist of knowledge of the components, set up of the system, inspection criteria and calibration of optical components. They must also be trained on the appropriate rigging of the load with the twin-lift system and, if possible, an update to FM 4-20.197 (FM 10-450-3) should be released to include twin-lift operations and information on it integrated into the Air Assault course. The FE should also be trained on the general control issues regarding load stabilization as if there is a failure in the automated load stabilization system, the FE of the master aircraft will take over relaying information on the stability of the load to the pilots in order to enhance situational awareness. In addition, flight training should be included in the qualification. This is to familiarize the FE with load oscillations and the methods of stabilization.

Takeoff and Landing Techniques

Prior to the arrival of the aircraft, the other elements of the twin-lift system should already be in place. This includes the load being appropriately rigged, pointed in the direction of takeoff, and all sling legs extended to the rear of the load as well as the spreader bar. The aircraft should arrive to the hook up point separately, positioning themselves over the sling leg from the spreader bar with enough space to attach the clevis to the center cargo hook with several feet of slack in the sling. Once both aircraft are "hooked up," they will takeoff simultaneously moving forward as they come to a hover over top of the

spreader bar. In the same manner, the aircraft and spreader bar should continue moving up and forward until they are centered over the load with the slings tight. Caution should be taken to ensure the twin-lift system is centered over the load as any misalignment will directly translate into oscillations as the load comes off the ground. Once the aircraft are centered over the load, they should increase thrust to lift the load vertically off the ground to a height of at least ten feet. The system will then be prepared to depart.

The twin-lift system can be brought to the above point by either the formation flight control system in the standard master/slave configuration or through pilots individually flying each aircraft. It should be possible to engage the formation flight system prior takeoff, although there are questions about the actions of the system on the ground with the possibility of uneven terrain or other unknown issues. Tests will have to be conducted during flight testing to determine if there are any unfavorable interactions with the twin-lift system on the ground. If there are, the system should be engaged once the aircraft are situated over the spreader bar to ensure synchronized motion and stability prior to the load coming off of the ground.

Once the twin-lift system is prepared to depart, with both the load stabilization system operational and the aircraft operating in a master/slave configuration, the pilot of the master aircraft should begin a slow acceleration until the system passes through effective translational lift (ETL). They should then begin a climb to the desired altitude at a rate less than 200 feet per minute while accelerating to the best climb airspeed (approximately 70 knots). Upon reaching the desired cruise altitude, the aircraft should accelerate to a maximum speed of 100 knots or the maximum speed where the load remains stable.

Landing operations should be executed in the exact opposite manner. Once the load is on the ground, the aircraft should move forward and down until the spreader bar is on the ground. At that time, the master/slave formation flight system should be turned off, the spreader bar released and the aircraft landed separately.

Cruise Flight
During cruise flight, turning the twin-lift system can become more difficult as the aircraft on the outside of the turn must increase airspeed in comparison to the aircraft on the inside to keep the system properly aligned; the steeper the turn, the larger the differential in airspeeds. Therefore, once the aircraft are being operated in the master/slave configuration, turns should be limited to less than 10°.

Load Stabilization System Failure
If there is a malfunction in the load stabilization system in one aircraft, master authority should be switched to the other aircraft. If that aircraft is operating properly, continue operations with no changes. If the system is malfunctioning in both aircraft, the Flight Engineer in the master aircraft should begin relaying information on the stability of the load to the pilots in order to enhance situational awareness. Oscillation tolerance should be reduced to a maximum of 20° before it is released and the system should be landed as soon as practicable.

Formation Flight Master/Slave System Failure

If there is a malfunction in the formation flight system in one aircraft, master authority should be switched to the other aircraft. If that aircraft is operating properly, continue operations with no changes. If the system is malfunctioning in both aircraft, the load should be released immediately and the aircraft flown away from each other.

Overview of Life Cycle Cost

A key element in the success of a business is the use of sound engineering design within reasonable economic constraints. In preliminary design, engineers make the decisions that drive Life Cycle Cost (LCC) numbers for the economic calculations. In general LCC is a measure of cost over a project's entire life span; it is composed of the total cost of ownership of machinery and equipment from cradle to grave. LCC includes the cost of acquisition, operation, maintenance, conversion, and/or decommission, and because of its comprehensive nature is a good way of evaluating alternatives for equipment and projects. The goal of LCC analysis is to select the most cost effective approach from a list of developed alternatives. LCC analysis provides better assessments of long-term cost effectiveness of projects than can be obtained by looking only at initial costs. LCC values are the summations of cost estimates of the entire life time of the equipment or project as determined from the detailed study and of total costs throughout time. Businesses summarize these cost increments and by taking in consideration the time value of money are able to represent them in net present value (NPV). A breakdown of the life cycle cost is shown in Figure 70.
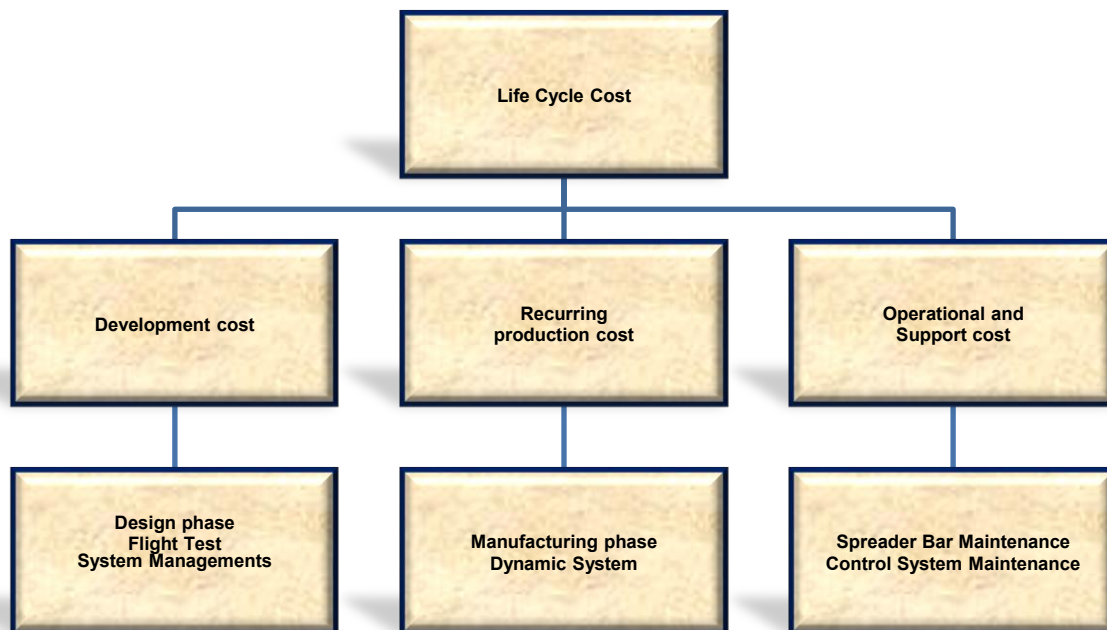
Figure 70: Life Cycle Cost Diagram

At the beginning of every analysis, the analyst must first begin by defining the entire problem. This is the basis of every cost analysis, and is extremely important to ensure the accuracy of the analysis. The analyst should develop a well structured cost structure to keep the process organized and ensure

everything is completely taken into consideration and nothing is counted twice. Once a sound cost structure is developed, a compiled database becomes crucial in the process of a successful analysis. The data will come in many forms, including contractor costs, government contracts, and cost/technical databases. A well organized database, along with sound analytic judgment, is critical to determining which data is appropriate for certain tasks. The analyst should research historical data and compare similarities between the current project and past information. Additionally, the analyst should make sure to note and address any differences in the data and also adjust for inflation rates. When it comes time to prepare the cost estimate, the analyst may choose to use several different types of cost-estimating techniques. For example, if analyzing some equipment that is fairly new and has very little information about it, the analyst should choose to use some sort of analogy cost estimate by using the historical data for similar equipment. The engineering approach is a little harder to apply than the others, since it consists of separating the system into smaller parts and estimating the cost of each part, as well as taking into account of the integration costs. The parametric approach consists of relating the cost to some sort of physical attribute of the system, whether it is horsepower, weight, fuel consumption, etc. The technique that relies solely on the analyst's judgment is the expert opinion approach. Once the cost estimate is complete, it is important to test its reliability and completeness. By testing certain key cost elements, the analyst can see how accurate the estimates were and be certain everything is accounted for, and can then conduct a cost-risk assessment.

Bell PC Cost Model

Background on equations/software

The PC Based Cost Model is a set of spreadsheets designed by Roger Biggs and Jim Key of Bell Helicopter Textron, Inc. The PC Bell cost model predicts and analyzes the development, production, and operating and support (O&S) costs of helicopters.

"This model utilizes a multi-level parametric approach to estimate development and recurring production cost for helicopter or tilt-rotor aircraft. Inputs for this approach use information available at a project's pre-design stage. Operating and support cost is predicted by companion model that utilizes the outputs from the recurring production cost model."[23]

Research, Development, Testing and Evaluation Cost

The PC Bell Operating and Support cost model was used to calculate the RDT&E costs. One of the largest costs associated with the twin-lift system will be seen in the RDT&E costs, as shown in Table 6. This is because while the system is comprised of new parts, the majority of the system is small additions that require a great deal of research and testing. Since the configuration for the design is a military utility, this is how the cost was modeled in the Bell PC Cost Model. As such, the calculated costs are higher than would be seen if the same configuration were run as a civilian aircraft.

Table 6: Total Development Costs, $2001

Engineering	
Design	$2,847,000
Flight Test	$5,730,000
Component Test	$0
Systems Engineering/Project Management	$1,171,000
Total Engineering	**$9,748,000**
Manufacturing Engineering	
Planning, Loft, Other	$1,034,000
Project Management	$268,000
Total Manufacturing Engineering	**$1,302,000**
Tooling	
Tool Make	$575,000
Outside Tooling	$213,000
Total Tooling	**$788,000**
Manufacturing	
Prototype (1)	$193,000
GTV (1) STA (1) FTA (1)	$435,000
Flight Test	$3,699,000
Component Test	$0
Total Manufacturing	**$4,327,000**
Logistics	**$912,000**
Other	
Travel and Per Diem	$338,000
Direct Expense	$1,242,000
Total Other	**$1,580,000**
ROM Adjustment @ 10.0%	$1,866,000
General & Administrative Cost @ 10.0%	$2,052,000
Total Program without profit	**$22,575,000**
Profit @ 12.0%	$2,709,000
Grand Total	**$25,284,000**

After obtaining the recurring cost, the following formula from was used to adjust the cost to 2010 dollars since the PC Bell Cost Model was designed in 2001.

$$FUTURE\_VALUE = PRESENT\_VALUE * (1 + i)^n$$

Where:

i =average yearly interest rate

n =number of years

It can be seen in Table 6 that flight testing will be the most costly development factor. This was calculated by using a single prototype, one ground test vehicle, one static test article and one fatigue test article. Total estimated RDTE Cost for the new design equals $25.3 million in 2001$ including a 12%

profit, or $39.3 million in 2010$. Unfortunately, at this time there is still no data available to properly validate this result.

Direct Operating Costs

In addition to the DOC of the aircraft, the addition of the subsystem to allow for twin-lift will add additional costs to the operation of the overall twin-lift system. These costs are seen in the costs to maintain and repair the system, as well as parts required on hand for these repairs. To analyze these additions, the Cost Trade-Off tool was utilized. The first thing that we had to determine for this analysis was determine the Maintenance man-hours per flight hour. This was done by finding the following parameters.

MTTR – Mean-time-to-repair: the sum of corrective maintenance times at any specific level of repair divided by the total number of failures within an item repaired at that level, during a particular interval under stated conditions. Corrective maintenance is all actions performed, as a result of failure(s), to restore an item to a specified condition. Corrective maintenance can include any or all of the following steps: localization, isolation, disassembly, interchange, reassembly, alignment, checkout. The average MTTR over all the substems of an aircraft is given by

$$MTTR = \frac{\Sigma[(1/MTBF)(MTTR)]}{\Sigma(1/MTBF)}$$

MMHTR – Maintenance man-hours to repair: the average number of man-hours spent on a repair event. This is a number intimately associated with maintenance crew size (MCS) and MTTR, and the two must be consistent:

$$MMHTR = MCS * MTTR$$

MMH/FH – Maintenance man-hours per flight hour: the average labor hours spent for a subsystem, for each flight hour:

$$MMH/FH = MMHTR / MTBMA = MCS * MTTR / MTBMA$$

Using this formula, the MMH/FH was able to be determined. For the twin-lift subsystem, this was found to be 0.12 man-hours per flight hour. This information fed into a larger determination for overall DOC.

$$DOC = DOC\ Reserves\ (A) + DOC\ Maintenance\ (B) + DOC\ Petrol-Oil-Lube\ (C),$$

in Dollars per Flight Hours ($/FH).

Because the subsystem we are analyzing does not require Petrol-Oil or Lube, this part of the equation was omitted. Therefore our analysis consists of only the changes to DOC based on Reserves and Maintenance. In addition, because our system consists of a control system as well as the spreader bar, we did a DOC analysis for these systems separately then added them together as outlined in the Cost TO tool paper. For the analysis of both these systems, we used a labor rate of $40/man-hour.

The first analysis done was for the spreader bar:

$$DOC\ Reserves = \frac{Manufacturing\ Cost}{MTBR(P1 + (1 - P1)P2)} = \frac{\$1,280,000}{2500(0.99 + (0.01)0.05)}$$

$$DOC\ Maintenance = \frac{\$}{MH}\frac{MMH}{FH} = \$40 * 0.12$$

$$DOC\ Spreader\ Bar = DOC\ Reserves + DOC\ Maintenance = \$516.91/FH$$

Next, the DOC was analyzed for the electronic subsystem:

$$DOC\ Reserves = \frac{Manufacturing\ Cost}{MTBR(P1 + (1 - P1)P2)} = \frac{\$500,000}{1500(0.95 + (0.05)0.05)}$$

$$DOC\ Maintenance = \frac{\$}{MH}\frac{MMH}{FH} = \$40 * 0.12$$

$$DOC\ Flight\ Controls = DOC\ Reserves + DOC\ Maintenance = \$349.95/FH$$

This gave the total additional DOC for the twin-lift system to be $866.86 per flight hour, which is not a significant addition to the overall DOC of the CH-47 in comparison to building a brand new heavy-lift helicopter.

Safety and Certification

Safety is defined as "the application of engineering and management principles criteria, and techniques to optimize safety within the constraints of operating effectiveness, time, and cost throughout all phases of a system life cycle". The goal is to implement safety early in the design process, and to involve not just the designers but also members from manufacturing as well as logistics[18]. Methods of implementing system safety include documenting the safety approach, identifying hazards, assessing mishap risk, and identifying mitigation measures[17].

Functional Analysis

The first step in accomplishing these system safety requirements is to develop a functional analysis. The functional analysis, shown in Figure 71, identifies the functions, or actions, that the system must perform in order to meet the mission requirements[12]. This is a top-down technique, in which each level describes the functions of the system in greater detail[12]. A functional analysis was developed for the twin-lift mission, and is presented in two levels. A more complete version which decomposes the mission in to three levels can be found in Appendix 2. The top level is the twin-lift mission in its entirety.

The second level describes six mission segments consisting of Pre-flight, take-off and climb, cruise, descend, payload release, and return to base. The third and most detailed level shows the specific functions that occur during each mission segment.
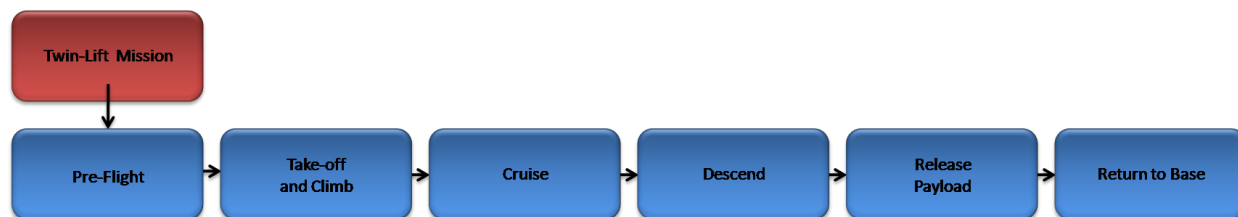
Figure 71: Two-Level Twin-Lift Mission Functional Analysis

Functional Hazard Assessment

At the start of an aircraft or system development cycle, a functional hazard assessment (FHA) is performed. This assessment includes the identification and classification of possible failure conditions. At this point, system safety objectives can also be established[19]. Table 7 lists the mishap severity categories that were used in developing the FHA[17].

Table 7: Mishap Severity Categories

Description	Result Criteria
Catastrophic	Could result in death, permanent total disability, loss exceeding $1M, or irreversible severe environmental damage that violates law or regulation.
Critical	Could result in permanent partial disability, injuries or occupational illness that may result in hospitalization of at least three personnel, loss exceeding $200K but less than $1M, or reversible environmental damage causing a violation of law or regulation.
Marginal	Could result in injury or occupational illness resulting in one or more lost work days, loss exceeding $10K but less than $200K, or mitigatible environmental damage without violation of law or regulation where restoration activities can be accomplished.
Negligible	Could result in injury or illness not resulting in a lost work day, loss exceeding $2K but less than $10K, or minimal environmental damage not violating law or regulation.

The full FHA developed for THOR was placed in Appendix 1. A shortened version is included in Table 8, in which catastrophic failures were identified. The assessment shows catastrophic failures occurring as a result of either loss of power or loss of control. When the aircraft looses power, the load control system and many aircraft systems will no longer be operable. This will result in unsafe conditions for both aircraft, as they are in very close proximity to one another. If control over the aircraft is lost during flight, a catastrophic condition can occur very quickly, if one aircraft veers towards the other aircraft or hits the spreader bar.

Table 8: Selected Hazards for the Twin-Lift System

Function	Failure Condition	Phase	Effect of Failure Condition on Aircraft/Crew	Classification
Take-Off in Twin-Lift Configuration	a. Loss of power	Take-off and Climb	Abort mission and jettison sling load	Catastrophic
Cruise with Sling Load to Destination	a. Loss of power	Cruise	Unable to maintain altitude, autorotation IAW Ops Manual, jettison load and decouple aircraft	Catastrophic
	b. Loss of control	Cruise	Cannot regain stability, jettison load and decouple aircraft,	Catastrophic

			attempt autorotation IAW Ops Manual	
Descend with Sling Load to release site	a. Loss of power	Descent	Unable to maintain altitude, jettison sling load and decouple aircraft, autorotation IAW Ops Manual	**Catastrophic**
	b. Loss of control	Descent	Cannot regain stability, jettison sling load and decouple aircraft, attempt autorotation IAW Ops Manual	**Catastrophic**

The functional hazard assessment serves as an input for the Preliminary System Safety Assessment, or PSSA. The PSSA normally takes the form of a fault tree analysis. Once the catastrophic failure modes were identified in the functional hazard assessment, a fault tree analysis was created for each mode, to identify specific failures that can cause the hazards identified in the FHA.

Fault Tree Analysis

Two fault trees were developed in response to the functional hazard assessment. Fault trees assist in identifying specific causes of failure. A fault tree was created for the two modes of failure identified in the functional hazard assessment; loss of aircraft power and loss of aircraft control. The fault tree for loss of aircraft power is shown in Figure 72. Loss of power can result from an electrical system failure, or a power train failure.
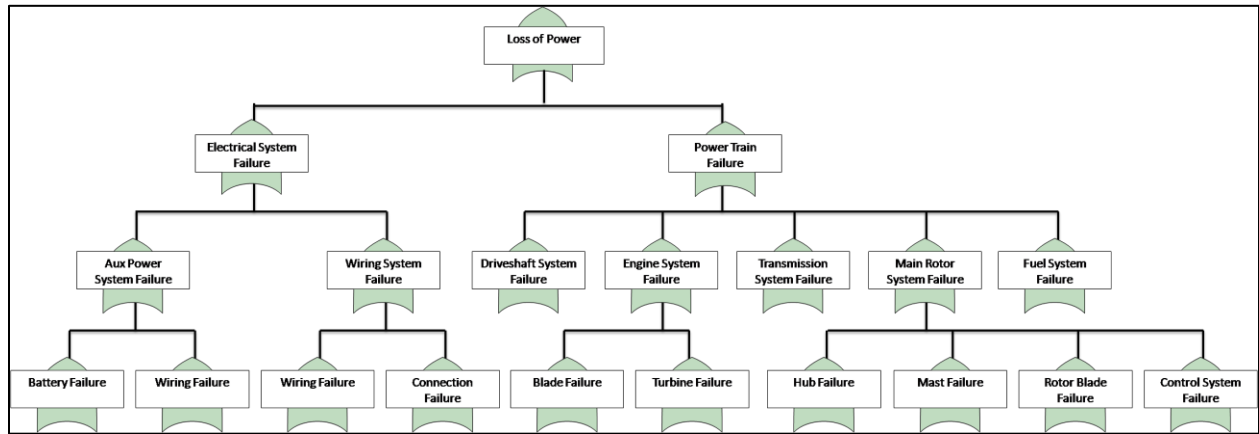
Figure 72: Fault Tree - Loss of Power

A fault tree for loss of control is shown in Figure 73. Loss of control can come from a failure in the flight control system (FCS) or in the main rotor system. The FCS has both electrical and mechanical components, as is shown in the figure. Although the main rotor system may not often be thought of as a control system, the main rotor is responsible for providing aircraft lift and control, via manipulation of the blades.
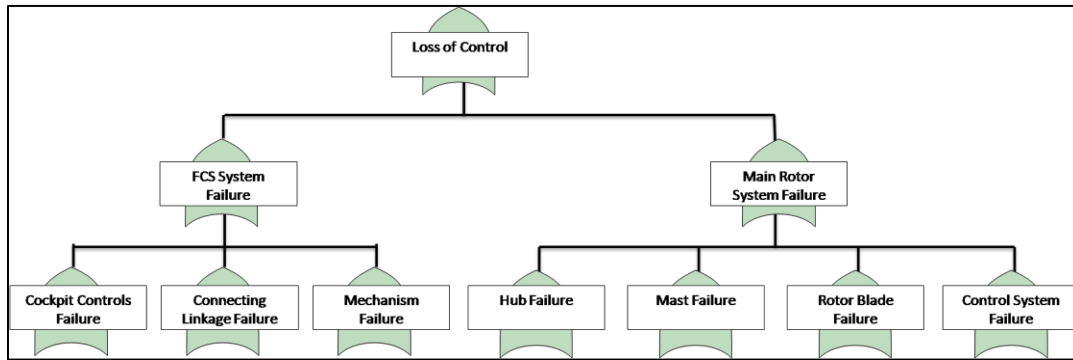
Figure 73: Fault Tree - Loss of Control

Risk Mitigation

An important part of the safety process involves risk mitigation. Risk mitigation involves reducing mishap risk to an acceptable level. Since catastrophic failures were identified in the FHA, this section focuses on mitigating these risks by implementing an additional safety system.

In order to mitigate the possibility of a catastrophic failure in an emergency situation, there are two critical safety considerations. First, the two aircraft are in close proximity to one another, and physically connected by a spreader bar and cables. Second, the aircraft are flying with a significant sling load. In the event of an emergency, the aircraft need to be separated from each other as well as from the load. To accomplish this, an emergency load release system (ELRS) was developed. This system allows for the aircraft to be separated from each other and the heavy sling load by disconnecting the cables tethering each aircraft to its respective side of the spreader bar. The ELRS is discussed in-depth in the next section.

Safety System	Feature	Safety Effect
Emergency Load Release System (ELRS)	Automatic jettison of the spreader bar and load.	Allows for safe separation of the aircraft from each other and the payload in an emergency situation.

Emergency Load Release System (ELRS)

The twin-lift system may suffer catastrophic failure if unstable flight conditions develop. The controls system and load stabilization system have been designed to mitigate and prevent dangerous situations, but the risk of unstable flight cannot be eliminated entirely. In such cases, it is necessary to quickly and effectively jettison the payload and spreader bar to regain aircraft stability.

There are several ways that the load can be jettisoned. Two manual release mechanisms are onboard each aircraft. A release switch that controls the center cargo hook is located in the cockpit of each helicopter. The switch opens the center cargo hook and releases the spreader bar and load. A separate load release lever is located in the cargo bay adjacent to the cargo hook. This lever also opens the hook and the load is released in a similar fashion. In some cases flight instability occurs too rapidly to depend on manual release systems.

Simulation indicates that the load must be released automatically when the system undergoes severe load oscillation. Stable flight is possible as long as the swinging is limited to 30°. At this point, the oscillations are critical and may result in a crash. A release mechanism independent of the controls system that releases the load when the load reaches this critical angle is required to prevent to save the aircraft and the lives of crew.

When the load oscillates, it is necessary to quickly release the load and spreader bar. The spreader bar must be released with the load because it is dangerous for the two helicopters to remain connected after the load is removed. The emergency release system must allow both helicopters free to take all necessary steps to regain stability as soon as it is activated. Therefore, the release system must cut the rope running from each helicopter to the spreader bar.

The emergency release mechanism used relies on a patented cable cutter to cut the rope. It consists of three parts:

- Cable Cutter
- Inclinometer
- Battery Supply

One release mechanism must be placed on each end of the spreader bar. An electrolytic inclinometer is placed on the each end cap of the spreader bar. This instrument measures the angular displacement of the oscillating system from gravity. Electrolytic inclinometers, such as those manufactured by Rieker, are compact and lightweight enough to be placed on the spreader bar. The instrument is capable of measuring angles with an accuracy of ±0.5° and a resolution of less than 0.03°. Digital output from the instrument is transmitted through two wires to the cable cutter. The wires must be sufficiently insulated to protect them from environmental damage.

The cable cutter is a cylindrical tube 13 inches long with a radius of 3.125 inches. Two pressure cartridges are at each end of the tube. Inside the tube, there are two independently propelled pistons attached to a flat metal plate. The metal plate has a circular hole through it, and sharp blade is placed around the edge of each hole. The cable from the helicopter to the spreader bar is run through a hole in the midpoint of the device. This hole is in line with the hole on the metal plate. Therefore, the rope runs through the two piston-operated blade pieces. The rope exits the device through a hole provided at the bottom of the release device. Each pressure cartridge receives input from the electrolytic inclinometer, so the two blades are independently operated. Power to the inclinometer and the pressure cartridge is provided by a battery supply located in the spreader bar. For redundancy, two independent battery supplies may be installed. If one supply fails, then the other battery supply can provide the power required to operate the system.

When the inclinometer senses severe load oscillations in excess of 30°, the emergency load release system is activated. The angular oscillation information is processed by the pressure cartridges via the wired connection previously mentioned. Each pressure cartridge is activated when unsafe oscillations are reported by the inclinometer. The pressure cartridge increases the pressure in a small cavity inside

the cable cutter. This sudden pressure increase forces each piston to accelerate away from the pressure cartridge. As the piston accelerates, the sharp blade slices the rope connecting the helicopter to the spreader bar. There are two independent pressure cartridge-piston systems. If one cartridge or blade fails, then the other blade will still safely sever the rope. After successful implementation of the emergency release mechanism, each helicopter will carry only an 11 foot rope. The sudden recoil force may accelerate the rope toward the helicopter, but it is not long enough to strike any rotors or engines. Pilots authorized to operate missions using the heavy lift system must be trained to properly respond to the forces associated with sudden loss of weight due to load release.

The emergency load release system must be maintained regularly. The pressure cartridges used to propel the pistons must be replaced at regular time intervals to ensure normal operation. Also, both battery supplies must be tested prior to every flight.

System Certification

This system design can be thought of as an aircraft modification, in which an improved capability was added to the aircraft. Because this modification impacts safety of the aircraft and crew, it requires airworthiness qualification. Techniques used during the qualification process include testing, analysis, modeling, and similarity.[18]

Table 9 lists the applicable requirements for this system to obtain airworthiness certification[20]. Implementing THOR involves modifying the aircraft avionics, as well as adding additional external load capability. For this reason, airworthiness requirements for structures, avionics, and electrical systems were listed.

Table 9: Applicable Airworthiness Criteria

4.0	Systems Engineering	9.0	Crew Systems
4.1	Design criteria	9.2	Crew Stations & Aircraft Interior
4.2	Tools & Databases	9.4	Human Performance
4.3	Materials Selection	9.8	Air Transportability & Airdrop
4.4	Manufacturing & Quality	11.0	Avionics
4.5	Operators & Maintenance Manuals/Technical Orders	11.1	Avionics Architecture
4.6	Configuration Identification	11.2	Avionics Subsystems
5.0	Structures	11.3	Avionics Air Vehicle Installation
5.1	Loads	12.0	Electrical System
5.2	Structural Dynamics	12.2	Electrical wiring system, including power distribution
5.3	Strength	13.0	Electromagnetic Environmental Effects (E^3)
5.4	Damage Tolerance & Durability	13.1	Component/subsystem E^3 qualification
5.5	Mass Properties	14.0	System Safety
5.6	Flight Release	14.1	System safety program
6.0	Flight Technology	14.2	Safety design requirements
6.1	Stability and control	14.3	Software safety program
6.3	Aerodynamics & Performance	20.0	Other Considerations
8.0	Air Vehicle Subsystems	20.1	Mission/test equipment and cargo/payload safety
8.10	External Cargo Hook Systems		

As shown in Figure 74, the twin-lift system was designed with a 5 year qualification plan, with the system fully implemented by the close of calendar 2014. A Significant milestone includes the configuration control board review, in which the modification design is reviewed and approved or

disproved. Also significant is the airworthiness qualification of the system. Once the system is deemed airworthy, production can begin.
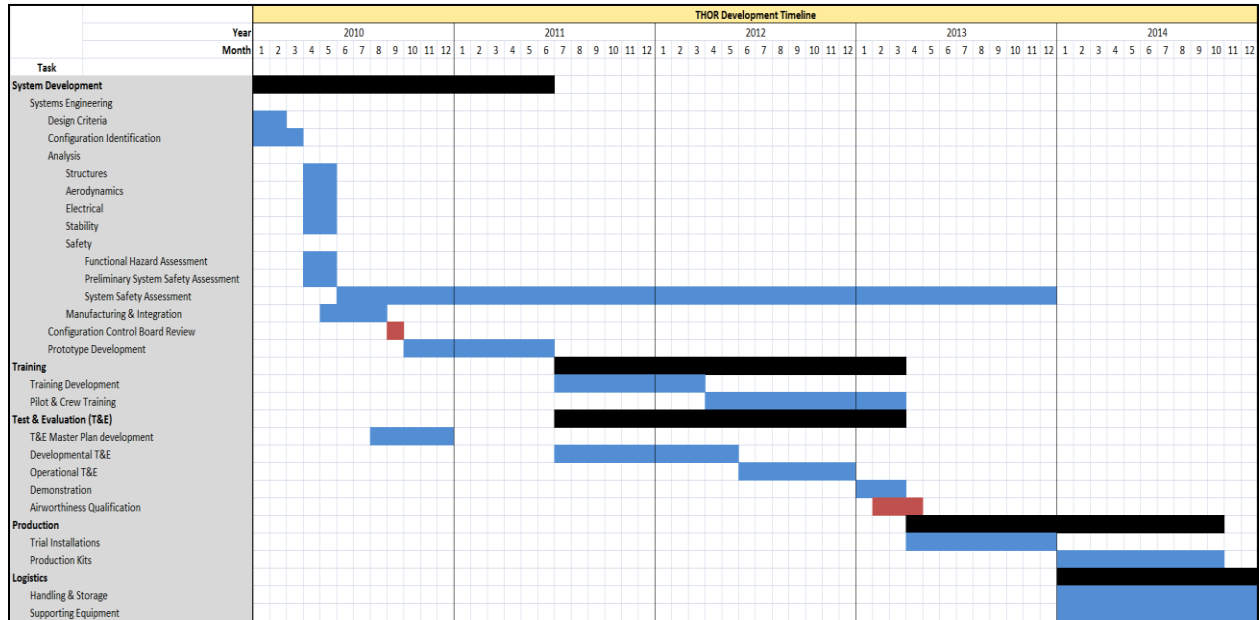
Figure 74: Twin-Lift System Development Timeline

Lift Improvement Flight Test

Introduction

In addition to the multi-lift system design task above, the RFP required that teams design and perform an experimental flight test in order to simulate the process of technological testing and evaluation. While completing this task, team members go through one small step of the same process that actual aerospace engineers undergo while they are trying to take their proposed system off the drawing board and onto the flight line. The methods used to develop this flight test experiment are the same as those used to create the tests and evaluation which every aircraft must undergo before taking to the sky.

Requirements Analysis

In order provide insight into the process of designing flight tests, the RFP instructed that we design, organize, and carry out our own flight test on an off-the-shelf remote control helicopter. We were required to devise an experiment to test the lift of the helicopter while in hover and then make a modification to the helicopter provide at least a 5% increase in lift. The helicopter was required to have a rotor diameter of at least thirty inches, and could be either gas-powered or electric. Prior to carrying out the experiment, we needed to perform a thorough analysis showing that the planned helicopter modification would indeed provide the necessary lift improvement. Then, after the successful completion of the flight test, the recorded data would be compared to the theoretical values from the analysis and conclusions would be drawn.

In addition to the requirements set by the RFP, during the process of developing our flight test, we came up with some goals of our own to ensure that our flight test was the best experiment we could perform. We wanted to record the most accurate and reproducible data that we could in order to guarantee the most precise results and conclusions possible. We also set the goal to be finished with all of the testing within a month of starting to plan the test so that we would be able to properly focus on the design task of the competition. Even though the RFP stated that up to $500 would be provided as reimbursement for any funds used for this test, we set a goal to keep expenses to a minimum, as we believe this accurately portrays situations in the real world. Our final and singularly most important personal goal was to ensure the safety of all team members and equipment to the best of our ability at all times during our flight test. With these goals in mind and the requirements set by the RFP, we set out to plan our flight test.

Planning

The first step in planning our flight test was to do some brainstorming and develop some ideas for our experiment. The first three big decisions we had to make were which helicopter to use, what modification to make to provide at least a 5% increase in lift, and how exactly to measure the lift and power of the helicopter. Once we had a good idea of what we wanted to do for our flight test, we performed an analysis to calculate the theoretical change in lift that our chosen modification would provide. Once these steps were complete, we would be ready to work out the last few details of our flight test and begin the testing process.

Helicopter Selection

The first decision we had to make was which helicopter to use for our flight test. Using the RFP requirement of a 30 inch rotor diameter as a starting point, we started investigating our options. We decided to talk to some of the professors at the Georgia Tech UAV lab about using one of their helicopters for our flight test. They had two helicopters that we seriously considered: the GTMax and a Mini 500. GTMax is a very large fully autonomous gas powered helicopter, and the Mini 500 is a large gas powered helicopter that requires a trained pilot. Both the GTMax and the Mini 500 had built in sensors to monitor and record the power produced by the motor as well as blade pitch. Unfortunately, none of the electric powered helicopter at the UAV lab fit our needs, and when we learned of this, the professors of the UAV lab referred us to Adaptive Flight Inc. (AFI) to ask if they had an electric helicopter that we might be able to use. Their Logo 500 had the capability to record the power generated by its motor, and was small enough to fly in an indoor facility. Our final option was to purchase a new helicopter for the test.

Once we had a couple of options to choose from, we started going through the goals we set for ourselves to try and make the best choice. Based on our goal to keep the flight testing as affordable as possible, we decided that buying our own helicopter would be the last resort. Since we set a goal to keep our data as accurate and reproducible as possible, we decided that we would prefer to test in an indoor environment to eliminate the wind as a source of random error. Because of the exhaust that is produced by gas powered helicopters, they need to be operated outdoors. That left us with either the

Logo 500 or brand new helicopter, so we started looking into the details of doing our flight test in conjunction with AFI.

We set up a meeting with the owner of AFI, Henrik Christophersen, to talk about the details of the flight test. One issue that came up during our meeting with Henrik was his concern for how large, expensive, and difficult to fly the Logo 500 was. None of our team members had enough practice flying helicopters to feel comfortable flying such a complex helicopter in a confined space, so we hired AFI's professional remote control helicopter pilot to fly it for us. Once that was settled, we decided that the Logo 500 would be perfect for our test and finalized the first step of our flight test.

Testing Methods

The next step was to determine exactly what we would be measuring during our flight test and the method in which we would be measuring it. After consulting with some of our professors, we came up with a short list of possible testing methods. The first idea we came up with would be simply load the helicopter with weight until it could no longer lift off the ground and maintain a stable hover. However, operating a helicopter near and possibly over its maximum gross weight is extremely unsafe. Operating the motor at its maximum setting over the course of several tests could easily cause irreparable damage to the motor, and operating a helicopter with little to no excess power could cause the pilot to lose control and crash the helicopter. We decided that even though this testing method would prove without a doubt what the helicopter's max payload was, it would be far too risky to try and perform. Another testing concept briefly considered was to attach the helicopter to a force scale and have it pull at maximum thrust; however this idea was quickly scrapped as it would be even more dangerous than the first.

After talking with AFI's pilot about our test, he told us about the Eagle Tree data acquisition system that was installed on the Logo 500. The Eagle Tree allowed us to record the voltage and amperage drawn by the motor of the helicopter during its flight, from which we could find the power output. By adding certain amounts of weight to the helicopter (which are well below the maximum payload weight) and recording the power required to maintain hover, we would be able to generate a plot of the power required to maintain certain amounts of weight, and then compare the curve from the baseline helicopter setup with the curve generated after the helicopter modification is made to see how much of a lift increase the modification produced. This testing method would be very safe because the helicopter would never be operating near to its maximum payload, so it would remain easily controllable to avoid any crashes and significantly reduce the chance to cause any damage to the motor. We decided that this would be the testing method we would use based on this level of safety. Now, the last major decision left to make was how to modify the helicopter to provide a 5% increase in lift.

Helicopter Modifications

Once we had a method for testing our chosen helicopter, we needed to find a way to modify the helicopter in order to increase its lifting capacity by 5%. We formulated several concepts for increasing lift. The first idea we came up with was to change the rotor blades, either by changing the length or the airfoil shape. This concept would be easy to test because the rotor blades of a Logo 500 only take about

a minute to change, and AFI already had a set of symmetric and semi-symmetric blades; however, this concept would be very difficult to analyze due to the lack of airfoil data for these blades. Another concept we thought of in order to increase the lift was to try a different fairing to help reduce the induced drag, however alternate fairings were not readily available and the effect of the fairing was not believed to have enough of an effect to cause a 5% change in lift. We thought to possibly add another small source of lifting power, but AFI did not want us to make permanent modifications to their helicopter.

The last idea we had was to change the motor pinion in order to change the gear ratio which in turn would change the RPM of the main rotor. This was a relatively simple process which could be done quickly to help keep the flight test moving, and AFI already owned several pinions which would help keep costs down. Finally, the effect of changing the RPM of the main rotor on the power required would be relatively simple to calculate, keeping the complexity of both the theoretical analysis and data reduction to a manageable level.

In the end, we decided to examine the effect of changing the motor pinion as our primary source of increased lift, and began to perform a full theoretical analysis on the effect of an RPM change. However, we were also curious about how much of an effect changing the rotor blades would have on the lift of the helicopter, so we decided to also include blade changes in our flight test and data analysis, but not as part of the theoretical pre-experimental analysis.

Now all three of the major preliminary decisions had been made, the next step was to go into a full theoretical analysis of our chosen helicopter, test method, and modification choices, the results of which can be found in the following section.

Theoretical Analysis

Once we developed a good idea of our baseline helicopter choice, testing procedure, and helicopter modification, the RFP required that an analysis be performed to show that the theoretical lift increase of our modification should indeed be at least 5%. This analysis was important to our flight test because it helped verify that the testing methods we had chose would actually yield the results we were looking for. The initial analysis helps eliminate possible testing methods which would not provide a 5% lift increase, which would take significantly more time and resources to determine experimentally.

Pinion Change Theory

The primary modification that we intended to perform on our helicopter was a change in motor pinions. The baseline helicopter setup consisted of an engine that operated at a constant speed of 19,800 RPM. The engine was connected to a motor pinion with 13 teeth, which in turn spun the main rotor pinion which had 153 teeth. This baseline setup yielded a gear ratio of 11.77:1, which rotated the main rotor at a speed of 1682 RPM. The purpose behind changing the motor pinion was to change the rotational speed of the main rotor. By changing from the baseline motor pinion to a new 17 tooth motor pinion, we changed the gear ratio to 9:1, which produced a main rotor speed of 2200 RPM.

Once we knew the speeds at which the main rotor operated with both motor pinions, we were able to calculate the coefficient of thrust using the following equation from basic rotorcraft power analysis:

$$C_T = \frac{T}{\rho(A)(\Omega R)^2}$$

C_T is the coefficient of thrust, T is thrust, ρ is the air density, A is the area of the rotor disc, Ω is the rotational speed of the main rotor, and R is the rotor radius. If we set the thrust equal to the weight of the helicopter, we can find a value for C_T of the aircraft when it is loaded with different amounts of weight. Once we know the coefficients of thrust, we can use it to find the coefficients of power required to lift the helicopter and any additional weight using the following equation:

$$C_{p,req} = C_T{}^{3/2} + \frac{\sigma C_d}{8}$$

$C_{p,req}$ is the coefficient of power required and C_d is the coefficient of drag of the helicopter. The results of these calculations as well as the decrease in power required when changing from the baseline 13 tooth motor pinion to the 17 tooth motor pinion can be seen in Table 10.

Table 10: Theoretical Power Calculations

13 tooth		
Weight (g)	Ct	Cp
0	0.002312	0.00010421
358	0.002492	0.00011357
895	0.002762	0.00012825
Average	0.002522	0.00011534
17 tooth		
Weight (g)	Ct	Cp
0	0.001352	6.0754E-05
358	0.001457	6.494E-05
895	0.001615	7.1505E-05
Average	0.001475	6.5733E-05
$C_{p,req}$ **Decrease**		
Average	70.995%	

Blade Change Theory

The secondary method of increasing the lift produced by our helicopter that we considered was to change the airfoil of the rotor blades. AFI possessed a set of symmetric rotor blades and a set of semi-symmetric rotor blades, and we wanted to explore the effect of switching between the two. Without knowing the exact airfoil cross-section of the blades we used, it would be very difficult to create a quantitative analysis with any degree of accuracy. However, by looking at graph in Figure 75, we can see

that two rotors whose only difference is the shape of their airfoil can have significantly different values of C_T for the same figure of merit. Once the shape of the airfoils are known, the C_T can be found, from which the $C_{p,req}$ can be found in the same as in the pinion change analysis.

Since we did not have the airfoil data, we did not perform this theoretical analysis, however we decided to test the effect of the blades anyways to see how they compared qualitatively with results such as those in Figure 75.
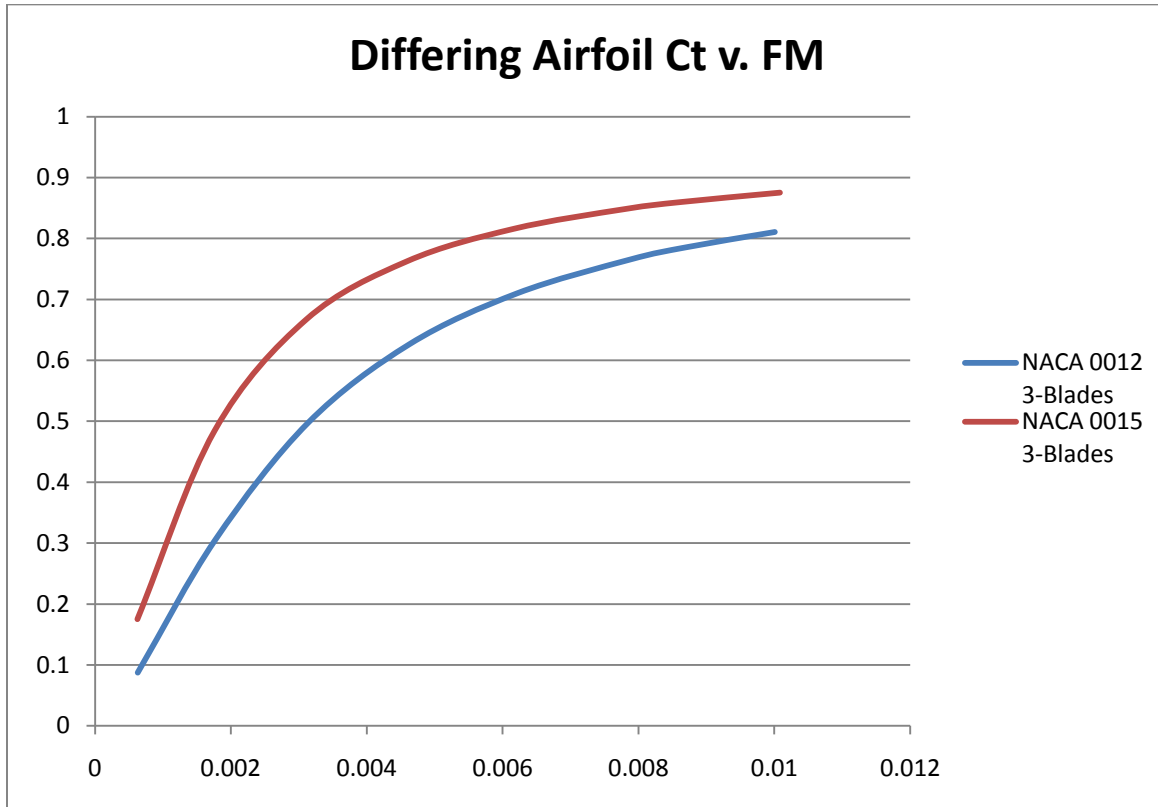
Figure 75: Example Effect of Airfoil Change

Procedure

When laying out the procedure section, we wanted to make sure we obtained the best data possible. In order to get good data, we knew that we had to have a good pilot to fly the helicopter, a good location to fly it in, and a testing order that would not disturb the results. For this reason, we carefully chose our pilot, flight location, and test order. If each mentioned point was not taken into careful consideration, we risked introducing multiple known and unknown factors that could significantly change the data. As a result, we feel that we got very reliable data with a low budget within a relatively short period of time.

Pilot

One of our main considerations was focused around flying the helicopter with a strong consistency. This meant that we must have a consistent pilot maintaining consistent flights. Before we completed selecting our baseline helicopter, we had 3 options for our pilot: learn ourselves, hire a pilot, or use an

uninhabited aerial vehicle (UAV) control system. Obviously, learning to fly a midsized professional helicopter was a daunting task, even for those of us with prior RC helicopter experience. Learning to fly ourselves also made flying with consistency even more of a challenge. Using a UAV system was a reasonable option. The UAV would give very consistent control and promised reasonable feedback within the realm of data. The main difficulty was finding a UAV outfitted helicopter and finding a reasonable location to allow the helicopter to be flown. This is because we did not feel totally comfortable allowing the UAV to command the helicopter within the relatively small constraints of an indoor room.

Fortunately, when we selected our helicopter, we were also provided a pilot. The company that we rented the Logo 500 from, Adaptive Flight Inc. (AFI) specializes in UAV helicopters. Yet, we did not use the UAV capabilities to maintain level flight. Instead one of their highly trained and highly experienced pilots fulfilled the need. We chose to use the pilot because we wanted to fly the helicopter indoors, further discussed in the next section, and both our team and AFI only felt comfortable with their professional pilot flying for the tests.

One of the main concerns with using a human to fly was whether or not we would get the consistency that we demanded. After researching the situation, and talking with the pilots and employees at AFI, we came to the conclusion that for a simple hovering maneuver, the pilot would be able to hold the helicopter as steady, if not steadier than the autopilot system. He mentioned that the main instance where the automated flight control would be more beneficial is when flying in a wind, and since we would be flying indoors, that would not be an issue.

During the flight tests, the pilot did indeed hold the helicopter at a consistent height and location for each individual test. We were able to confirm this because our helicopter was equipped with reflective tape that enabled it to be tracked in our specially equipped facility. It was clear that the helicopter maintained flight in an area of around a meter. Also, we were certain to keep the helicopter at just over 2 rotor diameters above the ground to nullify the in-ground effects.

Furthermore, because the pilot was very knowledgeable about the helicopter, he was able to provide other suggestions to keep our tests similar. For instance, he knew when to charge the battery and for how long to charge it so that the voltage remained fairly consistent (Volts were also recorded to show this trend). Also, when assisting us in modifying the helicopter by switching out the rotors and pinions, he consistently tightened the rotors the same amount as well as made sure all settings remained the same. Overall, using the professional pilot to fly the helicopter was very beneficial for many reasons.

Testing Location

Similarly to the pilot selection, our primary factor in determining where to test was maintaining the flight conditions. Changes in temperature, wind, or even humidity could alter the results depending on the amount of change. This would be especially true if we were not able to complete all of the flight tests within one period of time. We classified all of our options into 3 categories: outdoors (open field), small indoor room, or large indoor room (such as a hangar or gym.) The main advantage to flying

outdoors was that the space was basically unlimited. With unlimited space, we would be able to fly either by hand or by autopilot. Also, flying outdoors allowed us to use a gas, nitro, or electric helicopter. Unfortunately, flying outdoors would introduce multiple unnecessary variables such as wind and temperature change. The best way to get around this problem would be to fly early in the morning or in the evening when the conditions were calm and steady. Overall, flight conditions outdoors were highly unrepeatable. Flying indoors certainly eliminated this problem. There would be no wind and a negligible amount of temperature change. The only difference between flying in a small room and flying in a hangar is that the small room is equipped with a tracking system. The downside to flying in a small room is that we cannot fly with the UAV system and the limited space requires lower flight for safety.

After weighing our options, we felt that the best location for flight testing would be in a small indoor room. Specifically, we used a room located in one of the Georgia Tech Aerospace buildings known locally as the Indoor Flight Facility (IFF). The IFF is a relatively small room sizing with a width of around 35', a length of around 25', and a height of around 20'. Because the IFF is currently used by the institute for rotorcraft flight testing, it had been previously equipped with a Vicon Motion Capture system. The system works by emitting red light from numerous locations and tracking where the light is being reflected off of the object of interest. Also, because the room is indoors, we assured no wind and no significant temperature change.

Because of the small size of the IFF, and relatively large size of the helicopter, safety was a primary concern. Obviously, no one could be in the room at the same time as the testing. To overcome this, we installed a large sheet of Plexiglas in the doorframe to stand behind and observe the helicopter.

The IFF was also a very good choice for planning for unexpected circumstances or for the event that errors could occur. This was especially true in the early stages of our planning when we did not know approximately how long the testing would take or how many tests we would have to do. Beyond that, we knew that if the data collection process did not go as well as expected then we would need return and take more data. Not only was this planning important in the case that errors occurred or the time was longer than expected, but we also did not know how long the pilot and the helicopter would be available. If the pilot was only available for 1-2 hours, then we would most likely need to do testing on multiple days. If multiple days were required, then we needed for the conditions to be the exact same on both days. For instance, if we were outside and one day the temperature was 58 degrees Fahrenheit, and the next day it was 72 degrees Fahrenheit, then the data would show that the helicopter had much more lifting capability on the first day. With the IFF on the other hand, we knew that if testing had to be split up between multiple days then we would return to the same climate controlled room without wind. Fortunately, we were able to do all of the testing over a few hours on one day without having to return for more testing.

Testing Order
The order in which we performed all of the different tests was also very important in order to neutralize error from factors that were not accounted for. The order was especially thought through thoroughly because we were testing for lifting capability increases due to two different modifications. Because we

had separate modifications, we wanted to be sure that we identified which modification was responsible for the change in lifting capability. Beyond this, we wanted to ensure that as the voltage dropped and rose between charging that the data was not overly skewed.

As previously mentioned, the most important part of ordering the flight test was ordering it such that we were able to distinguish between the lifting capability change due to RPM change, and the lifting capability change due to rotor blade change. To do this, we ran the first half of all of the tests only with the 17 tooth pinion at 2199.6 RPM and then ran the second half of the tests with the 13 tooth pinion at 1682.1 RPM. Within each of the defined RPM sections (the 13 pinion section and the 17 pinion section), we adjusted the load and the blade type. All of the runs can be viewed in Table 11. As seen, for every run that was done in the high RPM section, the run exists in the same format under the low RPM section. This means that for every data point studied under the high RPM, there is a respective data point under the low RPM.

Next, we had to switch out the blades from the symmetric to the semi-symmetric type. Within each RPM speed, there are 6 runs for each type of blade. Notice that for each weight the blade style is not always ordered with the symmetric blade first. This is for two reasons. The first reason was simple practicality – it is easier to leave the current blade on then switch it out after every weight change. This is very important for saving time and money. The second equally important reason is that it helps balance out the voltages. Although we did record the voltage output to be able to recognize the drop, it is still very important to try to neutralize it as much as possible. When the blades are alternated, the level of the battery voltage is alternated as well. This actually proved to be a good decision after data analysis because our data showed that even though we recorded the voltages and took them into account, there still seems to be a trend in lift capability based upon the level of voltage.

The final parameter to change was the load levels. Unlike the blades, the loads were actually fairly difficult and time consuming to attach and detach. For this reason, they were alternated less often than the blades. Also, as seen in the Table, the loads were increased for the first half of the tests on the high RPM and then deceased on the low RMP. In other words, the helicopter starts with an empty load and ends with a full load for the high RPM, and starts with a full load and ends with an empty load under the low RPM setting. This is done for similar reasons to the pattern of the blades where they do not alternate consistently in a pattern format. First, it was easier to leave the entire load attached after the first half of the tests then to remove it and go back and reattach the weights. Second, it again reverses any tendency that would be formed by a drop in voltage.

Also, we ran each test twice. Meaning, after taking off and hovering for 45 seconds, we set the helicopter back down, slowed the blades, and took off again. We did this to prove the recorded data for each run to be repeatable. Also, this allowed us to gain extra data to create a more perceptive average. The extra data allows us to have more data as back up data as well. There is always a chance that we could have outliers within a certain section. In that case, we have other data to replace the recorded data with. Finally, the redundancy was again used to detect any changes due to voltage depreciation. We did not draw much if any of a correlation of voltage drop between each load.
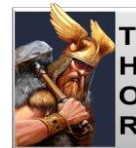
The battery was recharged partially between each weight change and was recharged fully during the motor pinion change. It is important to note that the battery was recharged to the same voltage during each load change. Similarly, when recharged to a full voltage, it was recharged to target value that the battery is always fully recharged to. The voltage is discussed in more detail under the execution section.

The testing order used proved to be very good for the limited time and resources that we had. All of the data recorded was very dependable and gave us a lot of insight based upon the order used. If we had more time and/or manpower, we would have run the tests at a larger range of loads, added on an extra RPM class, and run more tests to remove discrepancies due to voltage loss. In fact, our original test plan included extra weights and a 14 tooth pinion, but due to time the extra runs were cut out.

Table 11: Design of Experiments

Run	RPM	Load (g)	Blade	Re-run?
1	2199.6	empty	Sym	n
2	2199.6	empty	Sym	y
3	2199.6	empty	Semi	n
4	2199.6	empty	Semi	
5	2199.6	358	Semi	n
6	2199.6	358	Semi	y
7	2199.6	358	Sym	n
8	2199.6	358	Sym	y
9	2199.6	895	Sym	n
10	2199.6	895	Sym	y
11	2199.6	895	Semi	n
12	2199.6	895	Semi	y
13	1682.1	895	Semi	n
14	1682.1	895	Semi	y
15	1682.1	895	Sym	n
16	1682.1	895	Sym	y
17	1682.1	358	Sym	n
18	1682.1	358	Sym	y
19	1682.1	358	Semi	n
20	1682.1	358	Semi	y
21	1682.1	empty	Sym	n
22	1682.1	empty	Sym	y
23	1682.1	empty	Semi	n
24	1682.1	empty	Semi	y

Execution

After the detailed planning and theoretical analyses, we were able to complete the flight tests. Overall, the flight tests went as expected and in many instances were better. We also noted the specifics of the runs as well as the conditions in which the flight tests took place. Although the actual testing was very similar, the differences are important to note.

Testing

Once we gathered our flight team in the IFF room we began our testing. Our first step in the testing was to prepare the VICON motion capture system to recognize the helicopter. To do this, we attached multiple magnetic spheres that were coated in a reflective material that are seen by the motion capture system. The system was not only able to detect translational motion, but also yaw, roll, and pitch, although we had no need to utilize the extra capabilities. On the other hand, the motion capture system worked very well for recognizing where the helicopter was at all times. We were able to gather valuable data to show the consistency and stability of our manual hovering.

The helicopter was prepared for flight totally by the professional pilot. He went through all of the standard procedures to make sure the helicopter would operate with optimal settings. He also made the note to tell us that the Logo 500 helicopter operates like most large helicopters in the sense that the lift created by the rotors is mainly controlled by the blade pitch. Once the throttle was at a designated stick position, the helicopter reached its operating RPM. The operating RPM is of course dependent on the battery voltage, the number of motor pinion teeth, and the number of main rotor teeth. Anything above half throttle increases the angle of attack of the main rotors. It is important to note that as we spun the blades to the operating RPM, there was a clear audible difference in the frequency of the sound created by the two separate motor pinion RPMs. This is pointed out in the provided flight test video.

Along with this issue, we tried multiple methods to measure the in-flight RPMs. The first attempt to measure the RPM was done by an optical analog tachometer known as a stroboscope. The stroboscope works by spinning a disk that allows the view to be seen at a given frequency. When the stroboscope appears to cause the blades spinning in the viewfinder to stop spinning, we know that they are spinning at the same frequency and RPM of the stroboscope and hence the RPM is known. Unfortunately, the disk in our stroboscope quit working and we were unable to use this method. For the second attempt, we had a digital tachometer that works simply by optics and a laser. In order for this to work the operator has to be within a certain distance. We attempted to use the tachometer from just outside the door, but it was unable to correctly detect the RPM. For a final attempt, we went relatively close to the helicopter and throttled it up while keeping the blades at a negative angle of attack. Unfortunately we still were unable to get close enough to get dependable data. Instead, we used a relationship between our motor and the voltage output to determine the operating RPM for each pinion.

The actual hovering scenarios went very well. Our pilot was able to lift the helicopter off of the ground into the same spot and hold it with extraordinary consistency. Also, he was able to hover the helicopter at a high enough height so that it could be within reason considered to be flying in out of ground effect (OGE). This was at around twice the rotor diameter off of the ground. Once hovering, the helicopter

experienced very little bouncing, which would surely cause oscillations in the data. As mentioned before, the flight consistency can be seen in the data recorded by the Vicon system as well as the video provided.

The weights used were first massed on a scale with accuracy to the tenth of a gram. Each weight was weighed and recorded before being attached to the helicopter. Two of the weights were attached securely to the side of the landing skids. They did not shift or vibrate significantly during flight or between flights. Another two of the weights were securely positioned in the battery department with the battery. Again, they did not shift or vibrate during flights. The thin wire used to hold the weights to the helicopter is factored out and considered to be a part of the empty weight of the helicopter.

Miscellaneous

As mentioned within the "testing" order section, the battery was charged intermittently between the runs. Specifically, we charged the battery after each set of four runs. During the runs, the battery was only drained around half way (and slightly more for the heavier loads.) After each of the runs, we would return the battery voltage to a general amount to provide enough voltage for the next four runs. Also, after we finished all of the testing on higher RPM value, we charged the battery back to full. We were able to control the amount of charge being put into the battery and monitor the voltage with the professional battery charger. Before the first run and before the second set of runs with the 13 tooth pinion, we charged the battery to around 22.75 volts.

The room temperature was right around standard temperature at 71 degrees Fahrenheit.

Results

Once the testing was complete, we were ready to analyze the recorded data and determine changes in available lift due to the modifications made. We approached the results from multiple angles to gain as much perspective as possible on how our modifications changed the lift capability. We looked at the change in amperage drawn, the power used, and the coefficient of required power. Our ultimate goal was to compare the coefficients of required power because of the direct relation to thrust. The provided tables and graphs are intended to provide an abundance of insight as to how the maximum lifting capability changes under different scenarios.

Data

As mentioned within the testing method section, we used an Eagle Tree tool to record data. The Eagle Tree data chip is attached as a bridge between the battery and the leads to helicopter's onboard controller. It is simply used to measure the amperage drawn by the helicopter as well as the pack volts held by the battery at the given time. The Eagle Tree was set to record the data every 25 milliseconds, or 40 Hz. This was certainly a high enough frequency to gain ample data over a 45 second testing period. After every four flights, we took the Eagle Tree data and uploaded it to the computer. Once the data was taken into the Eagle Tree program, we were able to generate instant plots for visual analysis as well as some basic analysis.

Fortunately, the data stored by the Eagle Tree program was comma and space delimited, so we were able to import all of the data into Microsoft Excel. We needed to put the data into Excel to be able to analyze properly and present the data in a useful fashion. For this reason, Excel was used for all data reduction. Also, since there was a large amount of useless data from takeoff, landing, and between flights, we first used Excel to remove all of the unusable data. The useful data was recognized with the plots created by the Eagle Tree program and then associated with the data stored in the respective Excel file. Eventually, all of the data was broken down and separated into the useful data for each run. Figure and **Figure** show sample data captures from tests and include information on watts, current, and voltage that was gathered using the Eagle Tree program.

Data Reduction

After we had separated the useful data for each run, we were prepared to reduce and analyze the data. Because our ultimate interest was not how the power changed within each run, but rather what the required power was as a whole per run, we first took the average of the amperage and pack voltage for each run and its respective rerun. All of the average amperages (Amps) can be seen in Table 12. We also multiplied the pack voltage by the amperage to find the average power (in Watts) used during each run. The average powers for each run can also be viewed in Table 12.

Table 12: Amperage and Voltage per Run

Run	RPM	Load (g)	Blade	Amperage (A)	Power (Watts)
1 & 2	2199.6	empty	Sym	27.93822006	624.7200433
3 & 4	2199.6	empty	Semi	27.43785112	605.4489244
5 & 6	2199.6	358	Semi	28.9738354	649.4308447
7 & 8	2199.6	358	Sym	29.2145961	640.8699201
9 & 10	2199.6	895	Sym	31.29213068	682.6733299
11 & 12	2199.6	895	Semi	31.24153846	671.7308582
13 & 14	1682.1	895	Semi	21.19494649	477.8341573
15 & 16	1682.1	895	Sym	21.36293553	473.1262483
17 & 18	1682.1	358	Sym	22.77707278	510.9885424
19 & 20	1682.1	358	Semi	22.75523929	501.483387
21 & 22	1682.1	empty	Sym	25.43965861	566.8641088
23 & 24	1682.1	empty	Semi	25.56070106	558.8989103

Once we found the respective power output for each run, we did a preliminary analysis to study the differences in power used for each scenario. The preliminary analyses consisted of finding the percentage change in power used between the 13 tooth pinion gear and the 17 tooth pinion gear as well as the difference between the symmetric blade and the semi-symmetric blade. From our preliminary analysis, we found that the 17 tooth pinion used around 20% more power than the 13 tooth pinion. On the other hand, we found that the symmetric blades on average used about 0.47% more power than the semi-symmetric blade. Although this analysis is interesting because it shows which configurations would

drain the battery the quickest, it did not prove anything about the amount of lifting capability change between either the different pinion configurations or the different blade configurations. The used power data for the change in RPMs can be seen in Table 13, and the used power data for the change in rotor blades can be seen in Table 14. Also, a graph comparing the percentage change of the 13 tooth pinion to the 17 tooth pinion is shown in Figure 76, while a graph showing the percentage change of the symmetric blade to the semi-symmetric blade is shown in Figure 77.

Table 13: Pinion Change Summary

Percent Increases due to Pinion Change			
	Power		
	Sym	Semi	Average
0	23.51227	21.8553	22.68378659
360	21.31748	21.74958	21.53353225
1200	16.96408	16.7972	16.88063583
Average	20.59794	20.13403	20.36598489
	Amperage		
	Sym	Semi	Average
0	24.13638	22.14064	23.13850707
360	21.38744	22.11003	21.74873809
1200	16.96408	18.1836	17.57383952
Average	20.8293	20.81143	20.82036156

Table 14: Blade Change Summary

Percent Increases due to Blade Change			
	Power		Average
	13	17	
0	-0.99506	3.084761	1.044848379
360	1.86015	-1.33583	0.26216082
1200	-1.42516	1.602885	0.088863206
Average	-0.18669	1.117272	0.465290802
	Amperage		Average
	13	17	
0	0.786357	1.790984	1.28867053
360	0.095857	0.824111	0.459984151
1200	0.473549	0.161677	0.317613083
Average	0.451921	0.925591	0.688755921
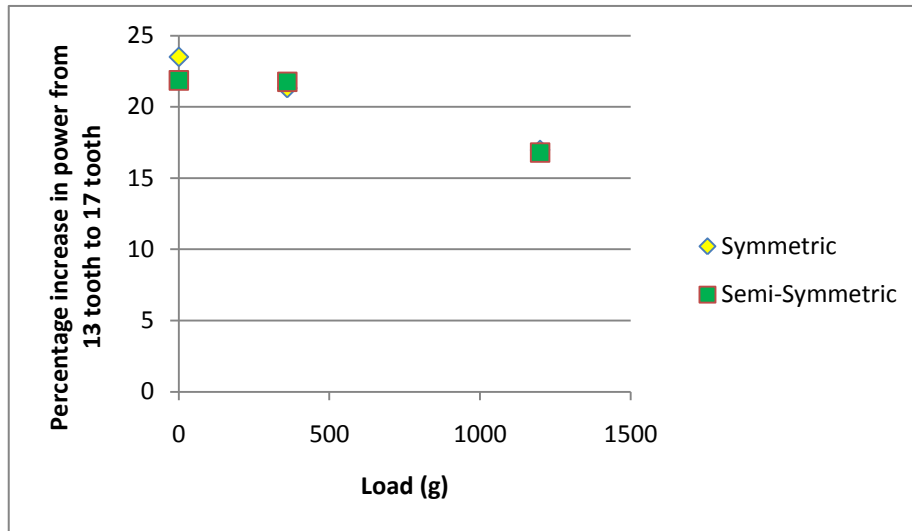
Figure 76: Pinion Change Plot
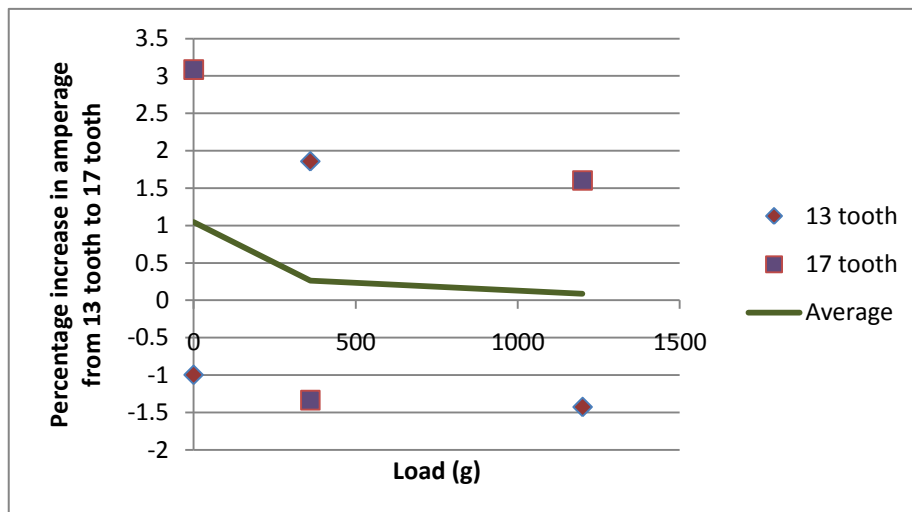
Figure 77: Blade Change Plot

Next, we calculated the coefficient of power required for each run. We decided to use the coefficient of power as a comparison tool for the lifting capability because the coefficient of power is directly related to the coefficient of thrust. The relationship is recognized in the following equation:

$$C_{p,req} = C_T \lambda_i + \frac{\sigma C_d}{8}$$

To find the experimental coefficient of power required, we used an equation that is independent of the coefficient of thrust. Instead, it is only dependent on the power used, the disk area, the air density, and the RPM. The RPM is found from the operating RPM of the motor, the number of pinion teeth, and the number of main gear teeth.

Since we were unable to use the tachometer or the stroboscope to obtain the actual RPM, we found it using calculations based upon the helicopter characteristics. First we researched the motor installed to find the RPM per Volts that it operates at. We found that our motor was right around 1000 RPM per Volts in tandem with our reasonably consistent battery. To account for losses, researched showed that the operation usually occurs at around 90% efficiency. So the RPM values were multiplied by 0.9 to take general losses into account. Next, the RPM of the rotors were based upon the gear ratio from the main gear that is attached to the rotor shaft to the motor pinion gear attached to the main motor. The main gear had 153 teeth and the motor pinion either had 13 teeth or 17 teeth. The gear ratio is the number of teeth on the driven gear divided by the number of teeth on the driving pinion. To find the rotor RPM, we simply divided the motor RPM by the gear ratio.

Once we found the blade RPMs for each installed pinion, we were able to find the coefficients of power during the testing. To find the coefficients of power, we simply used the blade RPM for the pinion that was installed, found the area of the blade, and used the power found by the Eagle Tree system. The coefficient of power was found from the following equation:

$$C_{p,req} = \frac{P_{req}}{\rho(\pi r^2)(\Omega R)^3}$$

The coefficient of power required values found are listed in Table 15. To find the change in power required, we simply divided the coefficient of power for the 17 tooth pinion configuration by the Cp,req for the 13 tooth pinion configuration. This gives the percentage increase of the coefficient of required power comparing the 17 tooth pinion configuration to the 13 tooth pinion configuration. In other words, the percentage describes how much more power is required to lift the same load with the lower RPM settings. Also, the same comparison methodology was used when comparing the semi-symmetric blade to the symmetric blade. From both tests, we were able to see a decrease in the coefficient of power required. A decrease in the coefficient of power required shows that less power is required to lift the same load; the maximum lifting capability of the system was increased. The results show that the 17 tooth pinion configuration is able to lift about 70% more than the 13 tooth pinion. The results also show that our second method, the changing of the blades from symmetric to semi-symmetric camber, raises the lifting ability by about 0.5%.

Table 15 – Percent more power required by the 13 tooth pinion

% More power required by 13 tooth pinion			
Weight	Sym	Semi	Average
0	69.343021	76.47182622	72.90742366
358	78.285891	72.66302264	75.47445664
895	83.061083	88.69455201	85.87781742
Average	76.896665	79.27646696	78.08656591

Table 16 – Percent more power required by the symmetric blade

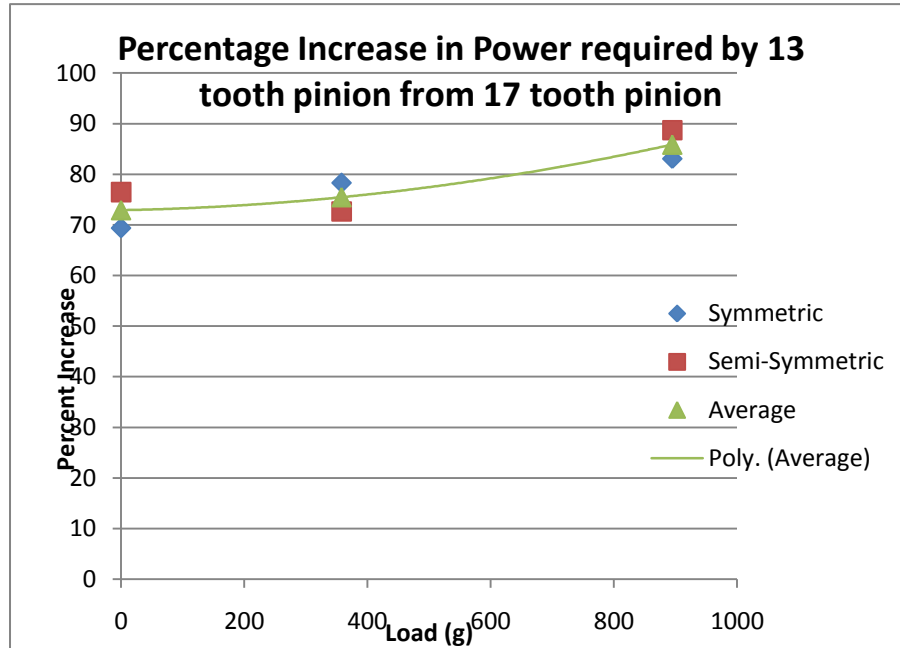| Blade Change			
Weight	13 tooth	17 tooth	Average
0	-0.98526	3.182947073	1.098843515
358	1.8954078	-1.318219597	0.288594116
896	-1.4051337	1.628996427	0.111931375
Average	-0.1649953	1.164574634	0.499789668

Figure 78: Percentage increase in power required by 13 tooth pinion from the 17 tooth pinion
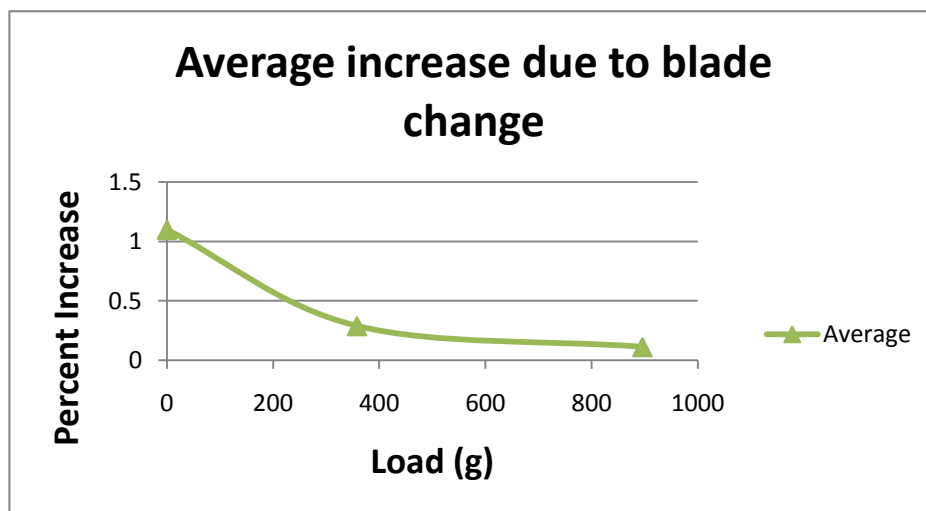

Figure 79: Average power increase due to the blade change

Error

For our calculations, there are a few places where error is present. The most noticeable and most critical of which is the calculation of the RPM. The most ideal situation would be to have a method to continuously record the RPM during flight and pair the RPM values to the respective data points taken for each run. Unfortunately we were unable to pursue this method because we could not afford the equipment or make major changes to the helicopter (since we did not own it.) The second ideal situation would have been to use either the tachometer or the stroboscope to measure the RPM during each flight for the run. Although we had prepared to try both methods, we were unsuccessful with both. Finally, we could have gone through each run and calculated the RPM for each voltage of each run by using the voltage to RPM conversion factor. This method would have been very tedious and would have only made a slight difference in the outcome of the data. Also, the changing of the efficiencies would have neglected this amount of data anyway. The efficiency factor is another clear source of error. Finding the efficiency of the motor to a reasonable accuracy would have been very time consuming and beyond the scope of the project. For this reason, we used a probable efficiency factor of 90%.

Error would also have resulted from the steadiness of the helicopter during flight. Yet, we do believe that the helicopter was held at a very steady position and the amount of error that would have resulted would be accounted for when averaging between the actual run and the redundant run. Along the same lines, the error due to the voltage decrease would have been minimized by repeated runs, the order of runs, and the abundance of runs. This factor could have been reduced more if we had more time to run more runs and mix them up more.

Finally, error would be a factor in the theoretical analysis. The theoretical analysis uses the coefficient of power required equation based upon the coefficient of thrust. In this particular equation, one of the factors is the induced drag. Because we were unable to perform an extensive induced drag calculation, we used a thought out estimate as to what the induced drag would be. Altering the induced drag coefficient does change the outcome of the coefficient of power required significantly. But because we used the same coefficient for all of the tests, it is still an effective method to predict the amount of thrust we gain.

Conclusion

In conclusion we found that switching the motor pinion from a 13 tooth pinion to a 17 tooth pinion increased the lifting capability of the helicopter by approximately 70%. For this reason, we have determined that changing the gearing system of a rotorcraft is an effective way to provide a helicopter with more lifting capability. The downside to increasing the number of teeth on the motor pinion is that the helicopter draws more power from the battery to turn the rotors at a higher RPM. Also, the increase in the number of teeth of the motor pinion is not conducive to forward flight or maneuvers. This is because it is harder to accelerate the blades or change their orientation. We also noticed that the more weight that was added to the load, the smaller the change in power required. On a side note, we experimentally determined that the heaviest tested load when using the 13 tooth pinion is right below

the maximum lift capability for that particular configuration. When holding the helicopter in steady hover, the pilot informed us that he had his control stick at full throttle. This was not planned or used for any reasoning in the data reduction.

On the other hand, changing the blades from a symmetric configuration to a semi-symmetric configuration is not a very effective method for increasing the maximum lift capability. We found that the change only produced around 0.5% lift increase, and that was across all weights. We noticed that as the load was increased, the effectiveness of the blade change became less. This means that at the maximum lift capability, the change in blade effectiveness would be next to none. We hypothesized that this is because at higher angles of attack, the added camber to the blades becomes less and less effective because the slopes of the lift curves come closer and closer together. It would be very interesting to perform more experimentation with blades that were more aerodynamically advanced than the semi-symmetric blade. Overall, this blade change is not recommended for increasing the maximum lifting capability by 5%.

We believe that our testing methods were highly reliable and are a recommendable method for future testing. If we were to make changes, we would like to run more tests and use helicopters that we are not concerned about breaking. We certainly consider the modification of adding more teeth to the rotor pinion to be a highly successful method for increasing the maximum lifting capability as long as steady hover is the primary flight necessity.
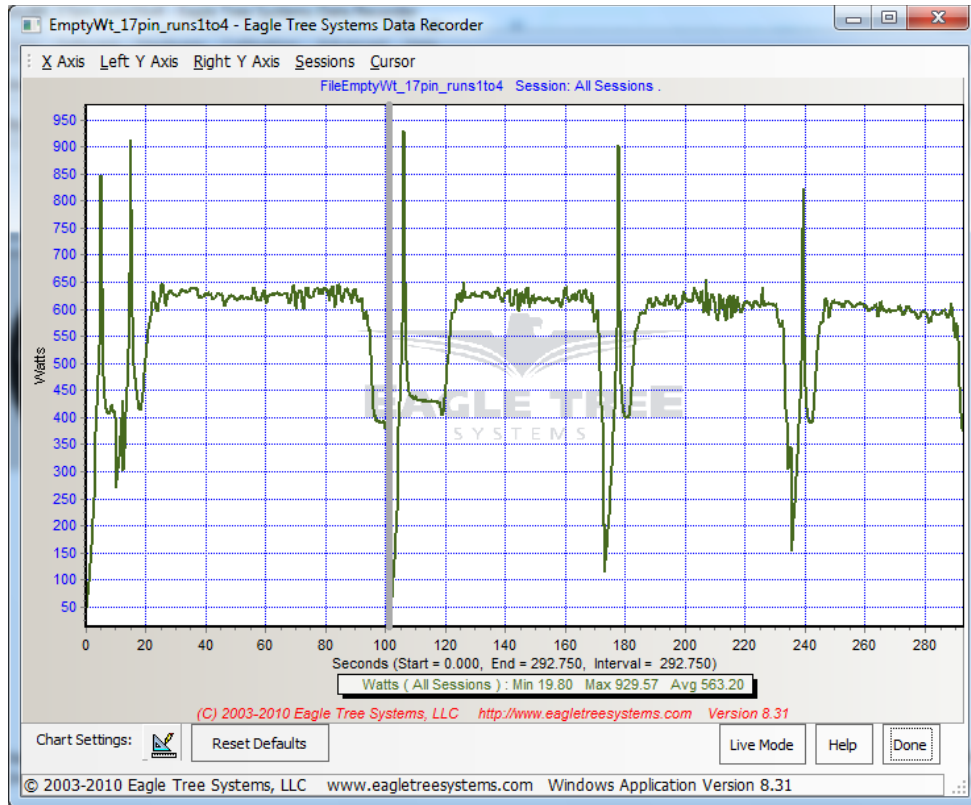
Figure 80: Sample Test Data - Watts
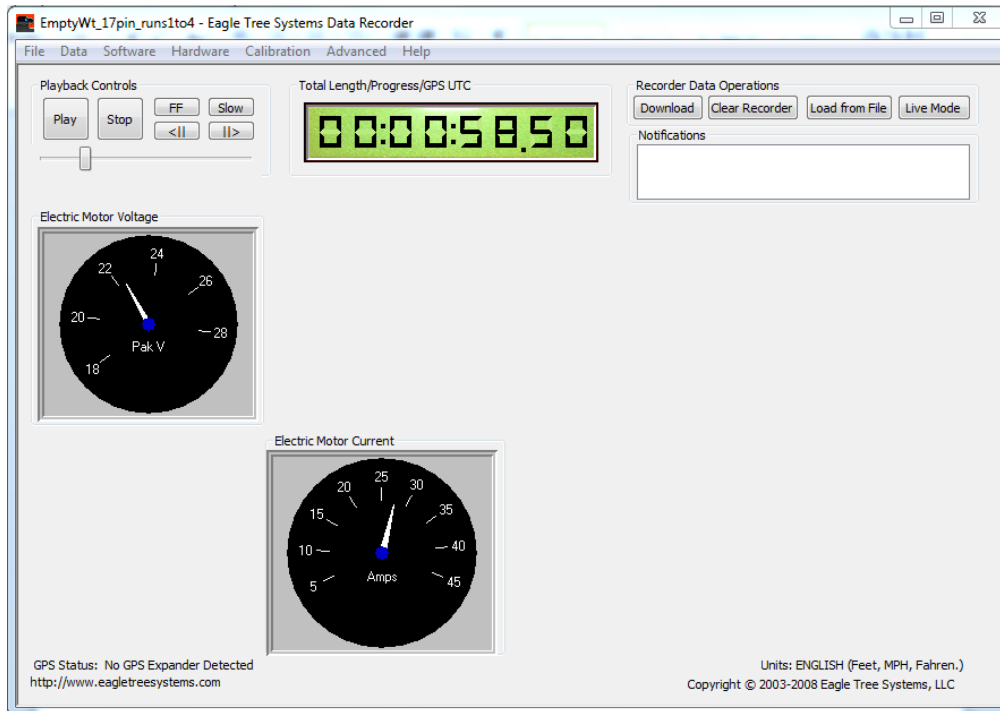
Figure 81: Sample Test Data – Voltage and Current

Conclusions

Team THOR has developed a twin-lift system which allows two CH-47F aircraft to cooperatively lift in excess of 90% more Payload than either aircraft alone could lift at its design gross weight. In order to accomplish this, the system uses the following:

      - A spreader bar made of five identical 20' sections to maintain portability as well as strength, modularity, increase maintainability and allow the aircraft to use 100% of its lifting capability

      - An innovative EGI/DAFCS formation flight system which allows safe, close proximity flight while operating in a master/slave configuration

      -An optical load stabilization system which implements control logic allowing the twin-lift system to operate safely across the entire flight envelope

These systems have been thoroughly researched, simulated and analyzed for their use in the creation of a safe, functional twin-lift system. When implemented, they can also be cross utilized to improve single aircraft sling load capabilities as well as formation flight while not in a twin-lift configuration.

While much work has been done in researching and testing the system, there is still additional work which needs to be accomplished prior to the system being ready for fielding. Probably the most important is the creation of a more detailed simulation model to determine the exact control logic which must be implemented to maintain system stability. Also, at the beginning of the project, the spreader bar was used to provide appropriate spacing between the aircraft and thus was placed in a position to prevent the aircraft from colliding. Once the EGI/DAFCS formation flight system was found, which allowed precision formation flight, this method of separation was no longer necessary. The spreader bar was still needed to maximize the lifting capability, but its placement only 12' below the aircraft was no longer appropriate. This placement led to lateral separation being the highest risk parameter in our simulations. A trade study on the appropriate placement of the spreader bar would alleviate much of this risk.

In addition to showing the feasibility of the system, THOR has done it in a manner which is significantly cheaper than developing a new heavy-lift helicopter to accomplish this seldom occurring mission. It was also accomplished with redundant safety measures that will allow it to pass certification and be fielded within the next 4 years.

All of this adds up to a superior lifting system, capable of accomplishing its required mission safely, quickly and in a cost effective manner.

References

[1] Cohen, C., et al, "Flight Tests of Attitude Determination Using GPS Compared Against an Inertial Navigation Unit", Navigation, Vol. 41, Fall 1994.

[2] Das, A. V., R. Fierro, V. Kumar, J. P. Ostrowski, J. Spletzer, and C. J. Taylor, "A Vision-based Formation Control Framework," *IEEE Trans. on Robotics and Automation*, Vol. 18, No. 5, October 2002, pp 813-825.

[3] Dieter, S., and L. Schmidt, <u>Engineering Design</u>, 4th edition, New York: McGraw-Hill Companies, 2009.

[4] United States, Office of the Under Secretary of Defense, "DoD Guide to Integrated Product and Process Development", Version 1.0, 5 February 1996.

[5] "Gain", Wikipedia, http://en.wikipedia.org/wiki/gain.

[6] Hamers, M., E. von Hinüber, A. Richter, "CH53G Experiences with a Flight Director for Slung Load Handling," *American Helicopter Society 64th Annual Forum,* Montréal, Canada, April-May 2008.

[7] Hanson, Curtis E., et al., *An Overview of Flight Test Results for a Formation Flight Autopilot,* NASA TM-2002-210729, 2002.

[8] Hayward, Roger C., Gebre-Egziabher, Demoz, Powell, J. David. *GPS-Based Attitude for Aircraft*, accessed 15 April 2010, http://waas.stanford.edu/~wwu/papers/gps/PDF/att_for_aircraft_rch1998.pdf.

[9] Johnson, E.N., A. J. Calise, R. Sattigeri, Y. Watanabe and V. Madyastha, "Approaches to Vision-Based Formation Control," *43rd IEEE Conference on Decision and Control,* Atlantis, Paradise Island, Bahamas, December 2004.

[10] Photomodeler, http://www.photomodeler.com.

[11] Schrage, Daniel. P, "Aerospace Systems Engineering – Systems Design & Analysis", Georgia Institute of Technology Lecture, 1 September 2009.

[12] United States, Department of Defense, "Systems Engineering Fundamentals", Defense Acquisition University Press, Fort Belvoir, VA, January 2001.

[13] "FalconView", http://www.falconview.org/trac/FalconView/wiki.

[14] United States, Office of the Deputy Under Secretary of Defense for Acquisition and Technology, Systems and Software Engineering, Enterprise Development. <u>Systems Engineering Plan Preparation Guide.</u> Version 2.01. Washington, DC, 2008.

[15] "Soaring in a Sim," Ares A Defense Technology Blog, April 2010, http://www.aviationweek.com.

16   "Thern Heavy Duty Power Winches", Winch guide, http://www.thern.com.

17   United States, Department of Defense, "Standard Practice for System Safety", MIL-STD-882D, 10 February 2000.

18   United States, Army Aviation and Troop Command, Aviation Research and Development Center, Directorate for Engineering, "Aeronautical Design Standard Handbook: Rotorcraft and Aircraft Qualification (RAQ) Handbook", ADS-51-HDBK, 21 October 1996.

19   SAE International, "Aerospace Recommended Practice: Guidelines and Methods for Conducting the Safety Assessment Process on Civil Airborne Systems and Equipment", ARP4761, December 1996.

20   United States, Department of Defense, "Airworthiness Certification Criteria", MIL-HDBK-516B, 5 February 2004.

21   Price H Manual.

22   US Army Field Manual 4-20-197

23   Pc Based Mode User's Guide Rev 3.1

      Cover page:
      Background image from: "Storm Images, Storm Backgrounds and Storm Myspace Layouts 1 of 4", Accessed 1 April 2010, http://www.layoutsparks.com/myspace-layouts/storm_0.

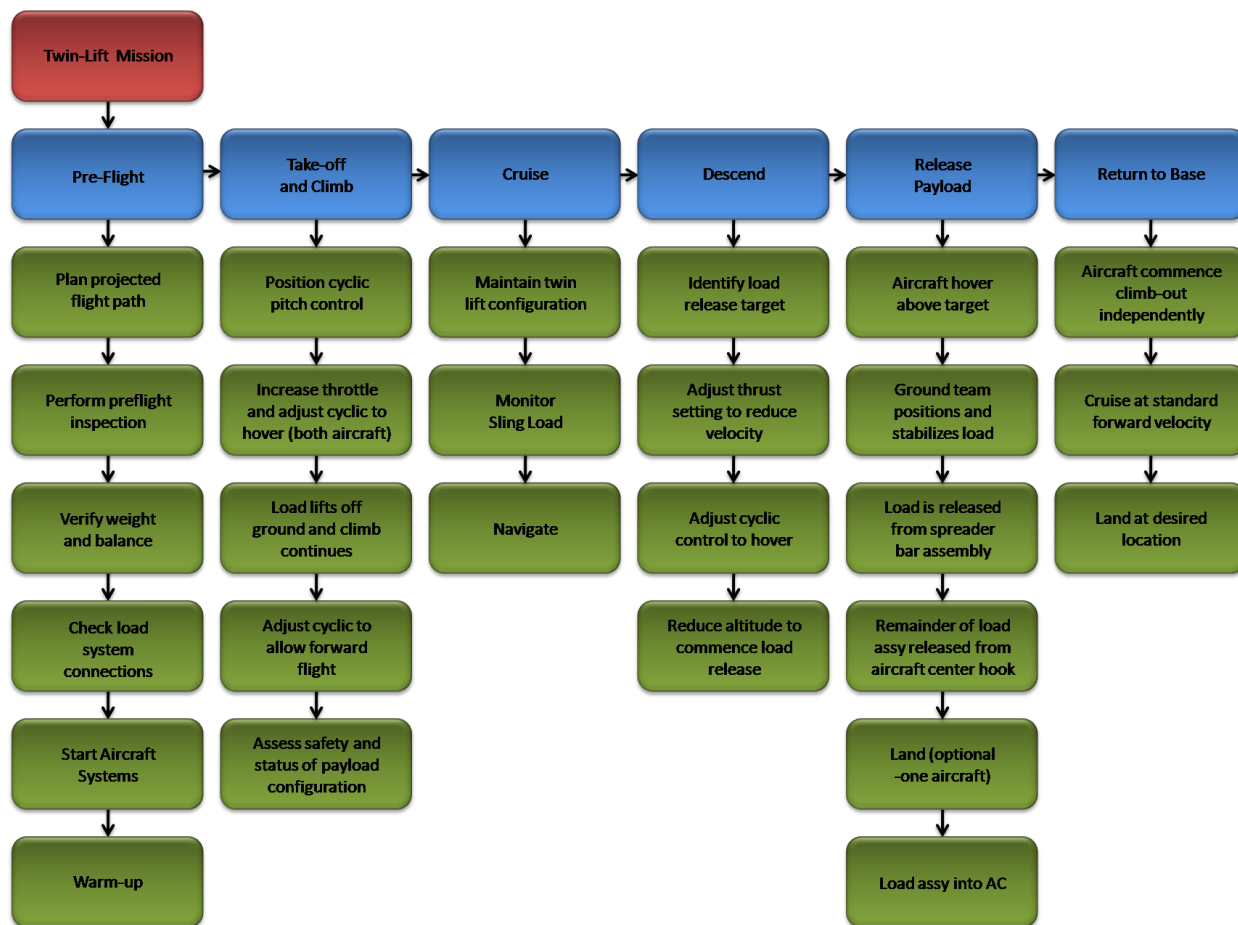   Thor image from: "The week that was…publishing", 21 December 2009, Accessed 1 April 2010, http://www.davidmaybury.ie/journal/?p=3058.

Appendix 1: Twin-Lift System Hazard Assessment

Function	Failure Condition	Phase	Effect of Failure Condition on Aircraft/Crew	Classification
Obtain Clearance for Take-Off	Unable to clear for take-off			
	a. Failure to perform pre-flight inspection	Pre-Flight	Mission delay or abort	Minor
	b. Aircraft systems fail to start	Pre-Flight	Mission delay or abort	Minor
	c. Failure to warm-up	Pre-Flight	Mission delay or abort	Minor
	d. Failure to secure load connections	Pre-Flight	Mission delay or abort	Minor
	e. Failure of load control system	Pre-Flight	Mission abort	Minor
Take-Off in Twin-Lift Configuration	Unable to takeoff and/or climb to desired altitude			
	a. Loss of power	Take-off and Climb	Abort mission and jettison sling load	**Catastrophic**
	b. Unable to climb	Take-off and Climb	Mission abort & emergency landing IAW Ops Manual	Marginal
	Unable to maintain sling load stability			
	a. Mechanical failure of load handling system	Take-off and Climb	Mission abort and jettison sling load and decouple aircraft	Critical
	b. Electrical failure of sling load control system	Take-off and Climb	Mission abort, land with sling load	Major
Cruise with Sling Load to Destination	Unable to cruise at desired speed and altitude			
	a. Loss of power	Cruise	Unable to maintain altitude, autorotation IAW Ops Manual, jettison load and decouple aircraft	**Catastrophic**
	b. Loss of control	Cruise	Cannot regain stability, jettison load and decouple aircraft, attempt autorotation IAW Ops Manual	**Catastrophic**
	c. Loss of Instrumentation	Cruise	Failure to reach destination, mission abort	Critical
	Failure to maintain twin-lift configuration			
	a. Failure of cues from load control system	Cruise	Aircrews can attempt to fly without controls system safely or can land as soon as practical	Major
	b. Failure to maintain aircraft separation or control of sling load	Cruise	Mission abort, jettison sling load and decouple aircraft	Critical
Descend with Sling Load to release site	Unable to descend at desired rate			
	a. Loss of power	Descent	Unable to maintain altitude, jettison sling load and decouple aircraft, autorotation IAW Ops Manual	**Catastrophic**
	b. Loss of control	Descent	Cannot regain stability, jettison sling load and decouple aircraft, attempt autorotation IAW Ops Manual	**Catastrophic**
	c. Loss of instrumentation	Descent	Unable to locate load release zone, mission abort	Major
	d. Loss of visual	Descent	Select more appropriate drop-off location IAW Ops Manual	Major
	Failure to maintain sling load stability			
	a. Mechanical failure of load handling system	Descent	Mission abort, jettison sling load and decouple aircraft.	Critical
	b. Electrical failure of load control system	Descent	Loss of cues from load controls system, aircrews can attempt to release load without cues.	Major
Release Payload	Failure to hover for desired duration			
	a. Loss of power	Payload Release	Mission abort, jettison sling load and decouple aircraft	Critical
	Failure to release payload in safe manner			
	a. Mechanical failure of load handling system	Payload Release	Unable to disconnect load from aircraft. Mission abort, land IAW Ops Manual	Minor

Appendix 2: Three-Level Mission Functional Analysis

Twin-Lift Mission

Pre-Flight	Take-off and Climb	Cruise	Descend	Release Payload	Return to Base
Plan projected flight path	Position cyclic pitch control	Maintain twin lift configuration	Identify load release target	Aircraft hover above target	Aircraft commence climb-out independently
Perform preflight inspection	Increase throttle and adjust cyclic to hover (both aircraft)	Monitor Sling Load	Adjust thrust setting to reduce velocity	Ground team positions and stabilizes load	Cruise at standard forward velocity
Verify weight and balance	Load lifts off ground and climb continues	Navigate	Adjust cyclic control to hover	Load is released from spreader bar assembly	Land at desired location
Check load system connections	Adjust cyclic to allow forward flight		Reduce altitude to commence load release	Remainder of load assy released from aircraft center hook	
Start Aircraft Systems	Assess safety and status of payload configuration			Land (optional –one aircraft)	
Warm-up				Load assy into AC	

Appendix 3: Trim Controller Inputs

Table 15: Unloaded Chinook Input Using Only Rotor Collective and Body Pitch Attitude

Velocity(knots)	Front Rotor Thrust(lb)	Rear Rotor Thrust(lb)	Body Pitch Attitude(deg)
0	12030.9479490182	12742.5413950593	6.42814445734860
10	12036.1216666510	12737.4103912854	6.32348847690977
20	12051.8853564222	12722.2806287443	6.00952699869193
30	12078.9634492041	12697.9448526907	5.48632130183453
40	12118.5524001478	12665.7339102481	4.75411301316642
50	12172.3031792148	12627.5297526563	3.81353244621824
60	12242.2946834403	12627.5297526563	2.66588696611287
70	12330.9963767209	12330.9963767209	1.31352263079818
80	12441.2185557382	12441.2185557382	-0.239754226639147
90	12576.0491946216	12576.0491946216	-1.98821822290231
100	12738.7774109332	12738.7774109332	-3.92376345870278

Table 16: Loaded Chinook Controller Input Using Only Rotor Collective and Pitch Attitude

Velocity(knots)	Front Rotor Thrust(lb)	Rear Rotor Thrust(lb)	Body Pitch Attitude(deg)
0	22165.0192330272	23228.0911777213	6.44141474747855
10	22169.1183511805	23224.0154287009	6.38418081410393
20	22181.5475215473	23211.9324139203	6.21247984168256
30	22202.7014438907	23192.2755488020	5.92632116609660
40	22202.7014438907	23165.7695242767	5.52574318336773
50	22274.0612658876	23133.4335802074	5.01084756105630
60	22326.3415007959	23096.5856303753	4.38184697418542
70	22391.4809132133	23056.8467618318	3.63912603354726
80	22471.1156756112	23016.1454715230	2.78331473728206
90	22567.0992543623	22976.7208331914	1.81537326823236
100	22681.4848327682	22941.1236146143	0.736686259618266

Table 17: Controller Inputs Without Loading

Velocity (knots)	Front Rotor Thrust (lb)	Rear Rotor Thrust (lb)	Front Rotor B1s (deg)	Front Rotor B1c (deg)	Rear Rotor B1s (deg)	Rear Rotor B1c (deg)	Vehicle Pitch (deg)	Roll (deg)
0	13835.27	11003.19	3.704082	-5.0439	-4.6593	-5.0439	6.959273	0
10	13835.76	11002.73	3.703583	-5.0311	-4.6590	-5.0311	6.88733	0
20	13837.35	11001.67	3.700168	-4.9924	-4.6557	4.99245	6.670837	0
30	13840.71	11000.69	3.689246	-4.9272	-4.6435	4.9272	6.308948	0
40	13847.24	11000.74	3.66519	-4.8352	-4.6154	4.8352	5.801497	0
50	13859.01	11003.09	3.622235	-4.7166	-4.5642	4.71662	5.149053	0
60	13878.77	11009.39	3.555109	-4.5720	-4.4833	4.57201	4.353173	0
70	13909.89	11021.66	3.459777	-4.4025	-4.3679	4.40259	3.416907	0
80	13956.44	11042.31	3.334318	-4.2104	-4.2156	4.21047	2.345426	0
90	14023.07	11074.09	3.179764	-3.9989	-4.0277	3.99891	1.146634	0
100	14115.03	11120.08	3.000586	-3.7724	-3.8098	3.77248	-0.1684	0

Table 18: Controller Inputs with Loading

Velocity (knots)	Front Rotor Thrust (lb)	Rear Rotor Thrust (lb)	Front Rotor B1s (deg)	Front Rotor B1c (deg)	Rear Rotor B1s (deg)	Rear Rotor B1c (deg)	Vehicle Pitch (deg)	Roll (deg)
0	25235.73	20350.95	4.74757	0.086276	-6.68407	0.086276	5.89075	0
10	25236.25	20350.31	4.745788	0.053359	-6.65936	0.053359	5.88885	0
20	25237.57	20348.74	4.73822	-0.04497	-6.5848	-0.04497	5.88021	0
30	25239.38	20346.92	4.719299	-0.20799	-6.45958	-0.20799	5.85765	0
40	25241.81	20345.54	4.682076	-0.43522	-6.28326	-0.43522	5.81235	0
50	25245.49	20345.38	4.619624	-0.72647	-6.05571	-0.72647	5.73561	0
60	25251.55	20347.43	4.525926	-1.08165	-5.77705	-1.08165	5.61993	0
70	25261.58	20352.92	4.396529	-1.50068	-5.44760	-1.50068	5.45978	0
80	25277.68	20363.4	4.229082	-1.98342	-5.06788	-1.98342	5.25227	0
90	25302.47	20380.7	4.023747	-2.52961	-4.63865	-2.52961	4.99768	0
100	25339.08	20406.85	3.783436	-3.13884	-4.16093	-3.13884	4.69973	0